INFRARED DETECTION OF SURFACE CHARGE AND CURRENT DISTRIBUTIONS.

James David Selim

Report Number NPS62-77-001

NAVAL POSTGRADUATE SCHOOL
Monterey, California

THESIS

INFRARED DETECTION OF SURFACE
CHARGE AND CURRENT
DISTRIBUTIONS

by

James David Selim

December 1977

Thesis Advisor: R. W. Burton

Prepared for: Rome Air Development Center
Griffiss AFB
New York 13441

REPORT DOCUMENTATION PAGE

READ INSTRUCTIONS BEFORE COMPLETING FORM

1. REPORT NUMBER: NPS62-77-001	2. GOVT ACCESSION NO.
3. RECIPIENT'S CATALOG NUMBER	
4. TITLE (and Subtitle): INFRARED DETECTION OF SURFACE CHARGE AND CURRENT DISTRIBUTIONS	5. TYPE OF REPORT & PERIOD COVERED: Final Report 1 Dec 76 - 1 Dec 77
	6. PERFORMING ORG. REPORT NUMBER
7. AUTHOR(s): James D. Selim in conjunction with Robert W. Burton	8. CONTRACT OR GRANT NUMBER(s)
9. PERFORMING ORGANIZATION NAME AND ADDRESS: Naval Postgraduate School Monterey, California	10. PROGRAM ELEMENT, PROJECT, TASK AREA & WORK UNIT NUMBERS: FY76196003
11. CONTROLLING OFFICE NAME AND ADDRESS: Rome Air Development Center Griffiss AFB New York 13441	12. REPORT DATE: December 1977
	13. NUMBER OF PAGES: 108
14. MONITORING AGENCY NAME & ADDRESS(if different from Controlling Office)	15. SECURITY CLASS. (of this report): Unclassified
	15a. DECLASSIFICATION/DOWNGRADING SCHEDULE

16. DISTRIBUTION STATEMENT (of this Report)

Approved for public release; distribution unlimited

17. DISTRIBUTION STATEMENT (of the abstract entered in Block 20, if different from Report)

18. SUPPLEMENTARY NOTES

19. KEY WORDS (Continue on reverse side if necessary and identify by block number)

Thermovision
Infrared
Surface Charge and Current Distribution

20. ABSTRACT (Continue on reverse side if necessary and identify by block number)

A technique was devised using infrared detection of localized I^2R heating of conducting materials to determine the surface charge and current distributions on various objects. The measurement process is explained and comparisons between experimentally

20.
determined and actual charge and current distributions
are presented.

Approved for public release; distribution unlimited.

INFRARED DETECTION OF SURFACE CHARGE AND CURRENT DISTRIBUTIONS

by

James David Selim
Captain, United States Marine Corps
B.S., Mathematics, University of Oklahoma, 1966
B.S.M.E., University of Oklahoma, 1967

Submitted in partial fulfillment of the
requirements for the degree of

ELECTRICAL ENGINEER

from the

NAVAL POSTGRADUATE SCHOOL

December 1977

ABSTRACT

A technique was devised using infrared detection of localized I^2R heating of conducting materials to determine the surface charge and current distributions on various objects. The measurement process is explained and comparisons between experimentally determined and actual charge and current distributions are presented.

TABLE OF CONTENTS

ACKNOWLEDGEMENT

When one spends an extended period in experimentation, advances are made haltingly and many "lost" hours are spent on fruitless theories. The frustration encountered is lessened when shared. My undying gratitude goes to my teacher, adviser, confidant, and friend, Professor Robert W. Burton.

Another major contribution was made by Pat and the kids. Their understanding, patience, and love is appreciated.

I. INTRODUCTION

Knowledge of the charge and current distributions is essential in many applications of antenna design and placement, electromagnetic scattering, and electromagnetic compatability. Although it is possible to measure these quantities directly on a given object using electrically small probes [Whiteside 1962], it is an extremely slow, tedious, and expensive process. To avoid this, computer analysis of structures has become increasingly important [Butler 1972, Chao and Strait 1971]. These models require assumptions concerning geometry, wire size, boundary conditions, and the like. In all such investigations, model verification has become important [Burton and King 1975, Burton, King and Blejer 1976]. Clearly, a technique yielding real-time measurement of charge and current magnitude distributions has obvious advantages.

La Varre and Burton have shown [1975] that surface currents on radiating and scattering structures can, under certain conditions, generate sufficient heat to be detectable by infrared measurements with equipment such as an AGA Thermovision 680 system.

A. FACTORS AFFECTING INFRARED DETECTION

The detectability of I^2R heating by surface currents is a function of the threshold temperature gradient of the measuring equipment, the conductivity and emissivity of the

surface under investigation, and the microwave power levels present.

A temperature gradient of 0.2°C can be detected by the Thermovision system. If a scattering or radiating structure has sufficient currents to cause a 2°C temperature difference, ten isotherms may be selected in various colors and displayed to indicate the temperature distributions.

The surface under consideration must be sufficiently conductive to allow representative charge and current distributions to form. However, the surface must not be so conductive that either no significant I^2R heating is produced, or any generated heat is quickly dissipated by the thermal conductivity of the material. High electrical conductivity in a material implies high thermal conductivity in that material.

The spectral emissivity (the ratio of the emittance of a body in a specified portion of the spectrum to that of an ideal radiator) must also be sufficiently high to allow good Thermovision detection of the surface. The more nearly "black" the surface in the three to five micrometer wavelength range, the better the detectability of a specific temperature difference on that surface.

Sufficient microwave power levels must be used to cause charge and current distributions to form, but practical and safety considerations dictate that minimum usable levels be employed. The experimental procedures in this work require an incident power at the surface of scattering objects of approximately three milliwatts per square centimeter.

B. THESIS OBJECTIVE

This work was done to indicate the feasibility of the infrared detection process, to reduce the process to common laboratory or applications procedures, to compare the results obtained with results from other techniques to exhibit the accuracy of the infrared detection procedure, and to use infrared detection to obtain current distributions on objects that have not been otherwise determined. The direction of future research was also indicated.

II. EXPERIMENTAL APPARATUS

A. AGA THERMOVISION SYSTEM 680

The AGA Thermovision System 680 is an infrared camera and display system that uses a single indium antimonide (InSb) photovoltaic detector, cooled to 77°K with liquid nitrogen, to detect emissions from objects in its field of view in the 2 to 5.6 micron wavelengths.

1. Camera

The camera (Figure 1) in this system has an 8°x8° field-of-view germanium lens, with a range of focus from 1.7 meters to infinity. Scanning is accomplished with two rotating eight-faced prisms that move the instantaneous field of view through the desired region. The cooled detector allows a minimum detectable temperature difference of better than 0.2°C at a 30°C object temperature.

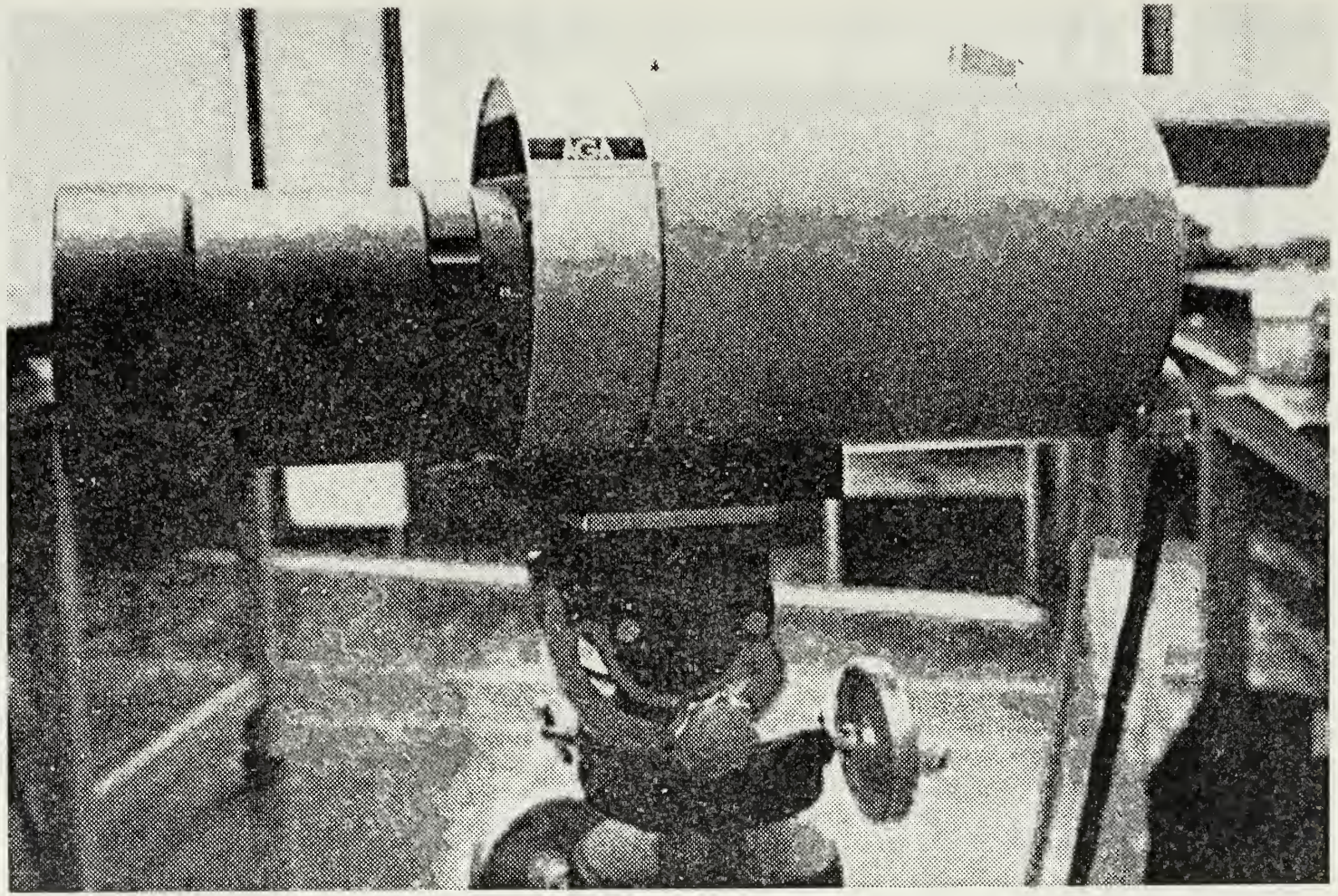

Figure 1 - AGA THERMOVISION CAMERA

2. Black and White Monitor

The black and white monitor (Figure 2) is the initial display of the camera's output. The display has 100 lines with a line frequency of 1600 lines per second, yielding 16 frames per second. The controls for focus, bias control of the detector (temperature window location), sensitivity (temperature window size), plus various other settings for the display are located on this monitor. The black and white monitor has the capability for two isotherms to be selected anywhere in the displayed temperature window that give highlighted output at the corresponding locations in the display.

3. Color Monitor

The color monitor (Figure 3) gives a display twice the size of the normal black and white output and permits the application of color to allow the temperature window to be divided into ten easily distinguishable regions. At the minimum settings, this quantizing allows the system to display the minimum detectable difference of 0.2°C in an easily understood format.

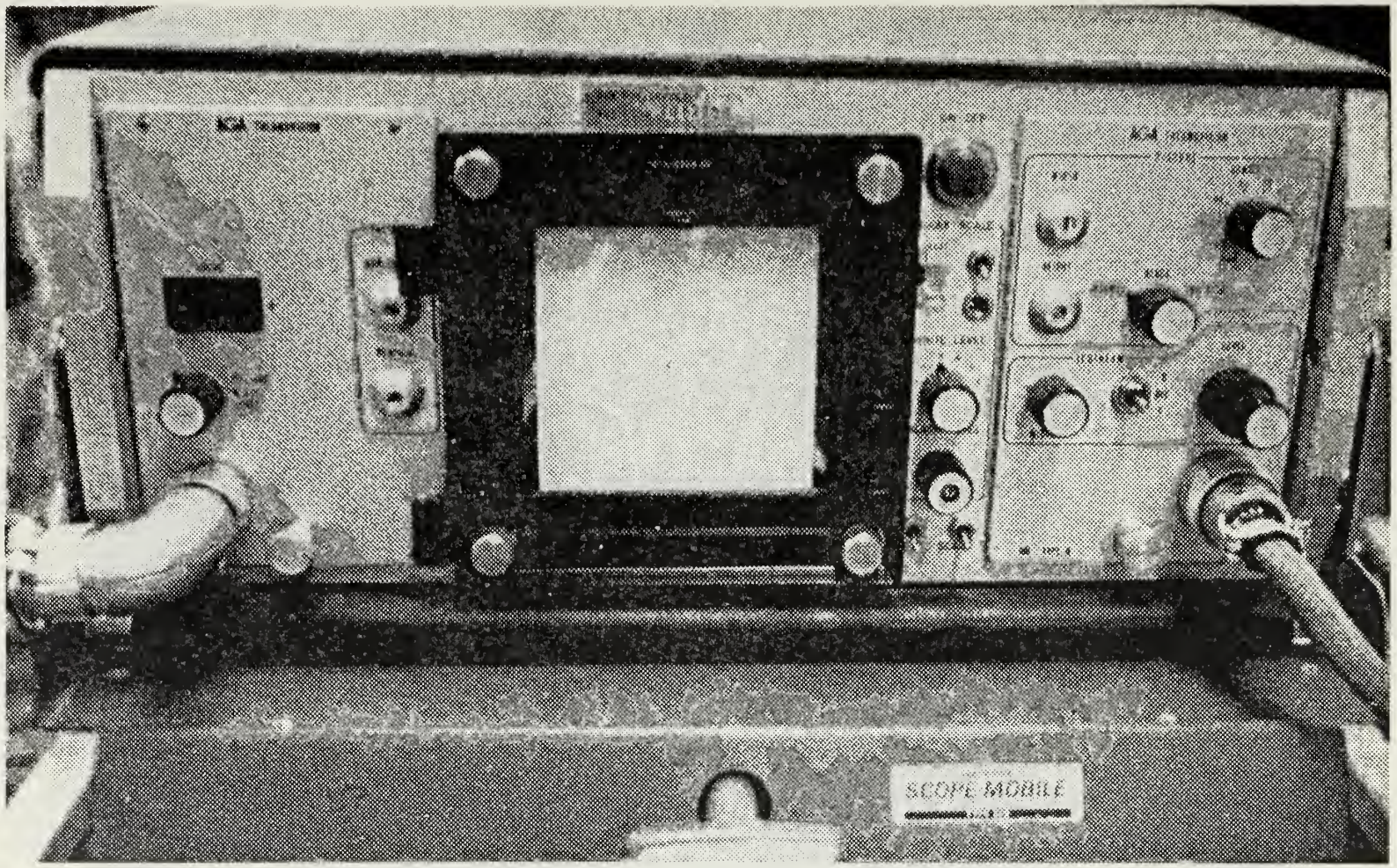

Figure 2 - AGA THERMOVISION BLACK AND WHITE MONITOR

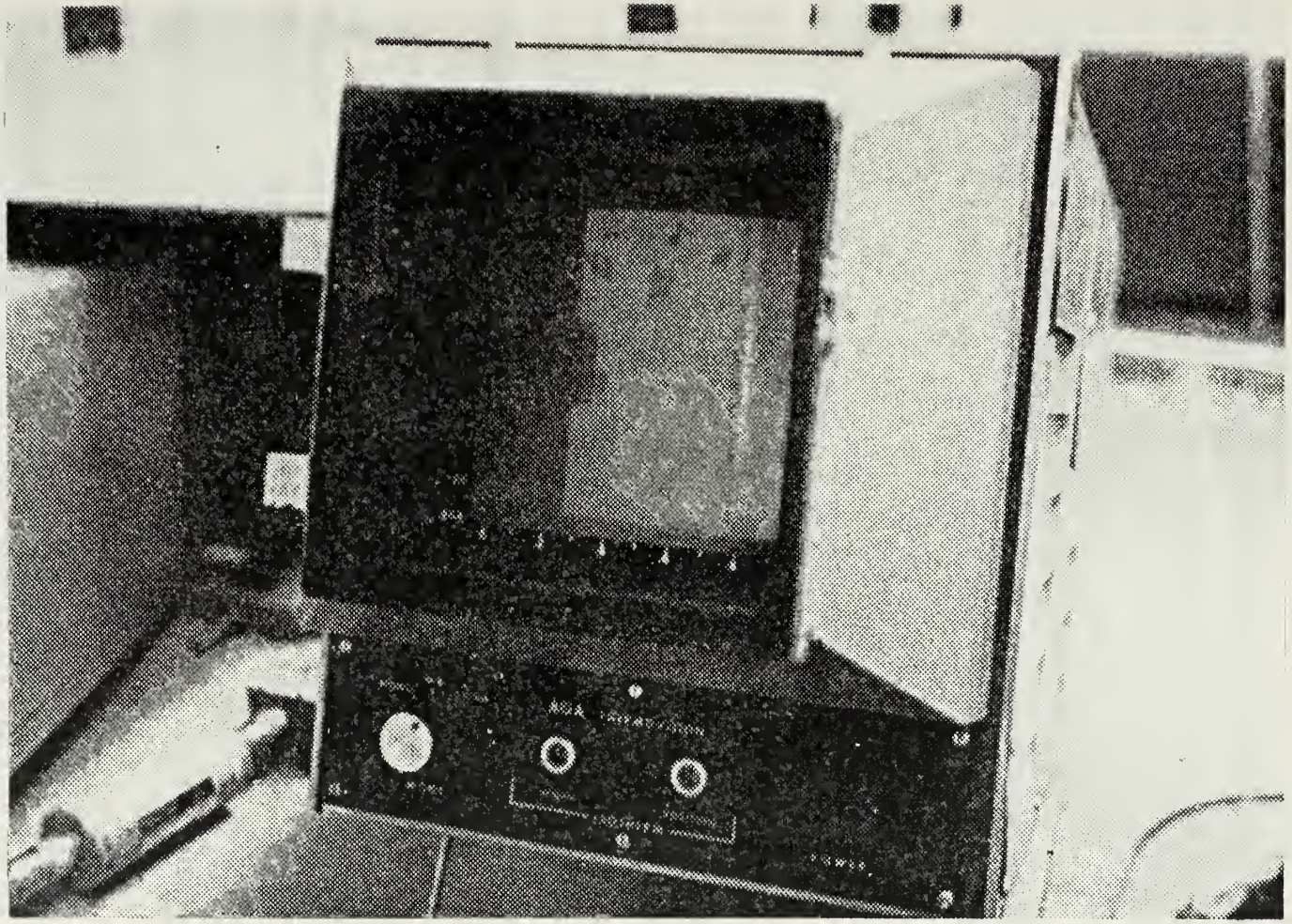

Figure 3 - AGA THERMOVISION COLOR MONITOR

4. Profile Adapter and Display

The profile adapter and its associated black and white display unit (Figure 4) give quantizing capability to the picture displays. Two modes exist in this display, one for surface temperature cross section of any selected scan line, and the other a diminished scale version that presents the surface temperature cross section of all 100 lines of the display. This relief map is a three-dimensional display of the emissions of the objects being viewed by the camera.

E. THERMOVISION PICTURE INTERPRETATION

Figure 5 is an example of a picture from the color monitor. The horizontal band at the bottom shows the ten isotherms in the selected temperature window, increasing in temperature from left to right. Thus, the relative temperature distribution of a homogeneous object can be determined by matching the colors in the display to the corresponding portion of the reference band. The color of any portion of the band may be chosen by the operator, and changed when desired. Normally the colors are arranged to provide maximum contrast between adjacent isotherms. For printing, the colors in the photographs are converted to half-tone black and white. This process diminishes the contrast between adjacent isotherms.

Unless otherwise indicated, all Thermovision pictures use a temperature window of 2°C, which makes each isotherm 0.2°C in width.

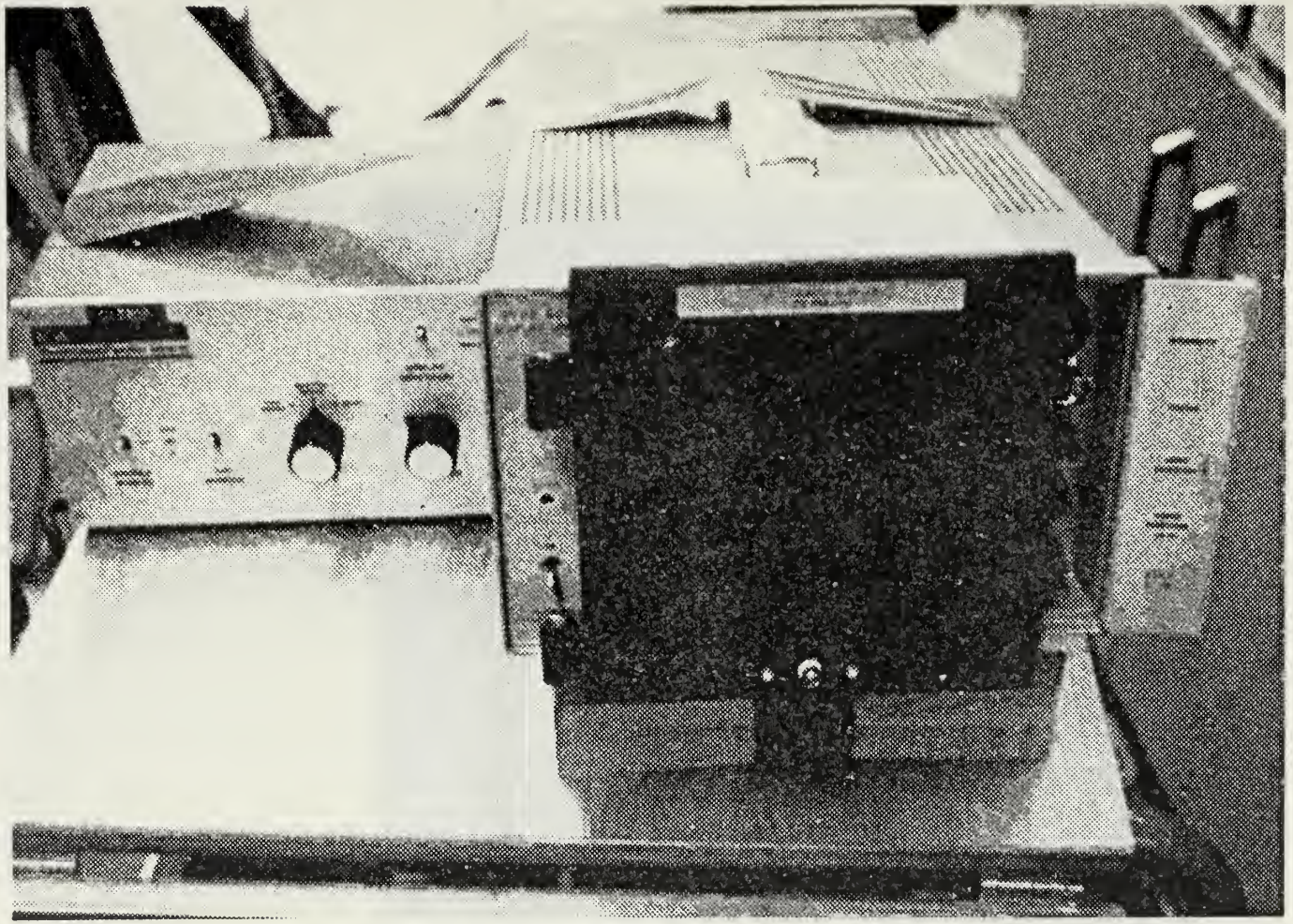

Figure 4 - AGA THERMOVISION PROFILE ADAPTER AND DISPLAY

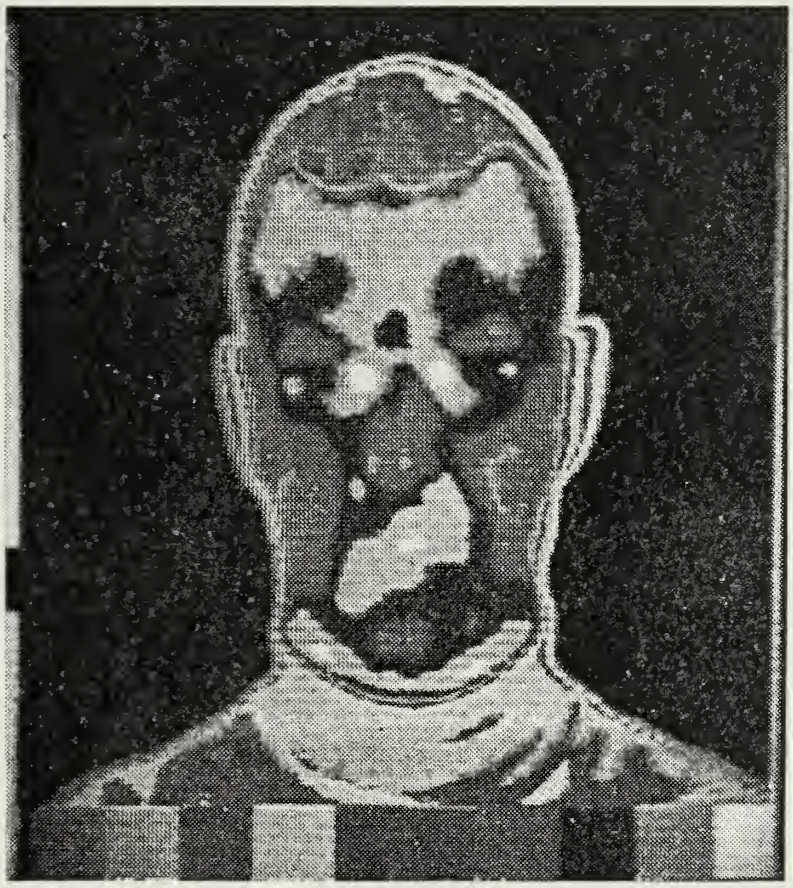

Figure 5 - THERMOVISION PICTURE EXAMPLE

C. LABORATORY ARRANGEMENT

Figure 6 shows the arrangement of the laboratory set up for the study of scattering objects. The object under study was placed on a 4x12 feet (3.8x11.5 wavelengths at 937.5 MHz) aluminum ground plane at a sufficient distance to insure an incident plane wave. The monopole was driven at its base and placed in front of a 60° corner reflector. The infrared camera was moved as desired around the ground plane to obtain the proper view of the object. To insure complete and uniform connections, all points of contact with the ground plane were taped with copper conducting tape.

To study radiating objects, the object, usually an antenna, was placed in the driven location and the corner reflector removed.

D. POWER GENERATING SYSTEM

Figure 7 is a schematic representation of the arrangement to provide the incident power to the driven element. The power generator (a Sierra Electronics model 470A, 80 watts maximum output) was connected to an isolater and then to a dual directional coupler. A dual stub tuner was then attached to cancel the reflected signal from the driven element. A power meter was connected at the return port of the dual directional coupler to allow determination of the occurrence of the minimum returned signal.

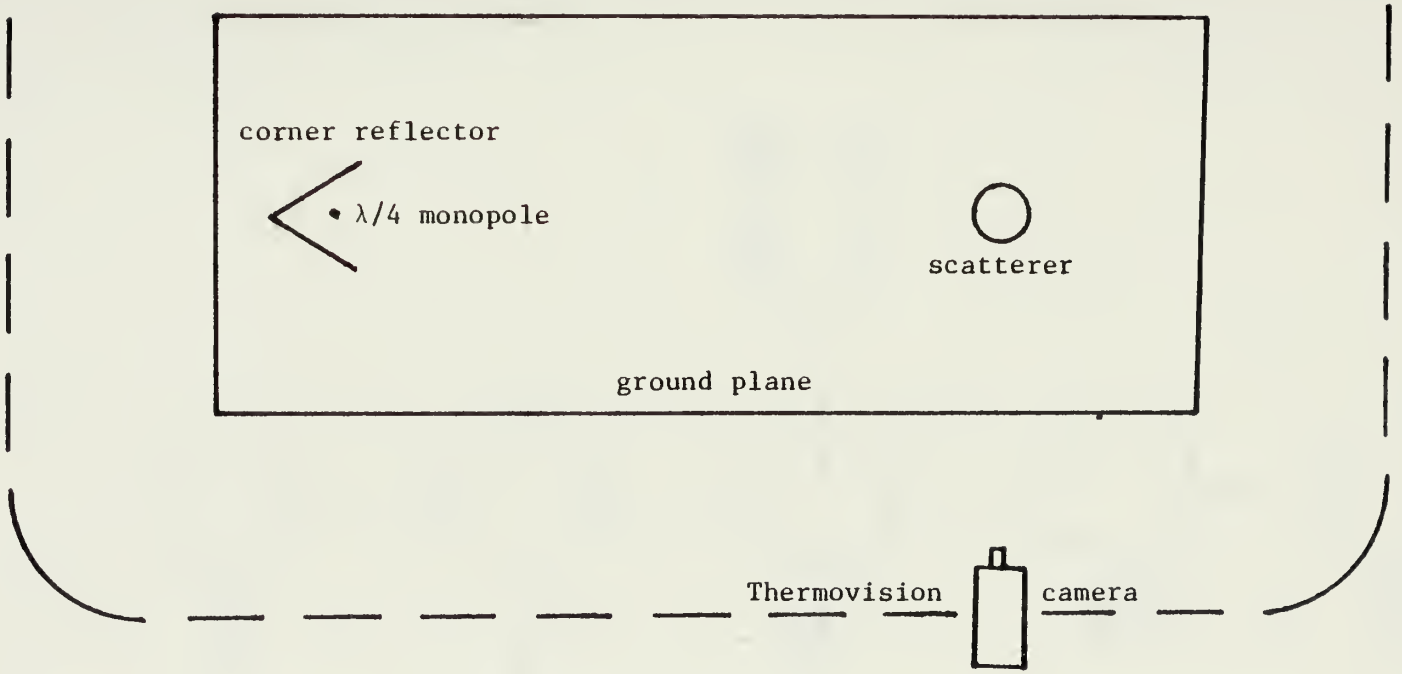

Figure 6 - LABORATORY ARRANGEMENT

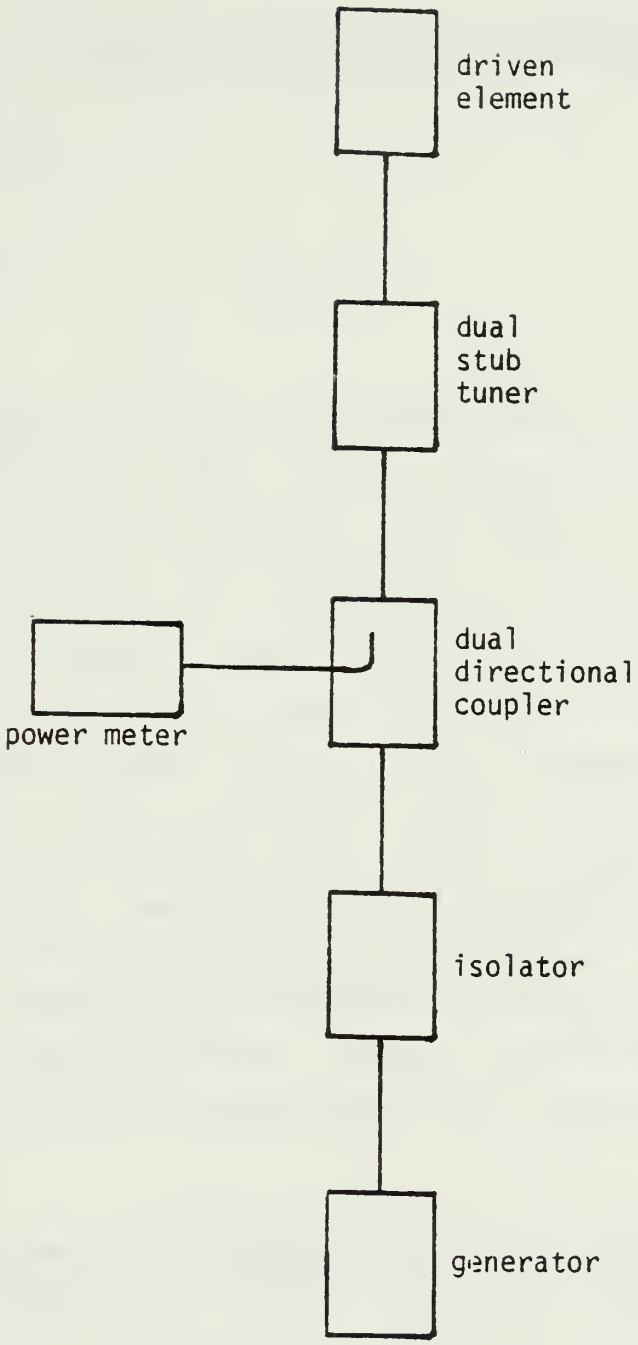

Figure 7 - POWER GENERATING SCHEMATIC

III. CHARGE DISTRIBUTION DETERMINATION

A. TECHNIQUE

To determine the charge distributions on an antenna, a sheet of resistive paper (2000 ohms per square, Sunshine Scientific Instrument Company, Philadelphia), was placed behind the antenna. A dielectric material was used as a backing for the paper to provide the required stiffness. The electric field lines, originating at the charge locations on the antenna, cause currents to flow on the resistive paper. Near large charge concentrations, where more lines of force converge, the resultant current magnitudes on the paper are higher, producing greater localized heating. When detected, this heating yields the relative charge distributions on the antenna. For radiating antennas, the current distributions may then be determined from the continuity equation. Figure 8 is an example of the setup for the charge determination on a scattering crossed dipole.

All measurements of charge distribution shown were made at a frequency of 937.5 megahertz (32 centimeter wavelength).

Only a few examples of this technique are included here to illustrate the procedure. Extensive examples and comparisons with known solutions are shown by Nanes and Burton [1977].

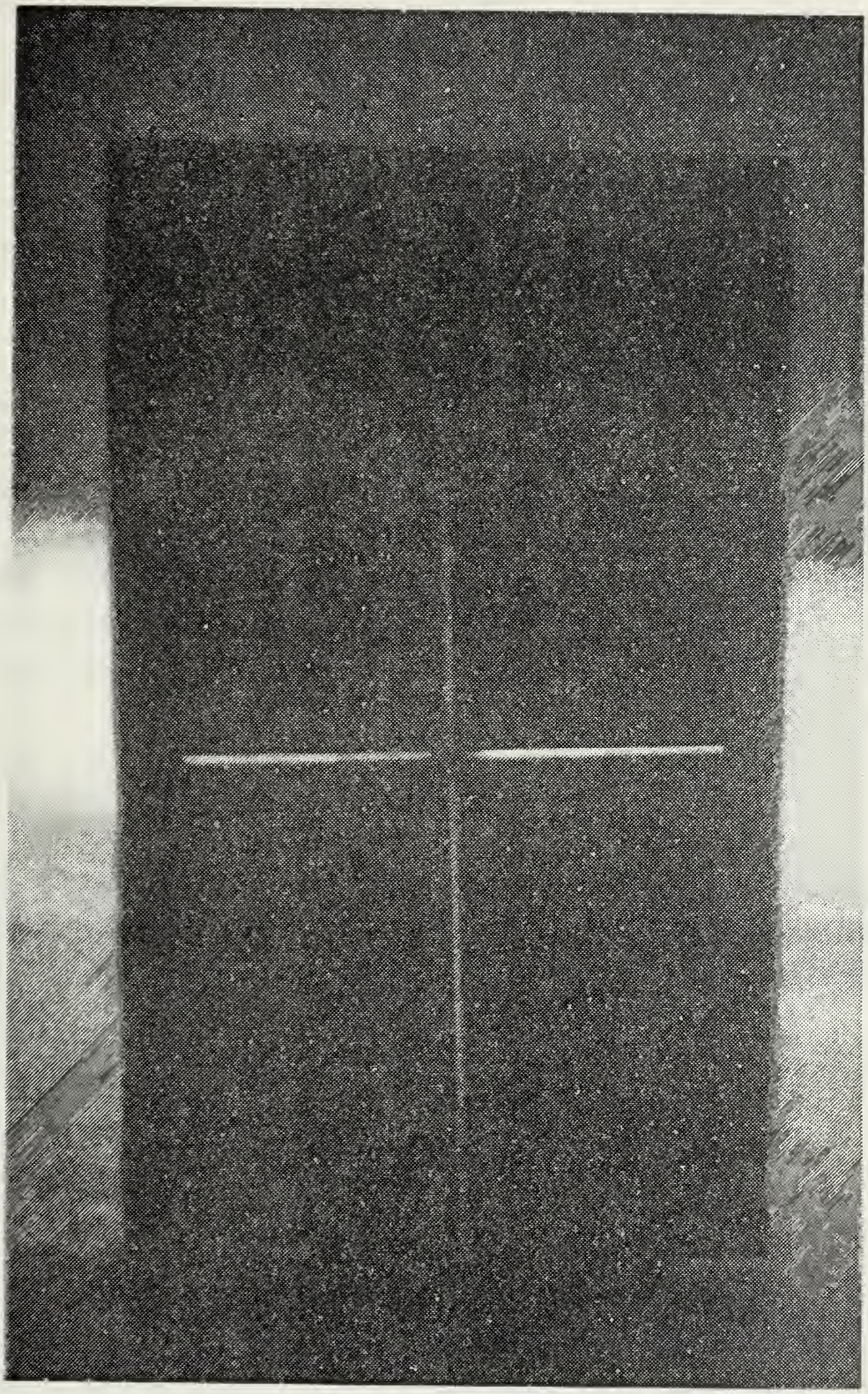

Figure 8 - CHARGE DISTRIBUTION DETERMINATION SET UP

E. THREE-QUARTER WAVELENGTH MONOPOLE ON GROUND PLANE

1. Radiating

The charge distribution on a radiating thin three-quarter wavelength (24 centimeters) monopole and the Thermovision charge picture is shown in Figure 9. The charge magnitude maximum locations are easily identified as the warmest points on the display. The charge minimum between the maximums is clearly seen as the coolest spot on the antenna. Note the driving point disturbance at the base of the monopole.

2. Scattering

The charge distribution for the scattering three-quarter wavelength monopole is shown in Figure 10. As expected, the distribution looks like the radiating case without the driving point disturbance.

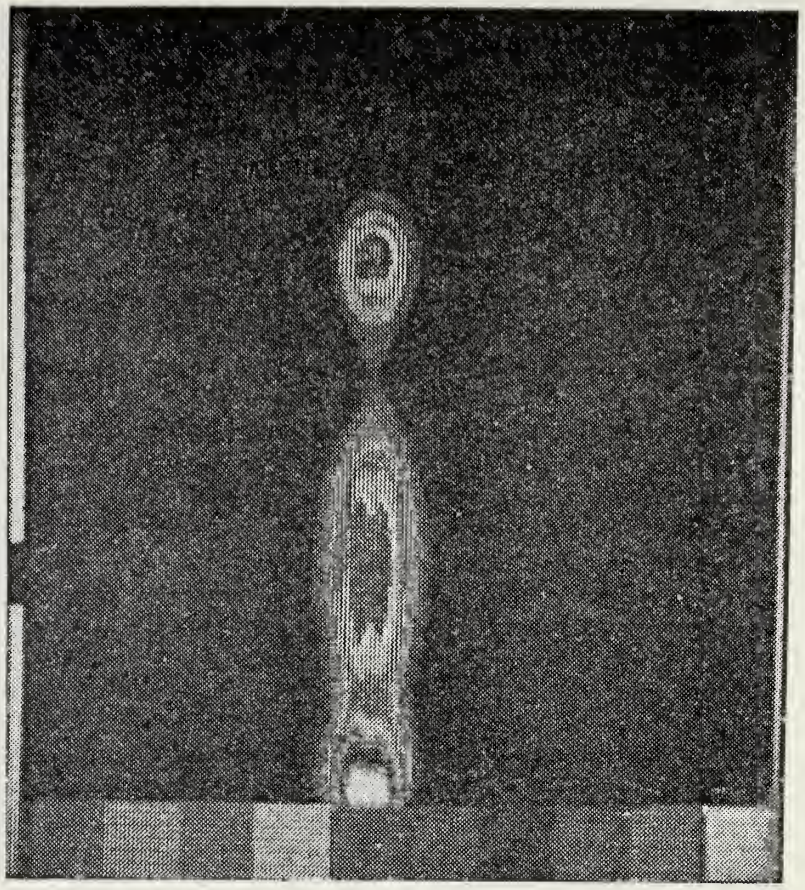

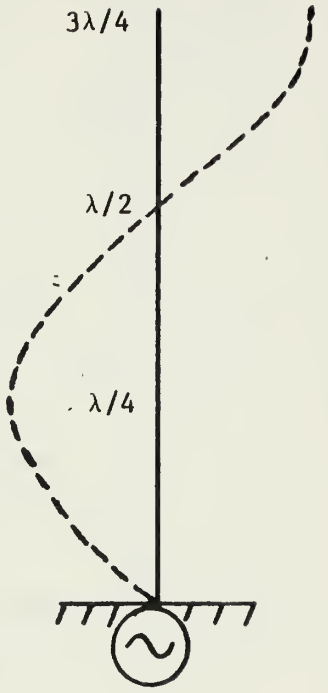

Figure 9 - RADIATING THREE-QUARTER WAVELENGTH MONOPOLE CHARGE DISTRIBUTION

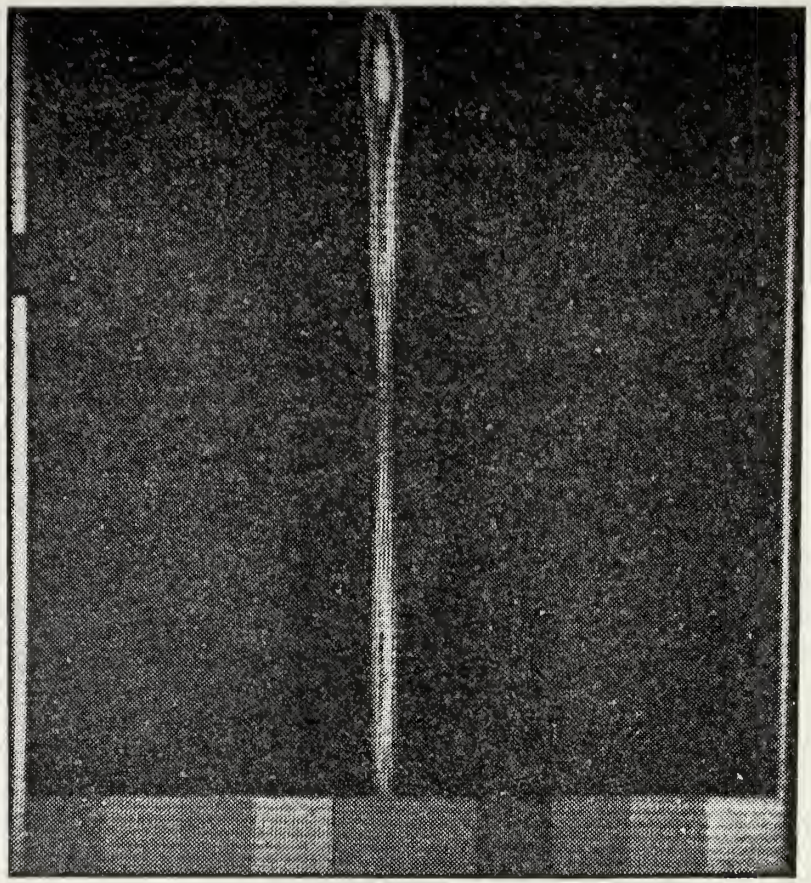

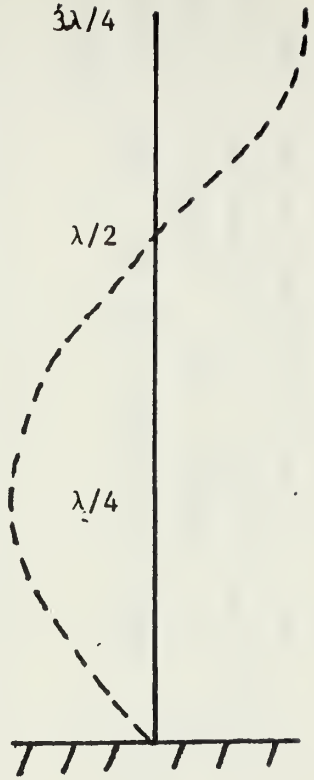

Figure 10 - SCATTERING THREE-QUARTER WAVELENGTH MONOPOLE CHARGE DISTRIBUTION

C. CROSSED DIPOLES ON GROUND PLANE

The charge distributions on two of the thin crossed antennas discussed by Burton and King [1975] are shown in Figures 11 and 12. The effects of the various resonant lengths seen by the source in these two radiating antennas is clear.

1. Horizontal Cross at One-Half Wavelength

Figure 11 shows the three-quarter wavelength monopole with one-quarter wavelength (8 centimeters) arms attached at one-half wavelength from the ground plane. The resonant length seen by the source is three-quarters of a wavelength, resulting in a charge distribution similar to the monopole, except there are now three locations (each tip) of the final charge maximums.

2. Horizontal Cross at One-Quarter Wavelength

When the horizontal cross is moved down to one-quarter wavelength from the ground plane, the charge distribution is as shown in Figure 12. The resonant length seen by the source is now one-half wavelength, which causes the significant redistribution of charge concentrations from the uncrossed monopole.

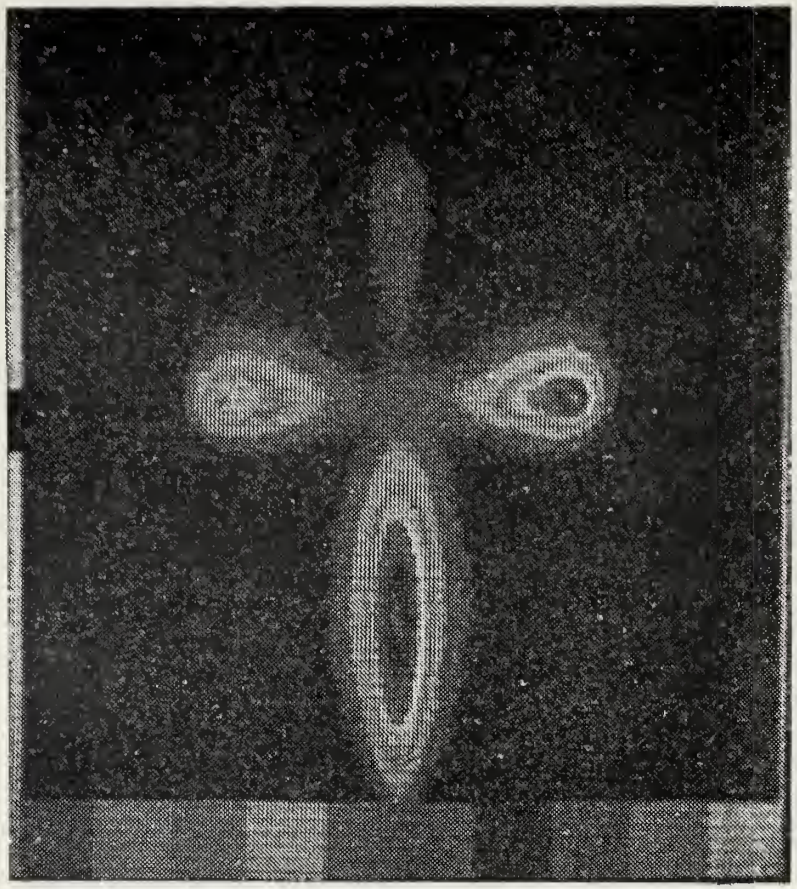

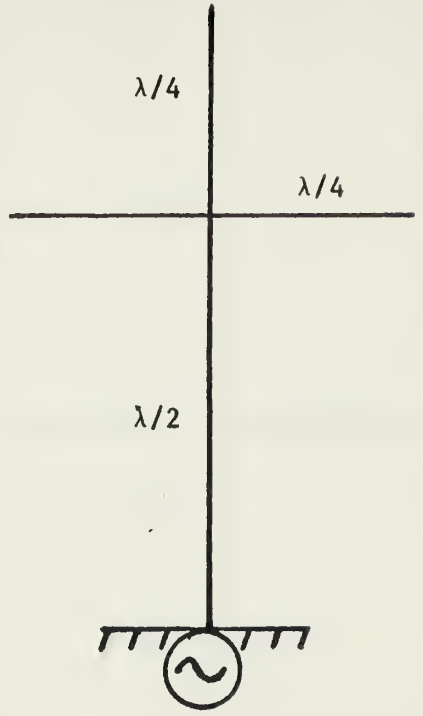

Figure 11 - HORIZONTAL CROSS AT ONE-HALF WAVELENGTH CHARGE DISTRIBUTION

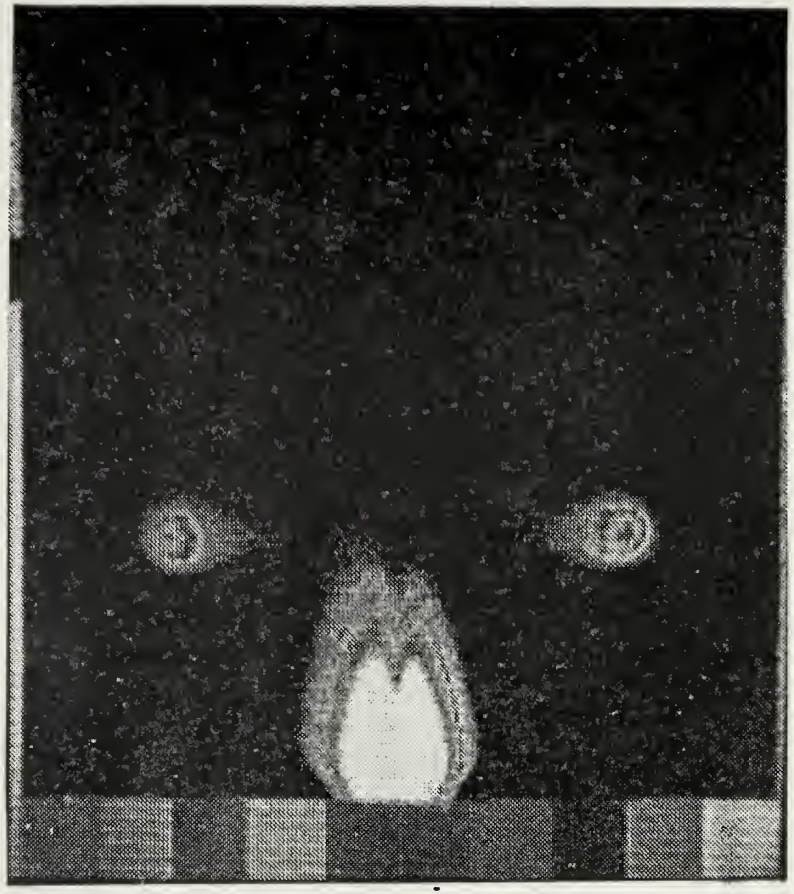

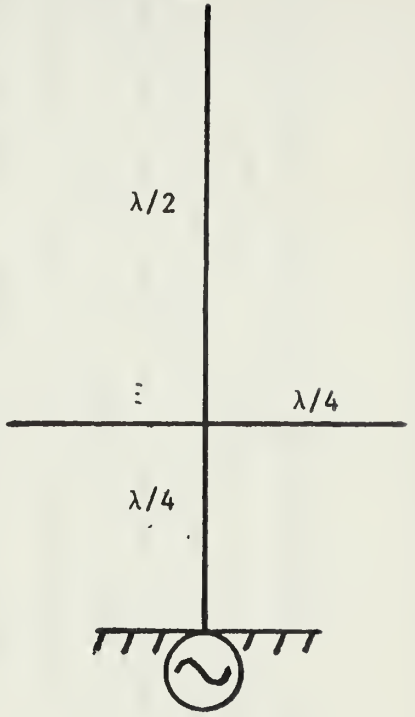

Figure 12 - HORIZONTAL CROSS AT ONE-QUARTER WAVELENGTH CHARGE DISTRIBUTION

IV. CURRENT DISTRIBUTION DETERMINATION

The technique for charge distribution determination is simple and convenient. However, two factors tend to limit its applicability to a general situation. Because the sheet of resistive paper must be situated adjacent to the object and respond to charge distributions despite the orientation with the source, direct charge distribution determination is presently limited to "thin" objects. Often, particularly in complex structures, objects of interest are not "thin." Additionally, primary interest often is directly in the current distributions on conductors. Thus, the thrust of this work was the direct determination of current distributions.

A. TECHNIQUE

Initially, a sheet of resistive paper was used to construct a model of the object. This model was then placed on the ground plane and irradiated. It was soon discovered that, because the skin depth of the resistive paper at 937.5 MHz is on the order of the paper thickness (approximately 0.8 millimeters), non-conducting objects used for support behind the model had a significant effect on the temperature distribution of the irradiated surface.

When five thicknesses of resistive paper were used for model construction, supporting structures no longer had an effect on the surface temperature distributions.

With an incident field strength of three milliwatts per square centimeter at the surface of a model, an obvious current magnitude representation is apparent within five to ten seconds. The surface then heats uniformly for approximately four minutes until steady state heating/cooling occurs.

Figure 13 shows the model used for a one-half wavelength (16 centimeters) square. Note the polystyrene foam used for support and the copper tape at the intersection with the ground plane.

All measurements of current distributions shown were made at a frequency of 937.5 megahertz (32 centimeter wavelength).

Burton and King, in work currently in progress at Harvard University, have measured the surface current and charge distributions on a flat surface with normal and 45° incident plane waves. Partial results of their investigation are shown in Appendix A, and provide a reference for the Thermovision pictures of the flat surfaces investigated herein.

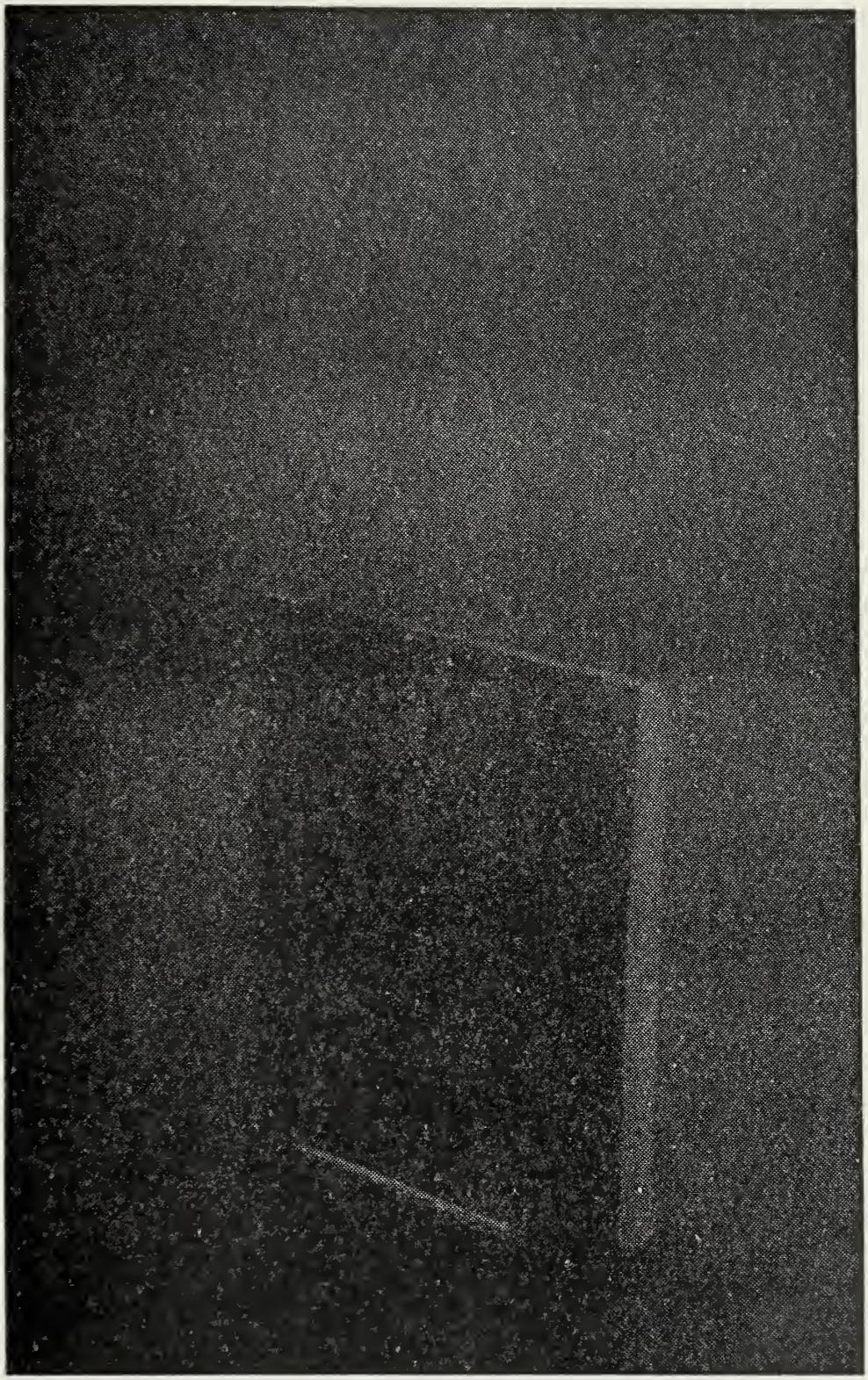

Figure 13 - CURRENT DISTRIBUTION DETERMINATION SET UP

E. ONE-HALF WAVELENGTH SQUARE ON GROUND PLANE

To illustrate the relationship between the Thermovision picture and the measured current distributions on a flat plate, several situations were viewed and displayed. Figure 14 shows the various incident angles of the plane electromagnetic wave on the one-half wavelength square.

To allow comparison between views, all Thermovision pictures were made with the camera normal to the surface of the model. Figure 16 has a marker superimposed on the Thermovision picture of the square with the normally incident signal to indicate the location of the temperature cross section in Figure 17. All temperature cross sections in this section were at the same relative locations as those shown in Figure 16.

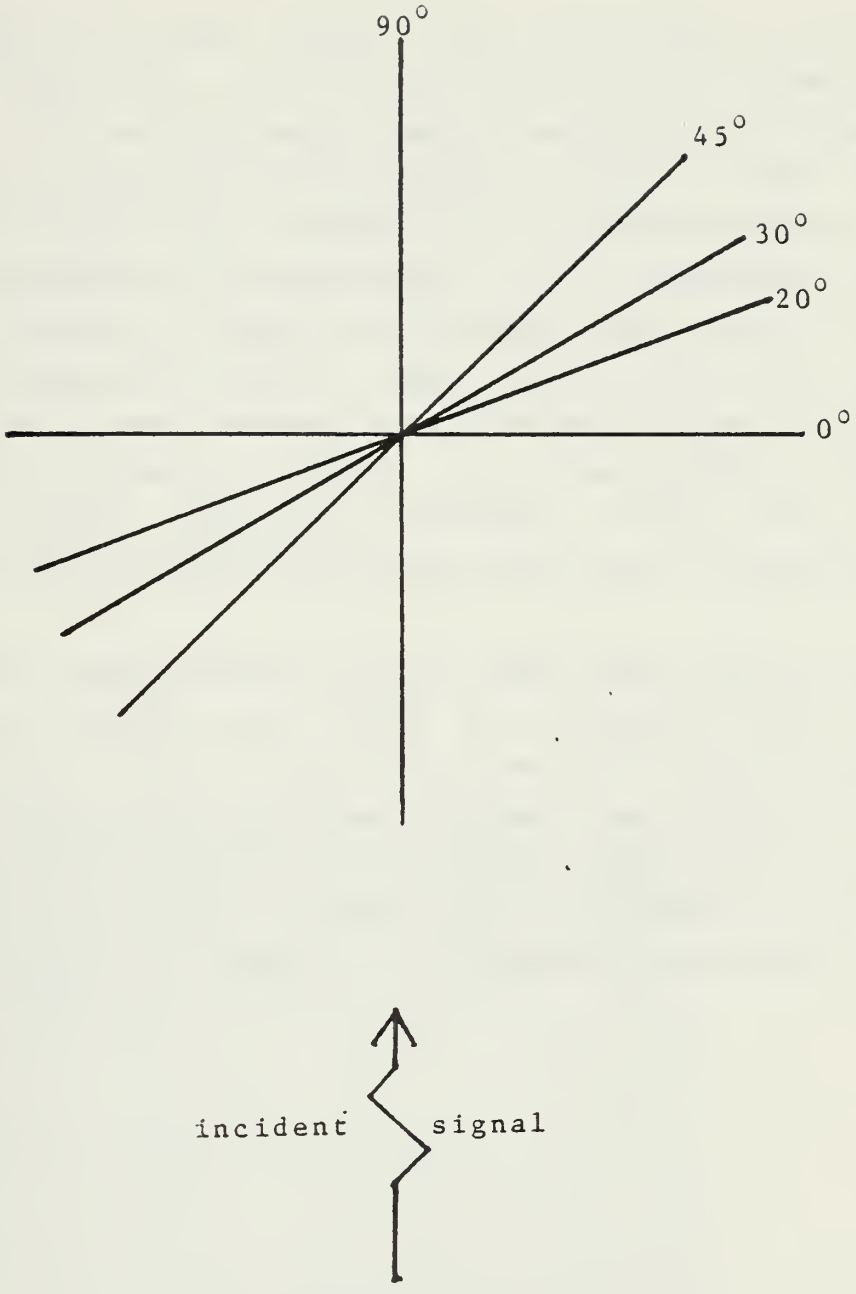

Figure 14 - ONE-HALF WAVELENGTH SQUARE ORIENTATICNS

1. Normal Incidence

When a flat surface is irradiated by a normally incident plane wave, the current distributions formed are a function of the resonant lengths seen by that signal. In general, the currents at the center of such a flat surface are less than the currents at the edges because of the mutual repulsion of the electrons. The magnitudes of the surface currents along the edges is a function of location along the resonant length seen by the incident signal. Intermediate areas between the center and the edges show the transition currents. Since, in rectangular objects, symmetry exists about the vertical center line of the surface, the currents seen on the two sides are identical.

The Thermovision picture shows these points clearly. Along each vertical edge, there is a "monocle-type" current distribution with the position dependent current magnitudes apparent. The current minimum along the vertical center line of the surface is also visible. Note that the current magnitudes in the lower center of the surface do not create enough localized heating to cause any detectable rise in temperature.

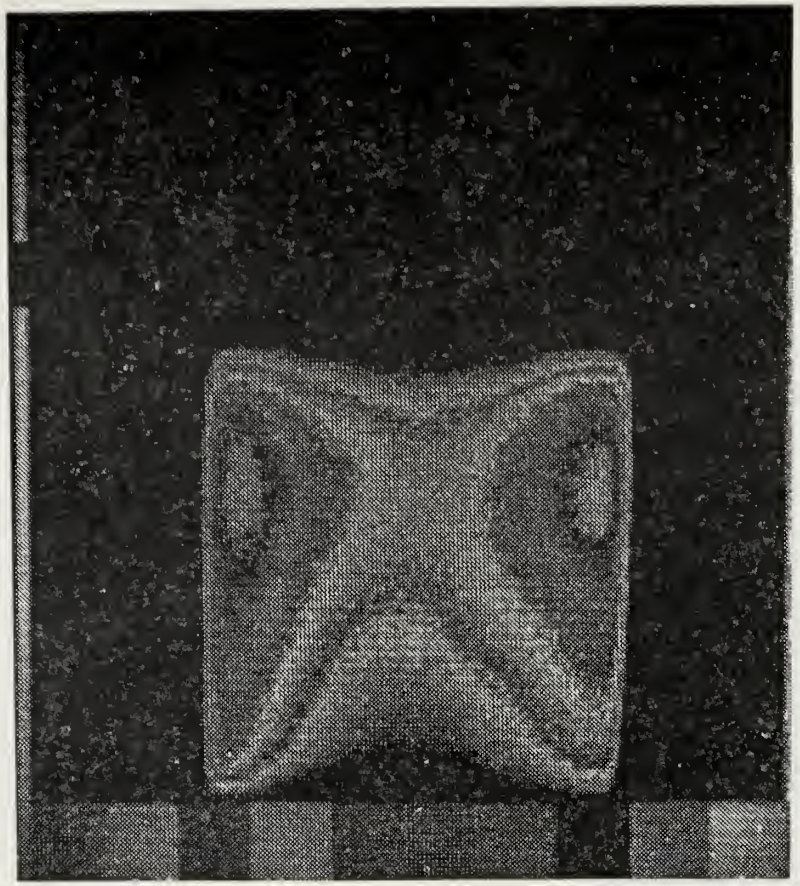

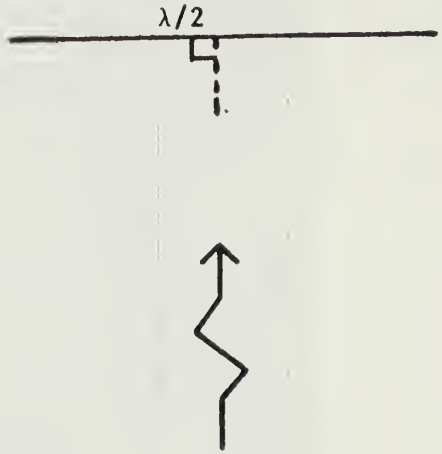

Figure 15 - ONE-HALF WAVELENGTH SQUARE CURRENT DISTRIBUTION, NORMAL INCIDENCE

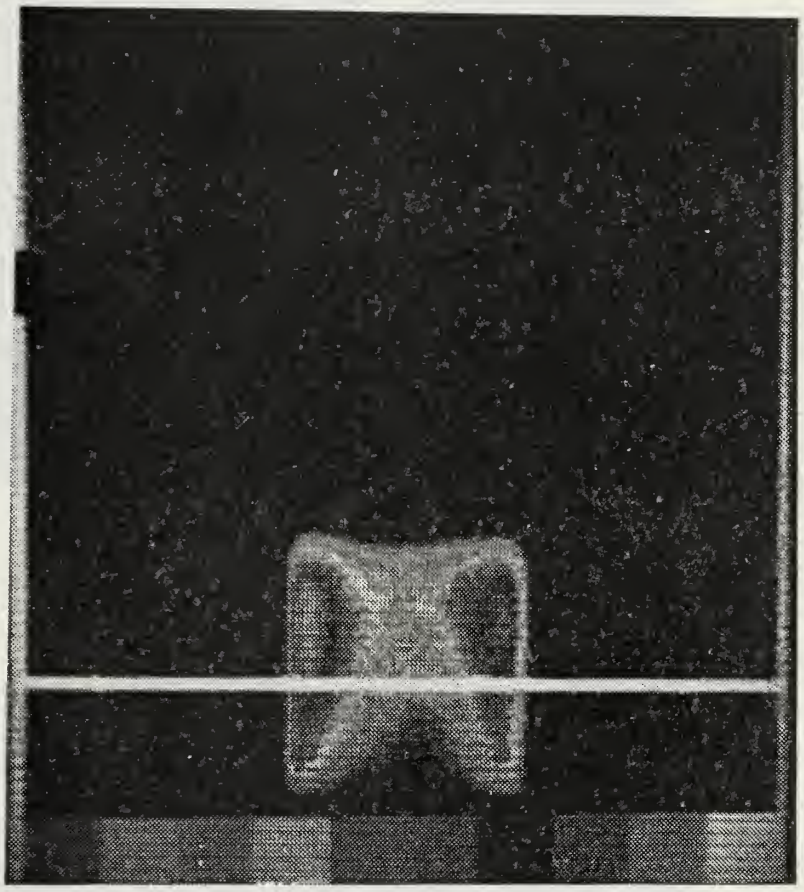

Figure 16 - ONE-HALF WAVELENGTH SQUARE CURRENT DISTRIBUTION, NORMAL INCIDENCE, WITH MARKER

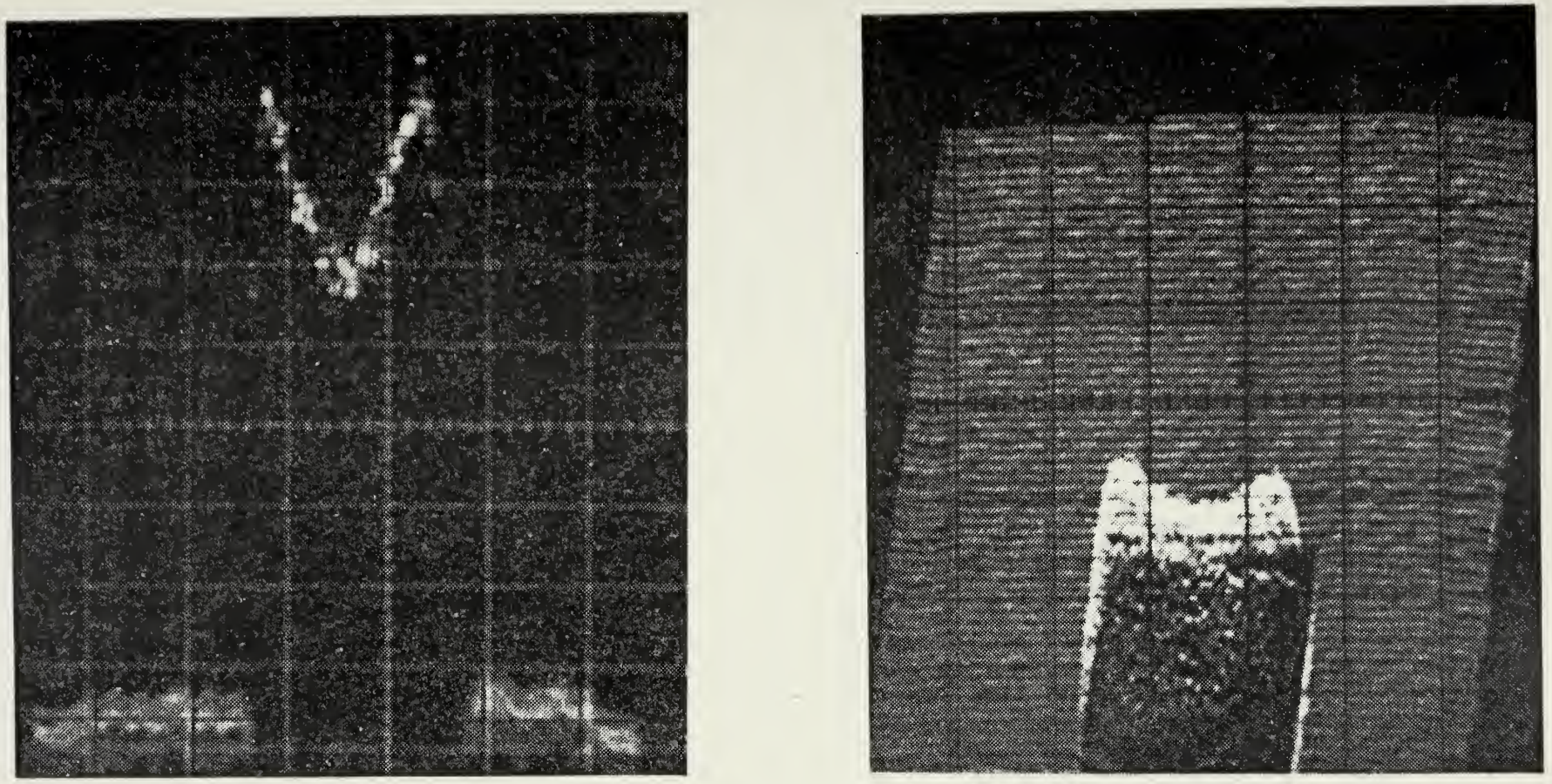

Figure 17 - ONE-HALF WAVELENGTH SQUARE, NORMAL INCIDENCE, TEMPERATURE CROSS SECTION AND RELIEF

2. Twenty-Degree Incidence

As the incident signal moves from the normal, the response of the leading edge is enhanced, and the trailing edge response is diminished. This reaction is apparent in Figures 18 and 19, which are the 20° incident views corresponding to the previous normally incident presentations. The relative magnitudes of the surface currents at the vertical edges can be seen in the temperature cross section in Figure 19. The current minimum towards the vertical center line of the surface remains, and the current increase at the trailing edge is still obvious.

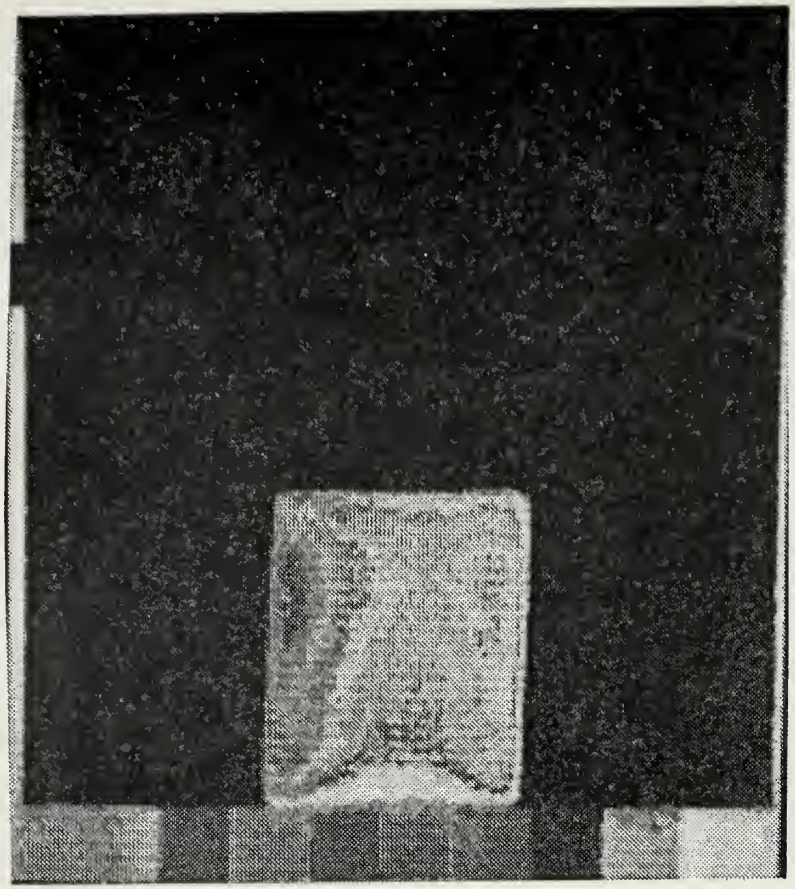

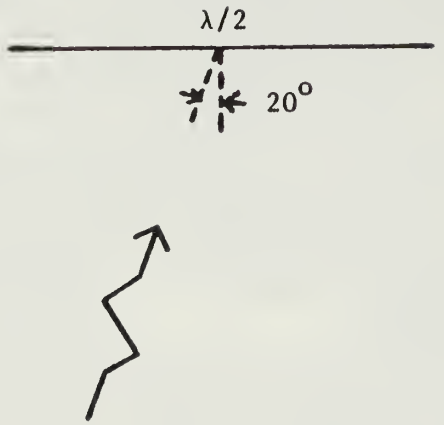

Figure 18 - ONE-HALF WAVELENGTH SQUARE CURRENT DISTRIBUTION, 20° INCIDENCE

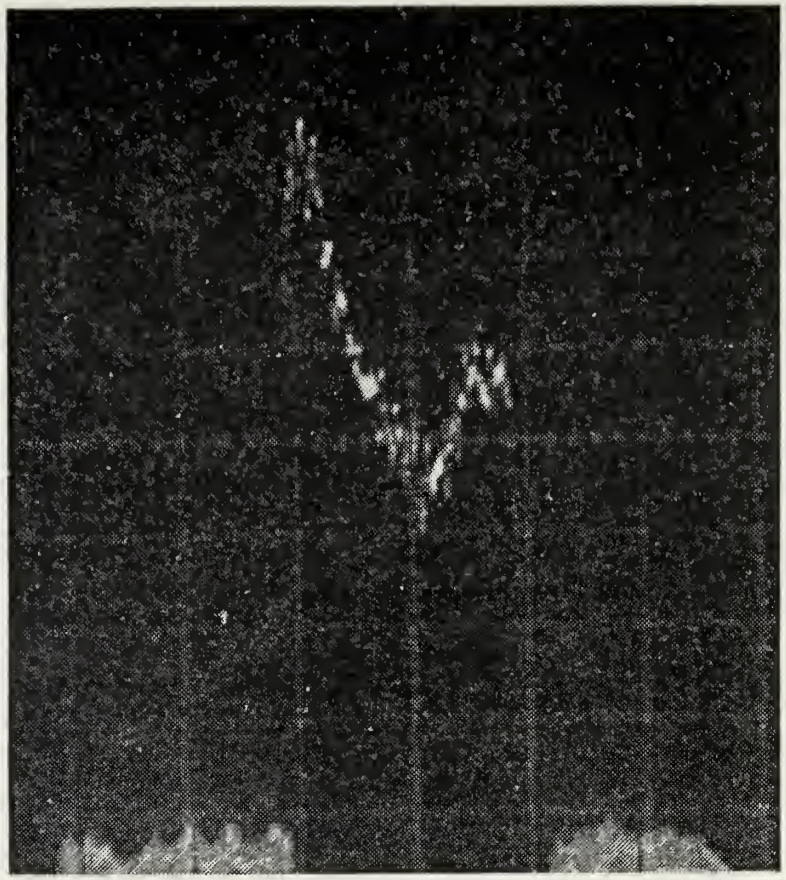

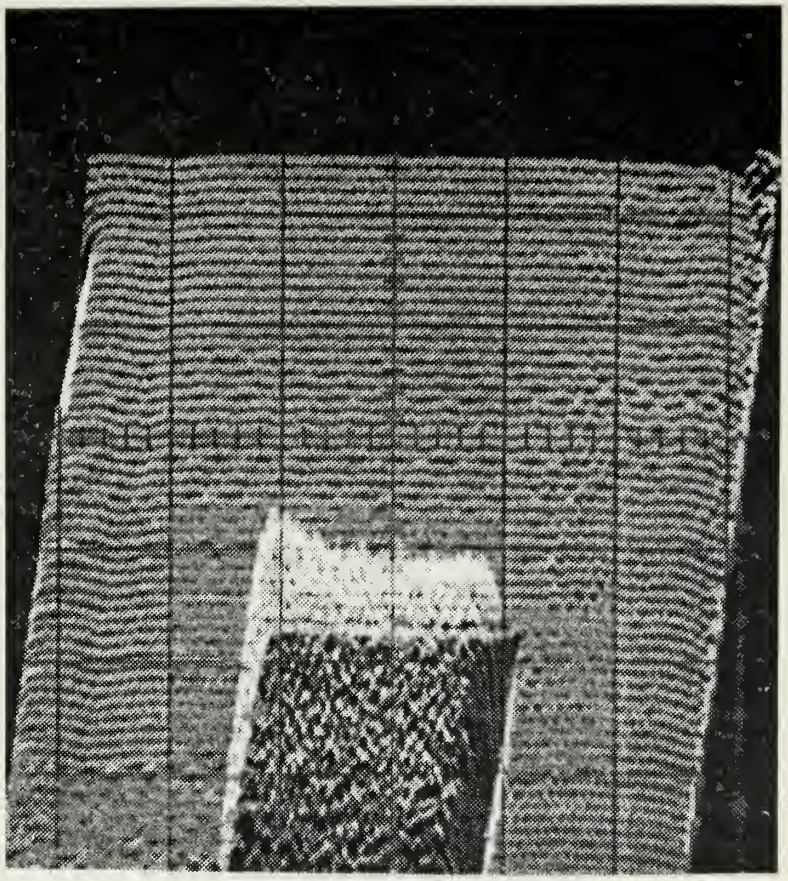

Figure 19 - ONE-HALF WAVELENGTH SQUARE, 20° INCIDENCE,
TEMPERATURE CROSS SECTION AND RELIEF

3. Thirty-Degree Incidence

The corresponding views for 30° incidence are shown in Figures 20 and 21. When the incident signal reaches 30° from the normal, the temperature difference between the current minimum location and the trailing edge in a horizontal cross section is barely detectable. The magnitude change from leading to trailing edge is now significantly greater than the 20° incidence case. However, the current magnitudes on the trailing edge are still sufficient to cause the apparent "monopole-type" current distribution.

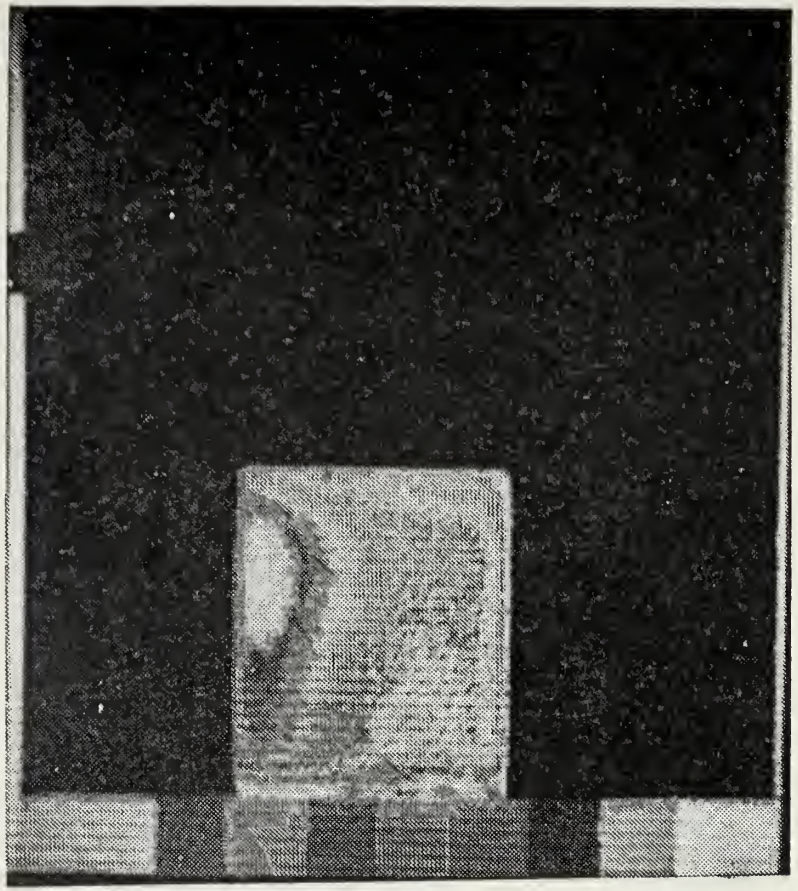

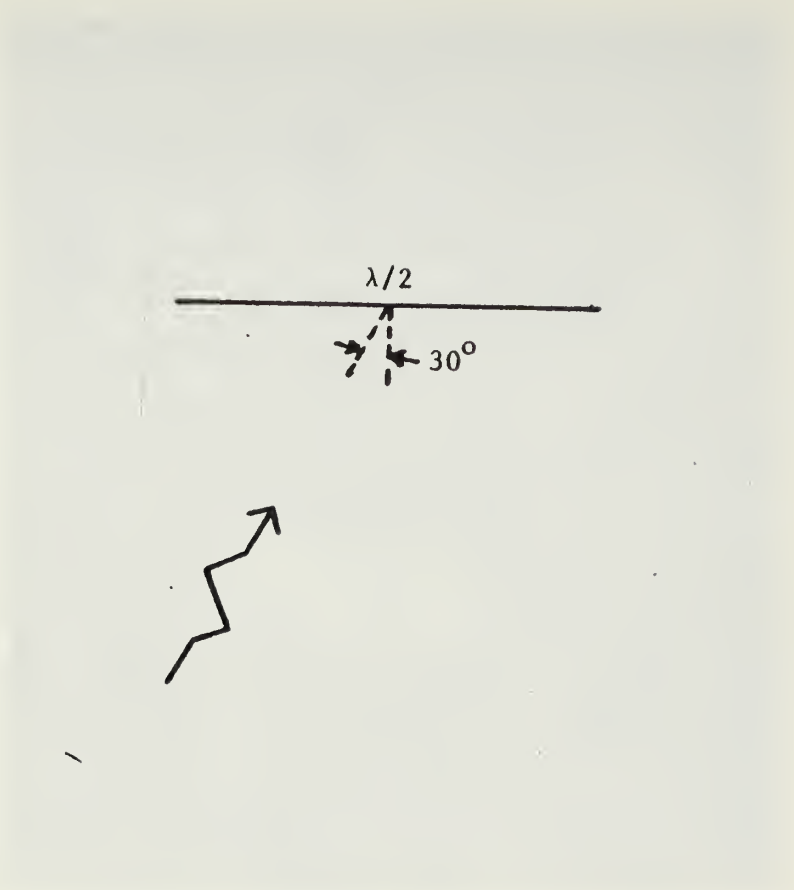

Figure 20 - ONE-HALF WAVELENGTH SQUARE CURRENT DISTRIBUTION, 30° INCIDENCE

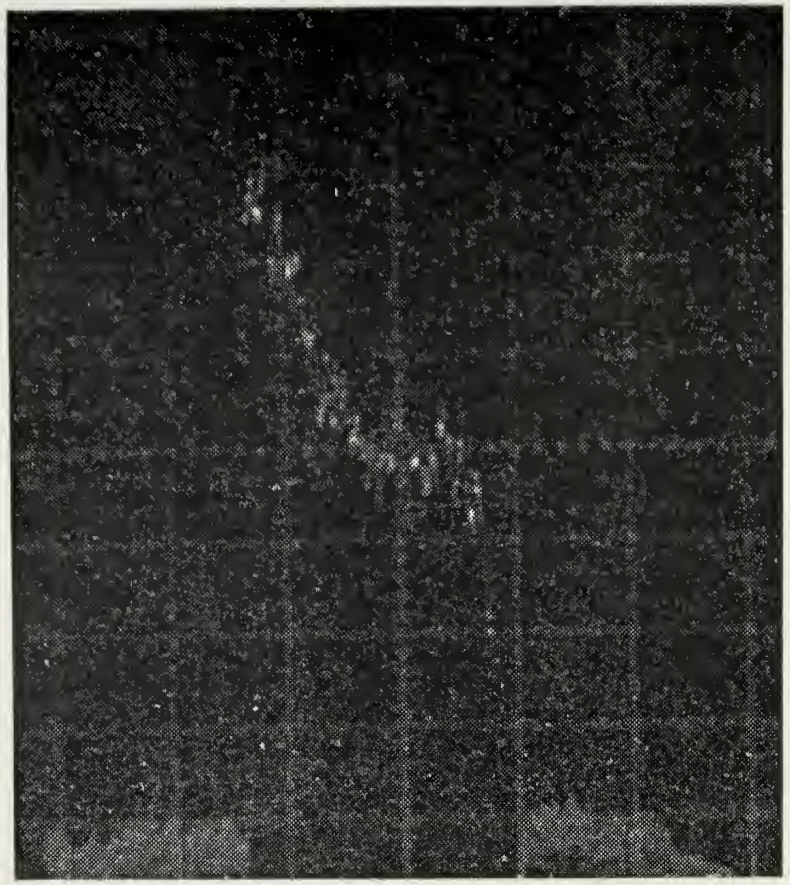

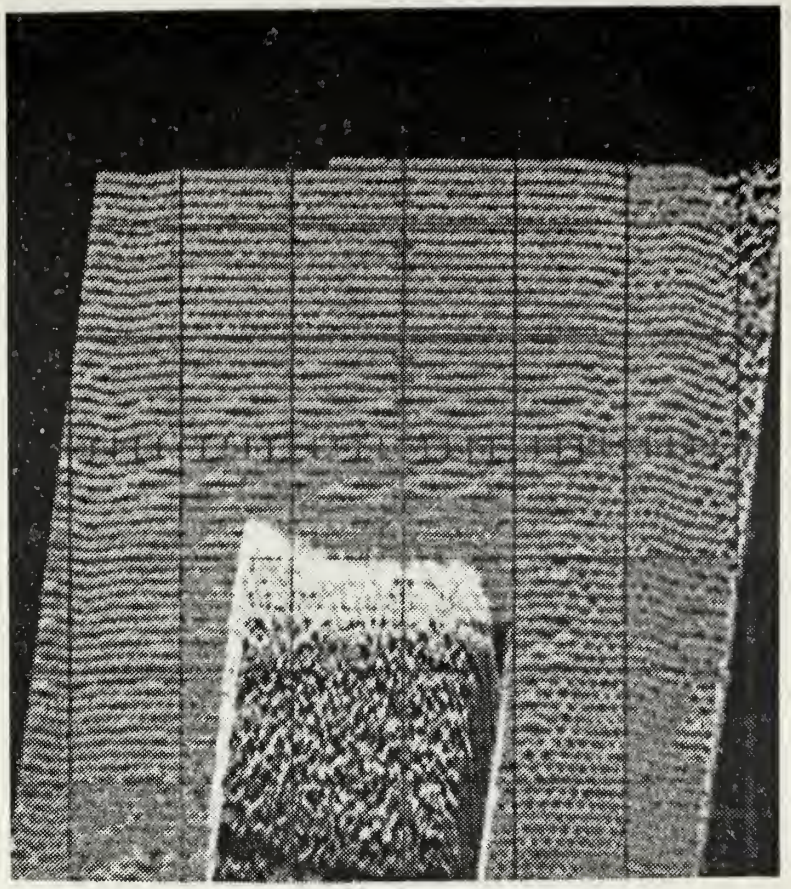

Figure 21 - ONE-HALF WAVELENGTH SQUARE, 30° INCIDENCE,
TEMPERATURE CROSS SECTION AND RELIEF

4. Forty-Five Degree Incidence

When the incident plane wave is 45° from the normal (Figures 22 and 23), the leading edge response is still greater than the previous cases, and the current on the trailing edge is barely larger than the more interior locations. Note that the locations of the current minima in this sequence have moved farther toward the trailing edge with an increase in incidence angle, and there is no longer the visible "monopole-type" current distribution at the trailing edge.

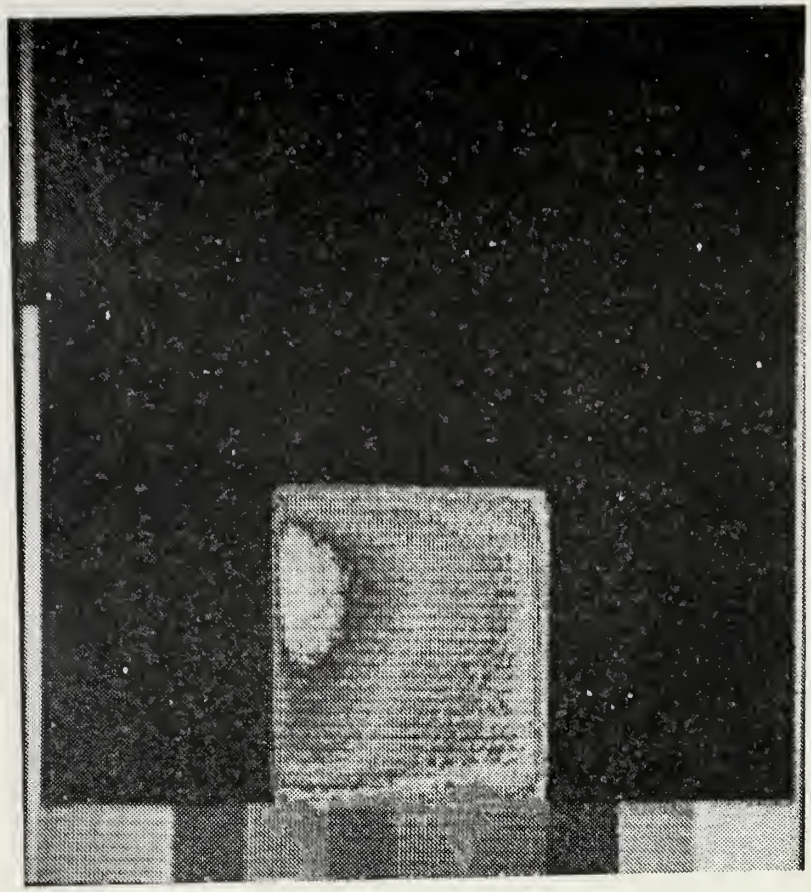

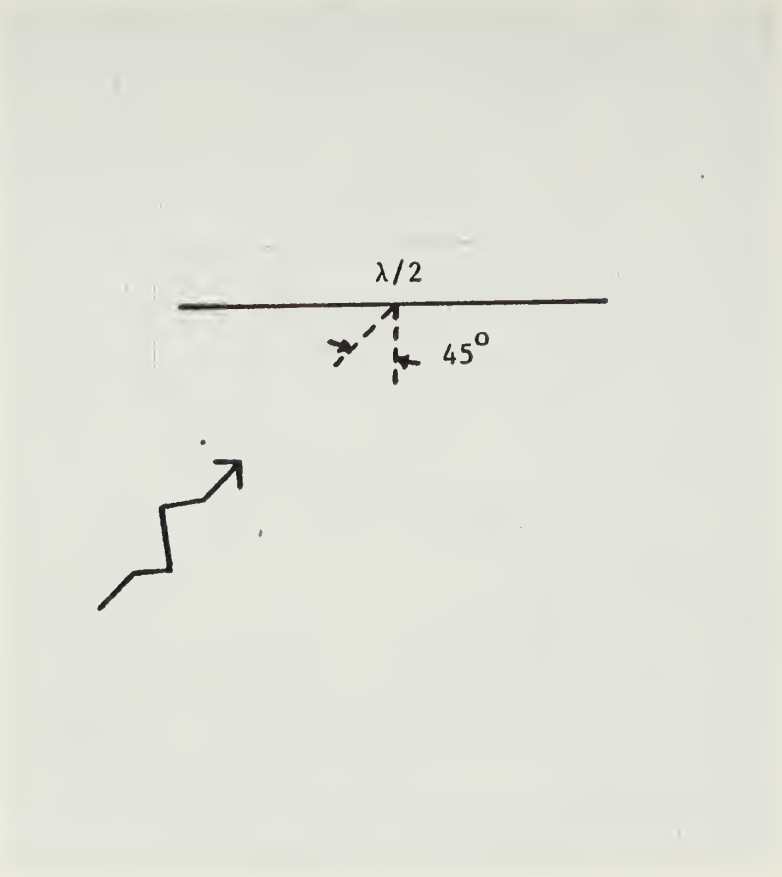

Figure 22 - ONE-HALF WAVELENGTH SQUARE CURRENT DISTRIBUTION, 45° INCIDENCE

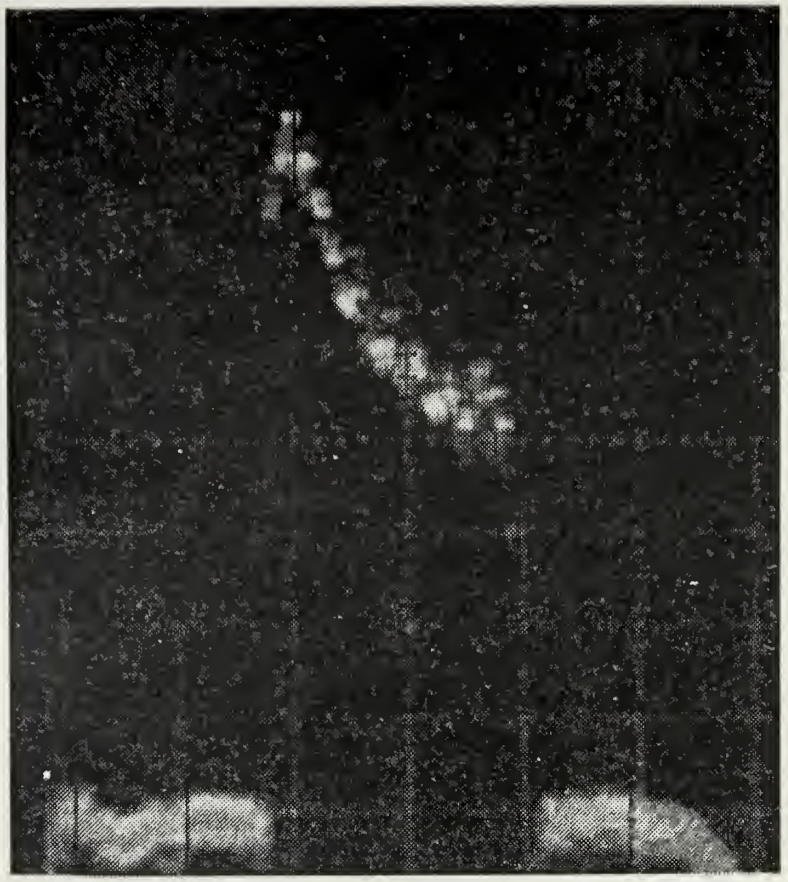

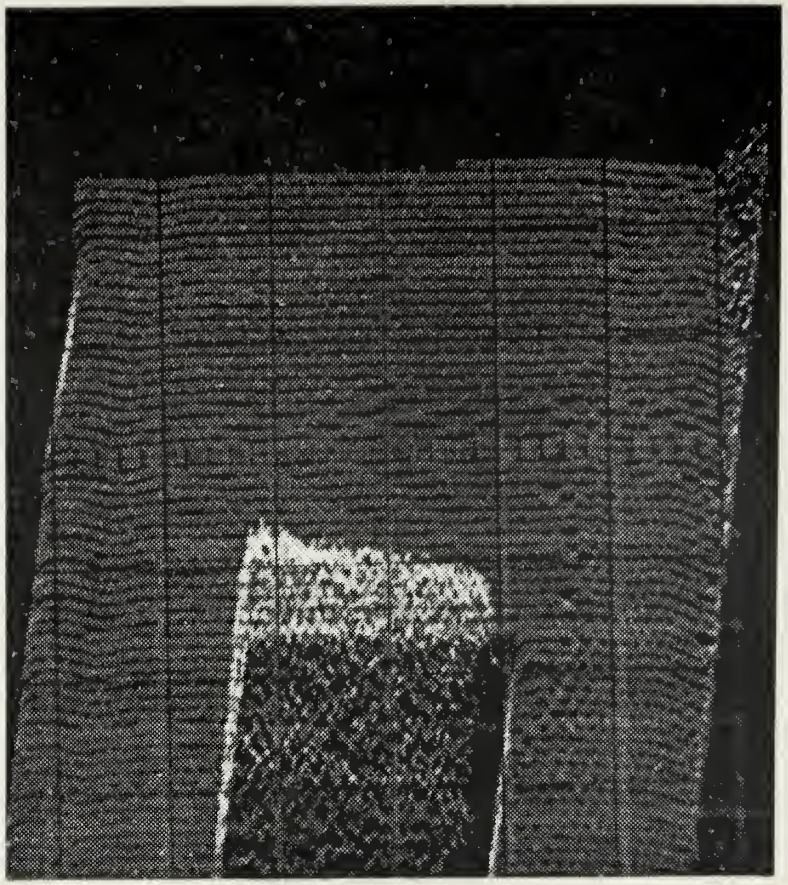

Figure 23 - ONE-HALF WAVELENGTH SQUARE, 45° INCIDENCE,
TEMPERATURE CROSS SECTION AND RELIEF

5. Ninety-Degree Incidence

When the incident signal is 90° from the normal (Figures 24 and 25), only the leading edge is being "driven," and the remainder of the surface is shadowed from the incident signal. Thus, the current magnitude is monotonically decreasing across the surface. The relative current magnitudes along the leading edge of the surface for this entire sequence remain constant, with the peak values of current occuring approximately three-quarters of the distance from the ground plane.

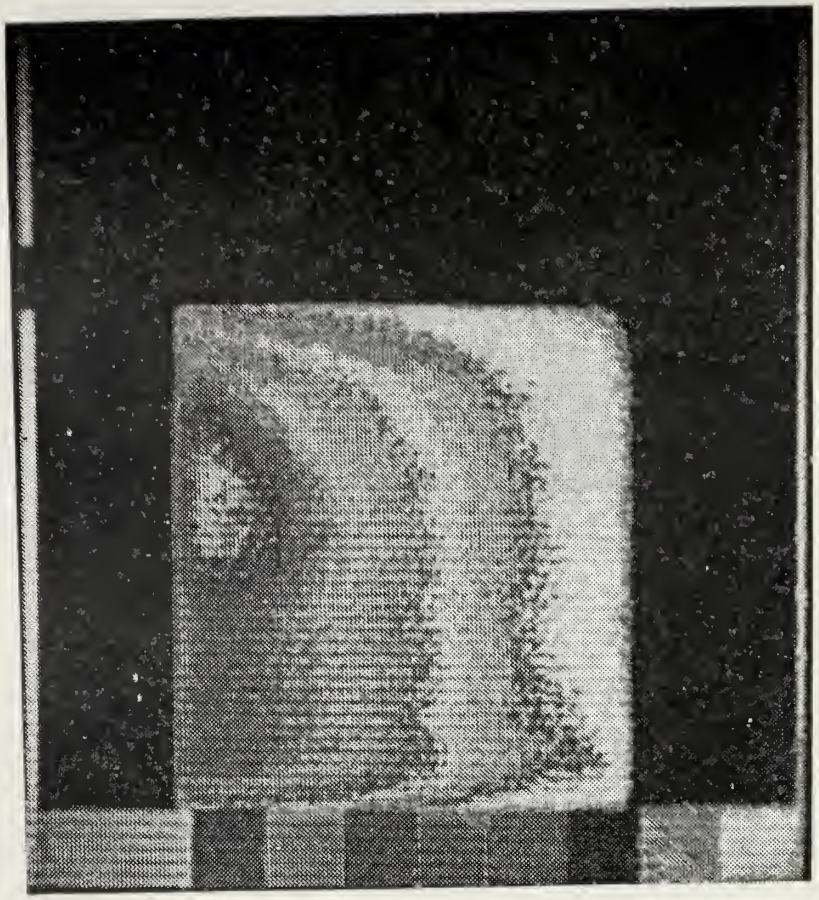

Figure 24 - ONE-HALF WAVELENGTH SQUARE CURRENT DISTRIBUTION, 90° INCIDENCE

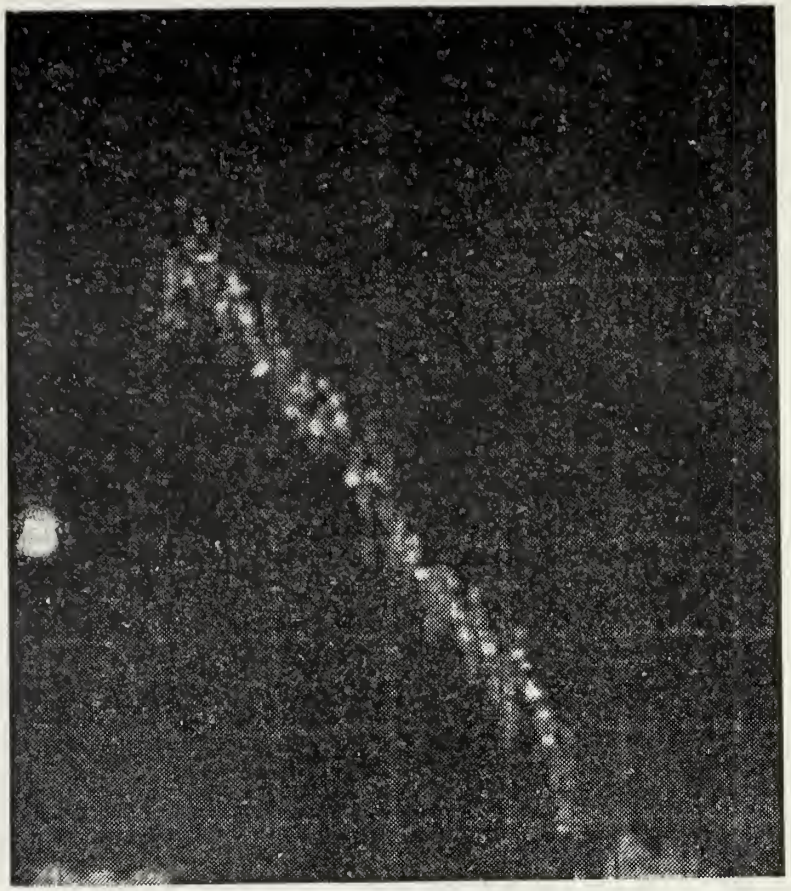

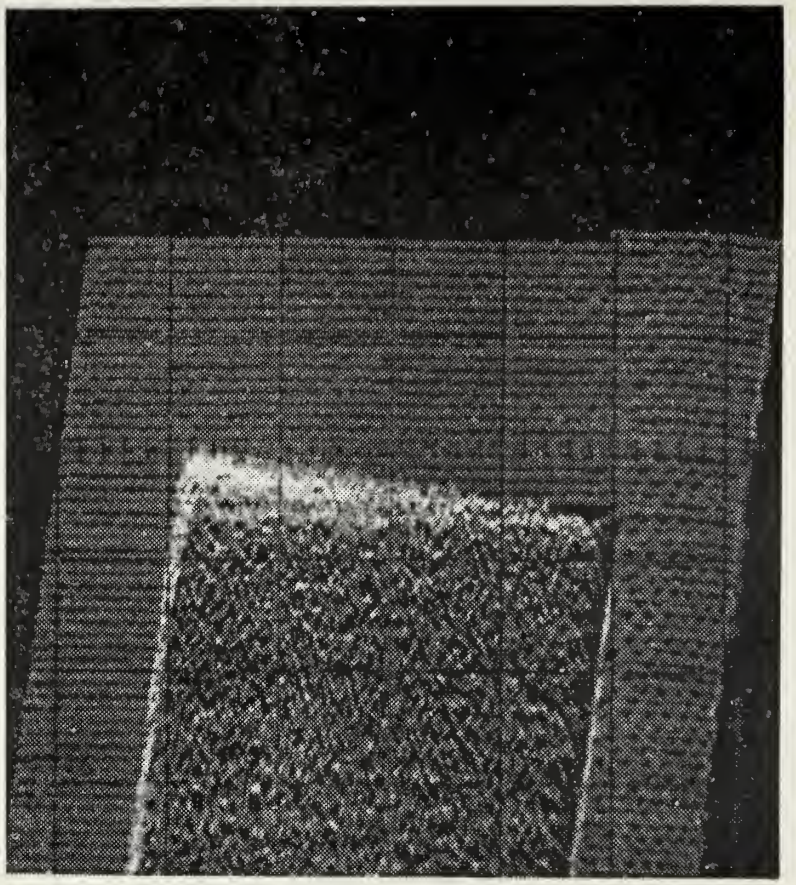

Figure 25 - ONE-HALF WAVELENGTH SQUARE, 90° INCIDENCE, TEMPERATURE CROSS SECTION AND RELIEF

C. THREE-QUARTER BY ONE-HALF WAVELENGTH FLAT PLATE ON GROUND PLANE

When the height of the vertical edge of the flat plate was increased to three-quarters of a wavelength (24 centimeters), the resonant length seen by the incident signal changed proportionally. This change caused a variation in the distribution along the edges of the surface, but the same general current arrangement occurs across the surface. All Thermovision pictures were again taken normal to the surface of the plate. For brevity, the temperature cross section and relief views of each situation were not included. No unexpected results were obtained in either of these views.

1. Normal Incidence

The normally incident plane wave again yields a current distribution that is symmetrical with respect to the vertical center line of the surface (Figure 26). The change in resonant length seen by the incident signal is apparent in the Thermovision picture with a local maximum occuring toward the top and the bottom of each vertical edge. The minimum current locations were again at the center of the plate, with the "monopole-type" current distribution at the edges.

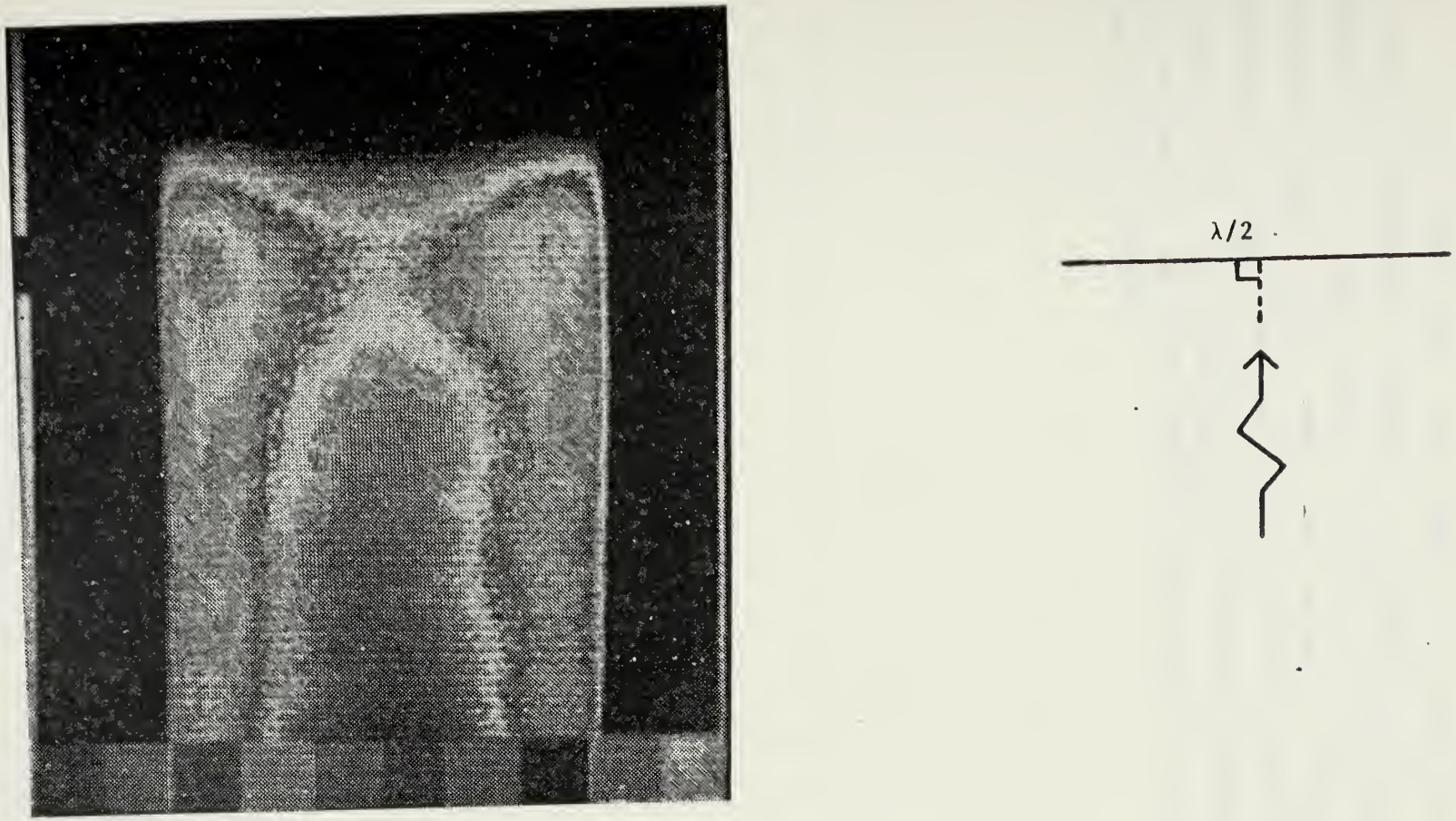

Figure 26 - THREE-QUARTER BY ONE-HALF WAVELENGTH FLAT PLATE CURRENT DISTRIBUTION, NORMAL INCIDENCE

2. Ten-Degree Incidence

The 10° view was added for the three-quarter by one-half wavelength plate to exhibit more clearly the transition of the surface current distributions as the incident signal moves off the normal (Figure 27). As expected, a small increase in the leading edge response and a decrease in the trailing edge response occurred. Plainly, the horizontal minimum remains very near the vertical center line of the surface.

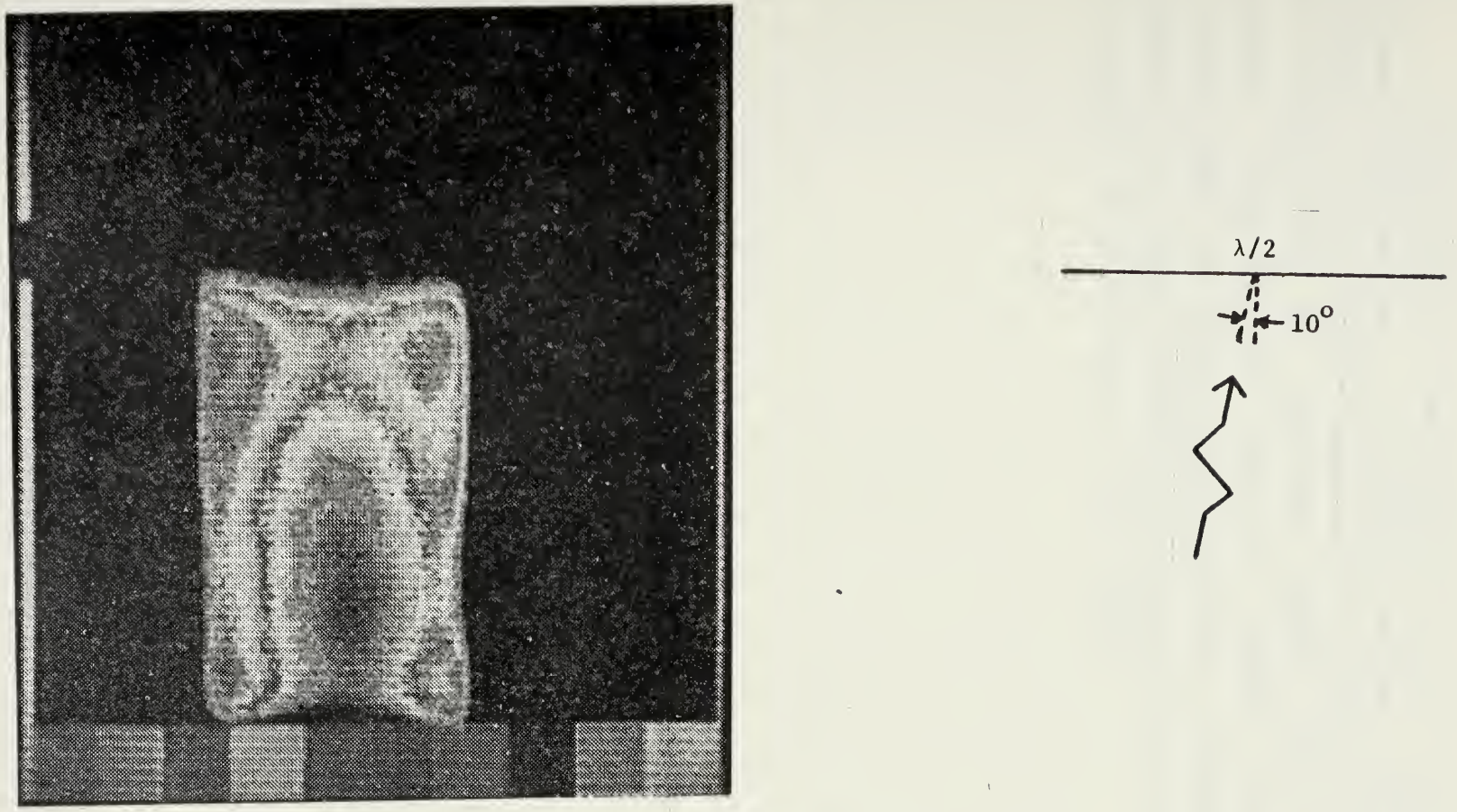

Figure 27 - THREE-QUARTER BY ONE-HALF WAVELENGTH FLAT PLATE CURRENT DISTRIBUTION, 10° INCIDENCE

3. Twenty-Degree Incidence

Figure 28 is a continuation of the transition of the current distribution. A visible current minimum remains slightly on the trailing side of the vertical center line of the surface, and the enhanced leading edge response is obvious. The minimum value of surface current on the trailing edge has become so low that the localized heating causes very little temperature rise from the minimum in the horizontal cross section at that heigth.

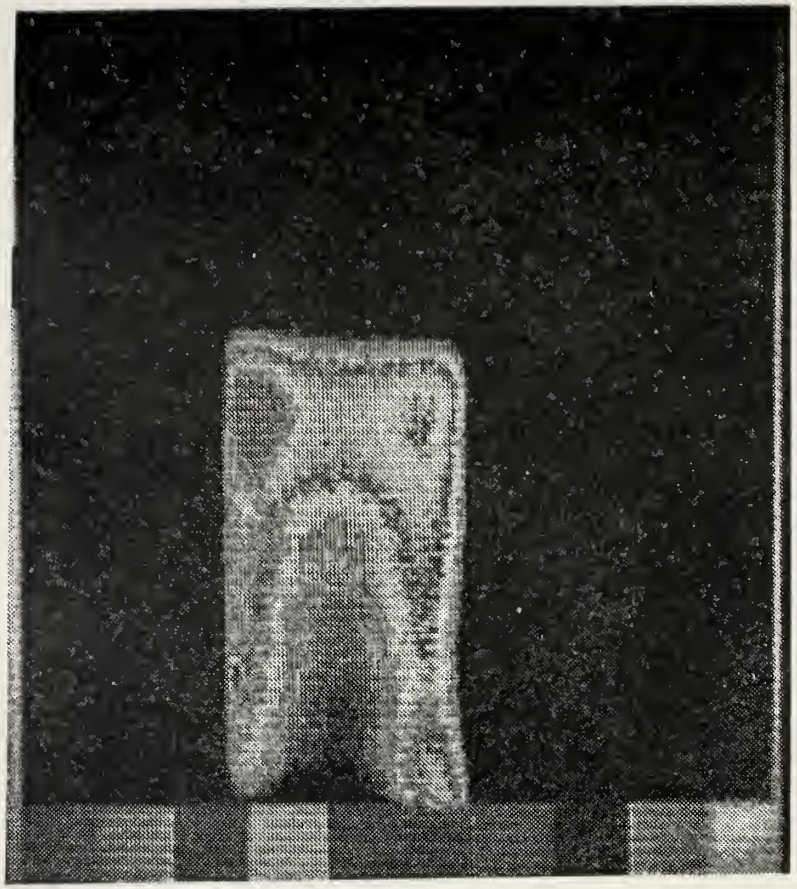

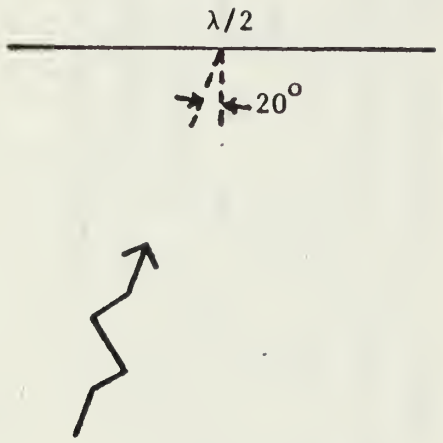

Figure 28 - THREE-QUARTER BY ONE-HALF WAVELENGTH FLAT PLATE CURRENT DISTRIBUTION, 20° INCIDENCE

4. Thirty-Degree Incidence

Several noticeable changes are evident when the incidence angle reaches 30° (Figure 29). Although two local maxima remain on the leading edge, the current levels on the trailing edge are so small that there exists only one obvious maximum on the trailing edge. Additionally, the minimum current magnitude in a horizontal cross section has moved to approximately two-thirds of the width from the leading edge of the surface.

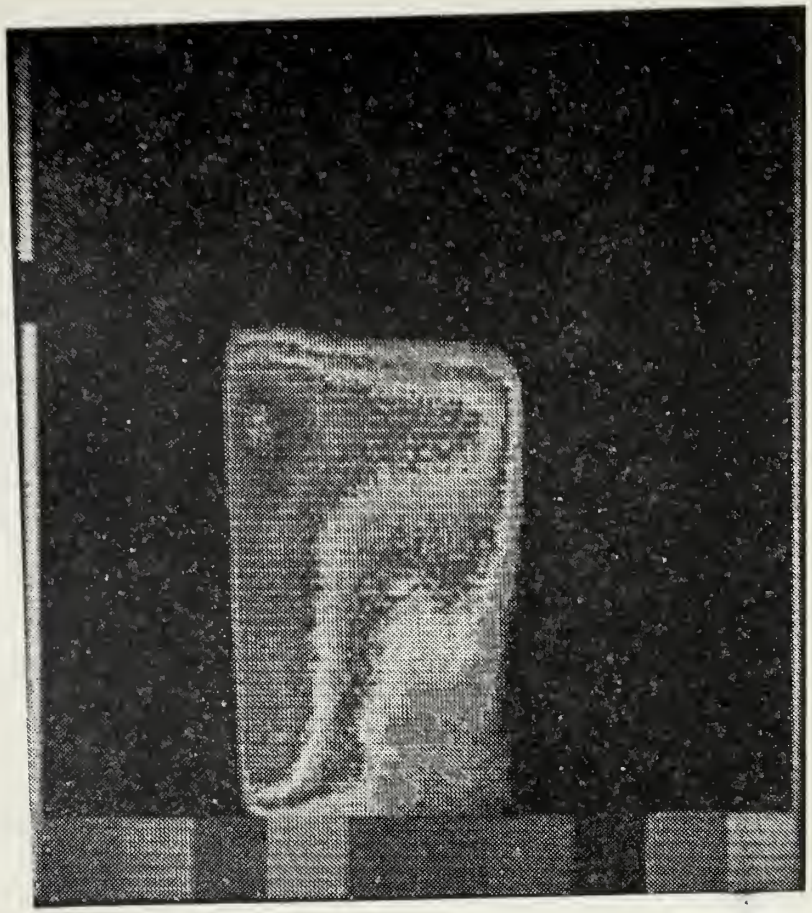

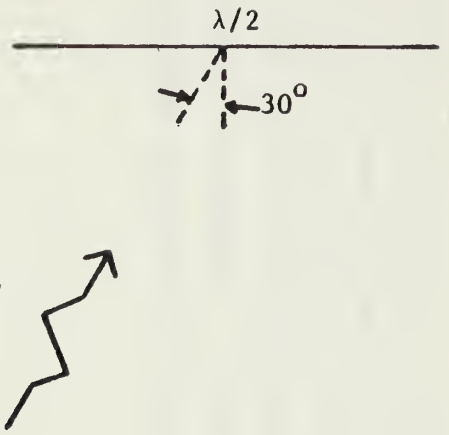

Figure 29 - THREE-QUARTER BY ONE-HALF WAVELENGTH FLAT PLATE CURRENT DISTRIBUTION, 30° INCIDENCE

5. Forty-Five Degree Incidence

Figure 30 indicates the current distribution on the surface with an incident signal 45° from the normal. When the signal is this far from the normal, the "monopole-type" current formation on the trailing edge is absent and the horizontal current minimum is nearly at that edge. The distinctive current formations on the leading edge remain evident.

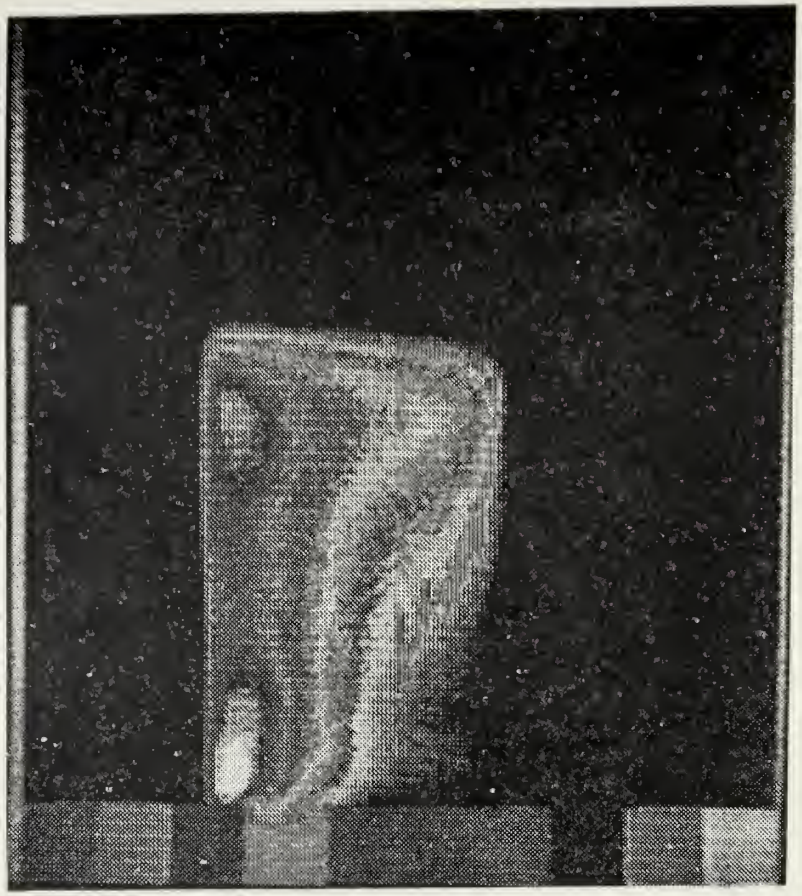

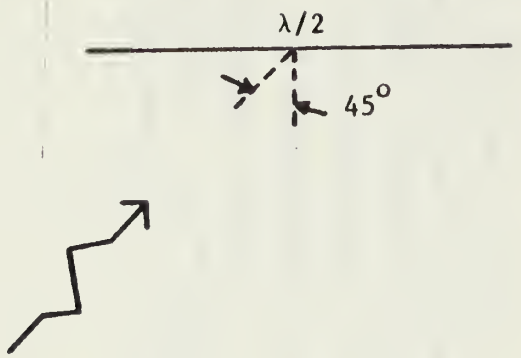

Figure 30 - THREE-QUARTER BY ONE-HALF WAVELENGTH FLAT PLATE CURRENT DISTRIBUTION, 45° INCIDENCE

6. Ninety-Degree Incidence

At 90° incidence (Figure 31), the leading edge is again the only "driven" portion of the surface. Thus, the current magnitudes decrease horizontally across the surface until they are insufficient to cause detectable heating of the surface. The insufficient heating causes the inability of the Thermovision picture to clearly define the trailing edge of the surface. The "monopole" current distribution on the leading edge remains as in the previous presentations.

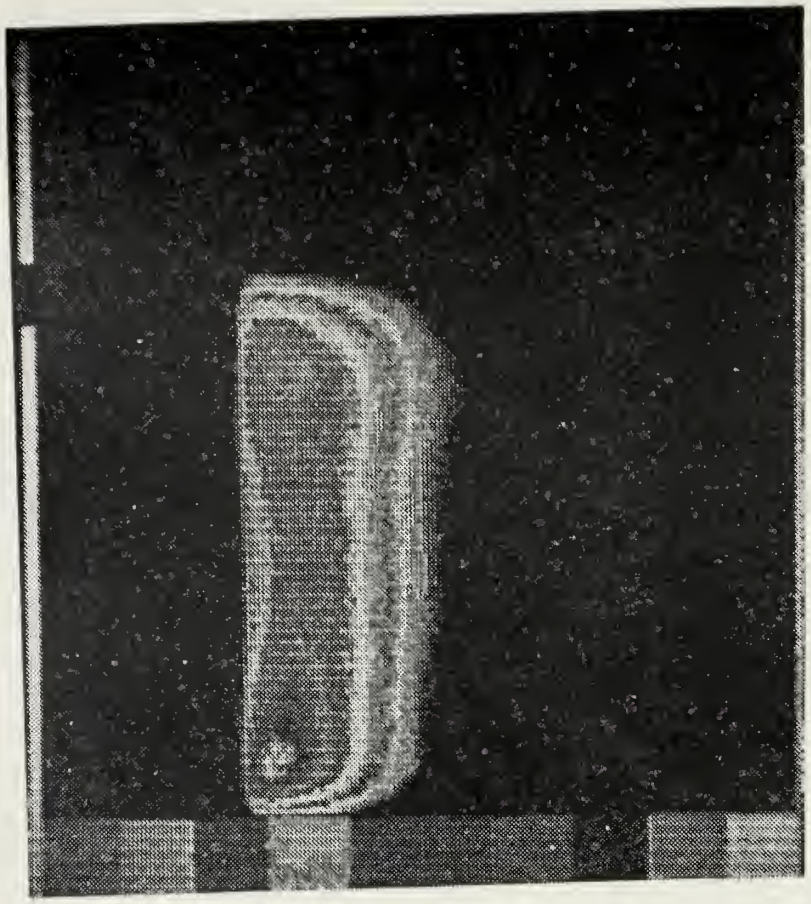

Figure 31 - THREE-QUARTER BY ONE-HALF WAVELENGTH FLAT PLATE CURRENT DISTRIBUTION, 90° INCIDENCE

D. ONE BY ONE-HALF WAVELENGTH FLAT PLATE ON GROUND PLANE

An increase to one wavelength in the height of the flat surface again causes an increase in the resonant length seen by the incident signal. A significant redistribution of the current magnitudes on the surface results.

For comparison, Thermovision pictures of the same incident angles as previously studied were taken, yielding the same type of transitions (Figures 32 through 37). All pictures were again taken normal to the surface under study.

1. Normal Incidence

With normal incidence (Figure 32), the symmetrical current distributions are again apparent. With the increase in the height of the surface, the two local maxima at each vertical edge have changed locations along the edge. This caused the appearance of a distinct oval current minimum in the center of the surface. The minimum for any horizontal cross section of the plate remains in the center, and the maximum at the edges.

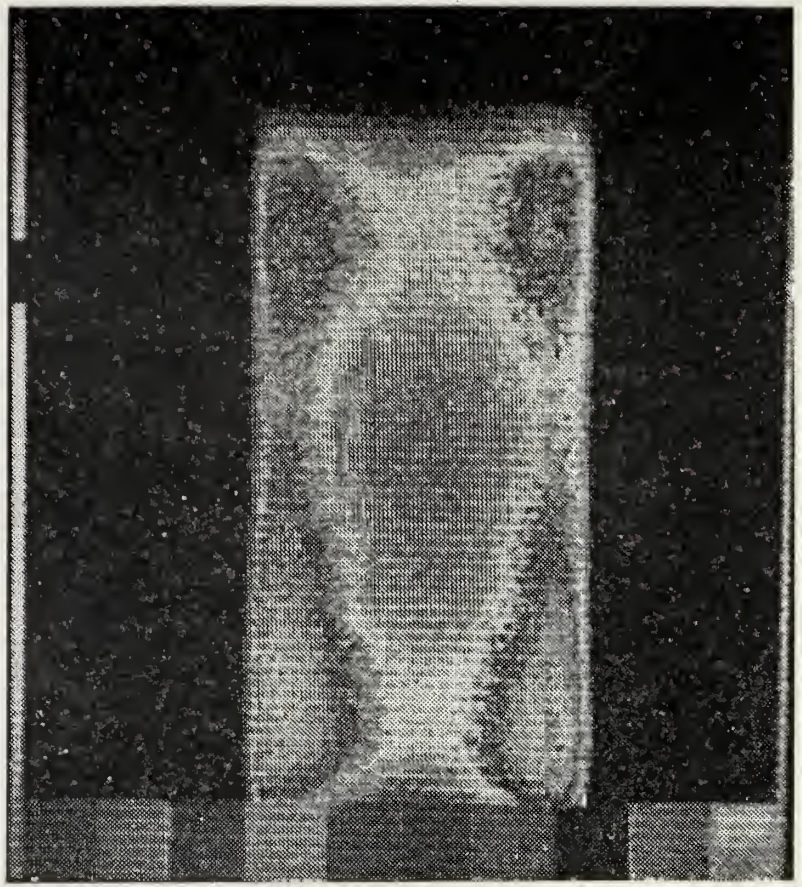

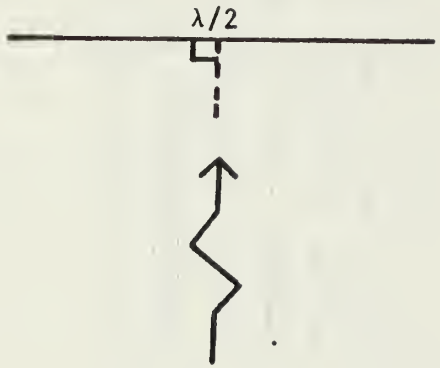

Figure 32 - ONE BY ONE-HALF WAVELENGTH FLAT PLATE CURRENT DISTRIBUTION, NORMAL INCIDENCE

2. Ten-Degree Incidence

With a 10° incident plane wave (Figure 33), the expected shift toward the leading edge occurred. Again, the two distinct localized maxima remain apparent at the trailing edge of the surface, and the enhancement of the leading edge currents is visible. A change in the bias setting of the Thermovision camera makes the oval shaped minimum toward the center more obvious than in the previous picture.

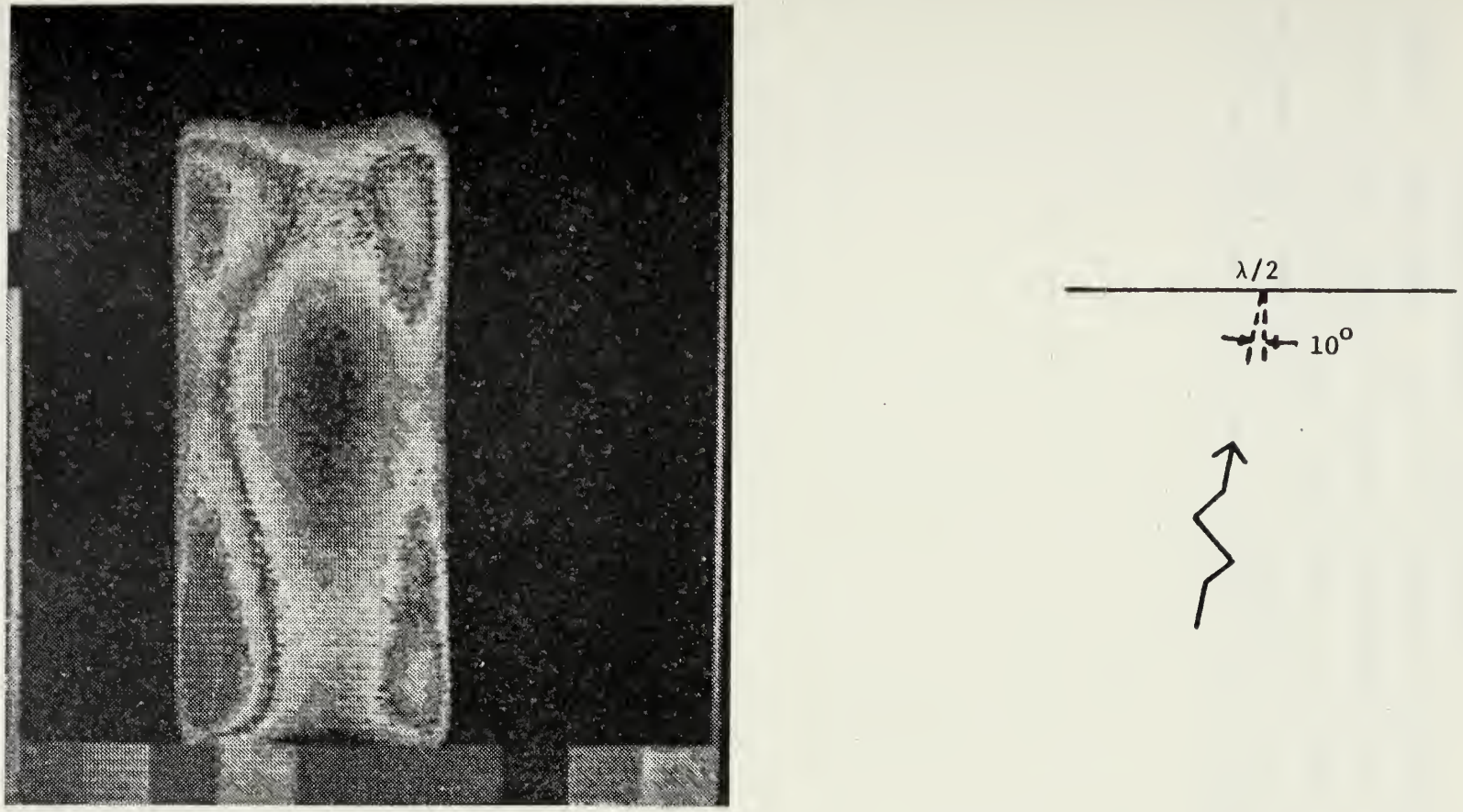

Figure 33 - ONE BY ONE-HALF WAVELENGTH FLAT PLATE CURRENT DISTRIBUTION, 10° INCIDENCE

3. Twenty-Degree Incidence

In this surface, the currents at a 20° incidence remain consistent with the previous examples (Figure 34). The two local maximum current locations are still evident, but are significantly diminished. The oval shaped current minimum also remains in the interior of the plate, but it also has shifted noticeably toward the trailing edge.

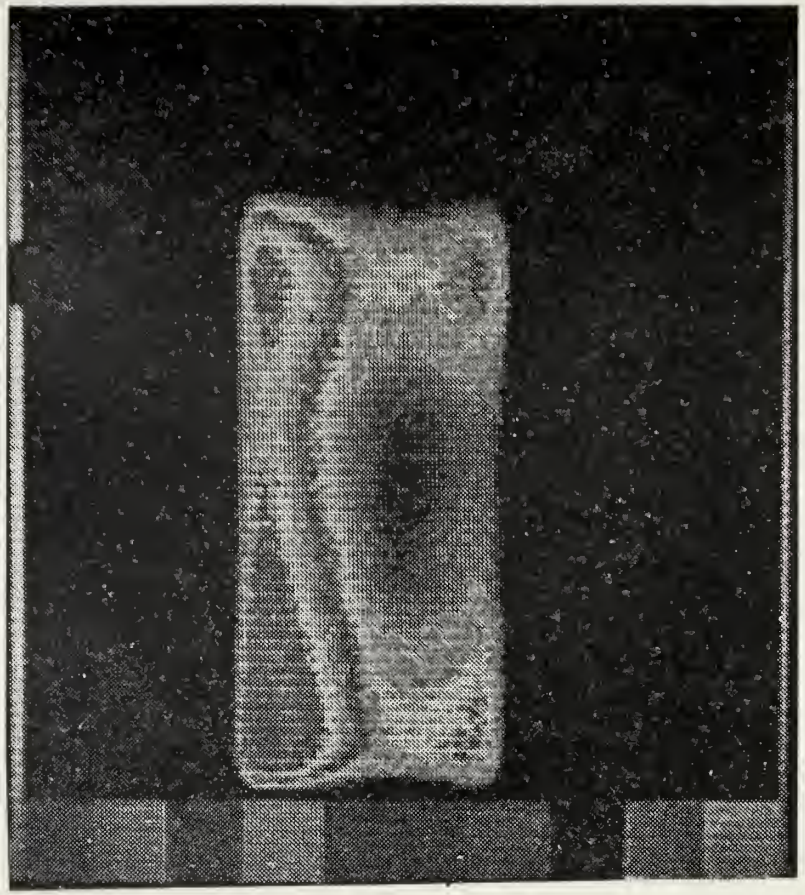

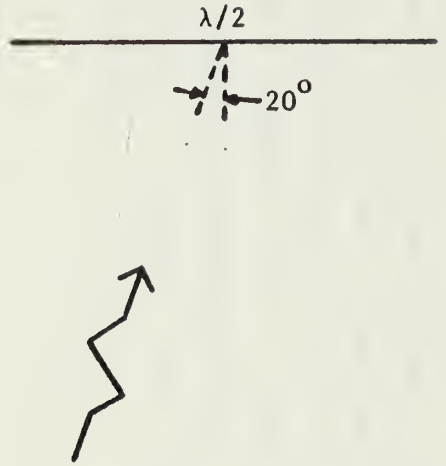

Figure 34 - ONE BY ONE-HALF WAVELENGTH FLAT PLATE CURRENT DISTRIBUTION, 20° INCIDENCE

4. Thirty-Degree Incidence

For the 30° incident signal, the changes in surface currents are as expected from the previous cases (Figure 35). The lessened response of the trailing edge and the shifted current minimum in a horizontal cross section remains. The localized heating on the trailing edge is now barely sufficient to cause the "monopole-type" current distribution profile.

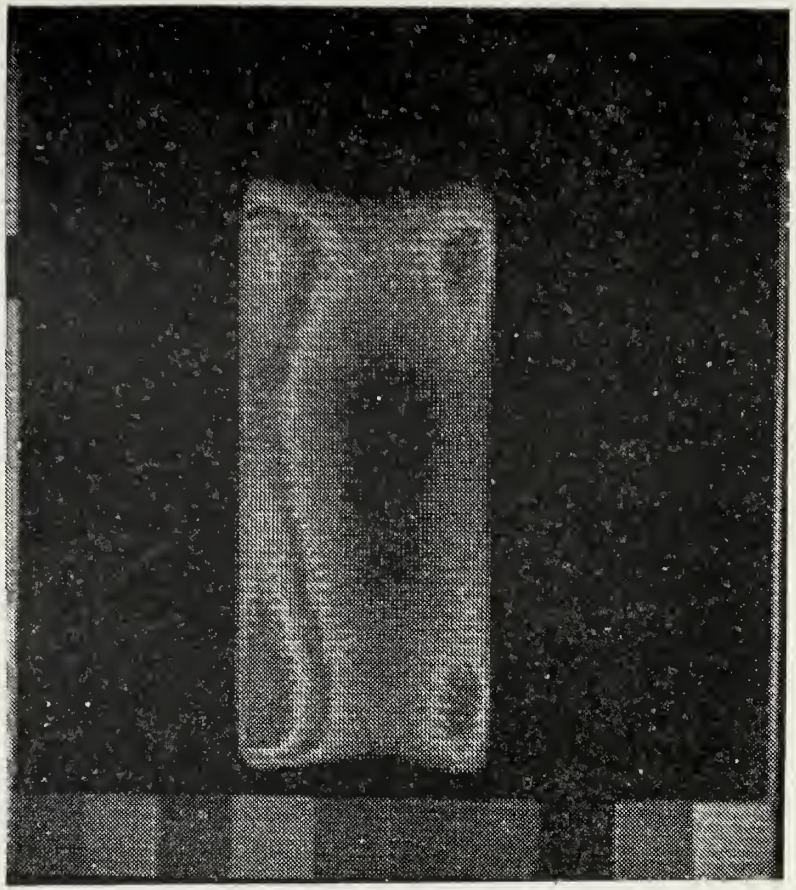

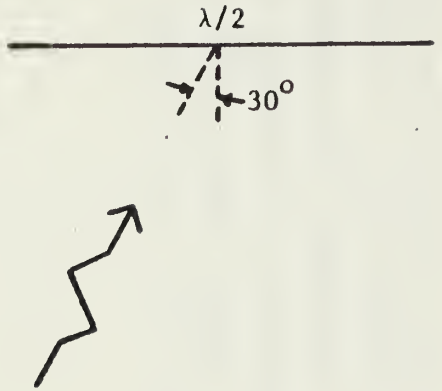

Figure 35 - ONE BY ONE-HALF WAVELENGTH FLAT PLATE CURRENT DISTRIBUTION, 30° INCIDENCE

5. Forty-Five Degree Incidence

For the 45° incident signal (Figure 36), the greatly diminished response of the trailing edge does not cause an obvious "monopole-type" response, and the significant shift of the current minimum in a horizontal cross section toward the trailing edge again occurs. The similarity among the 45° incident cases for all these surfaces is apparent.

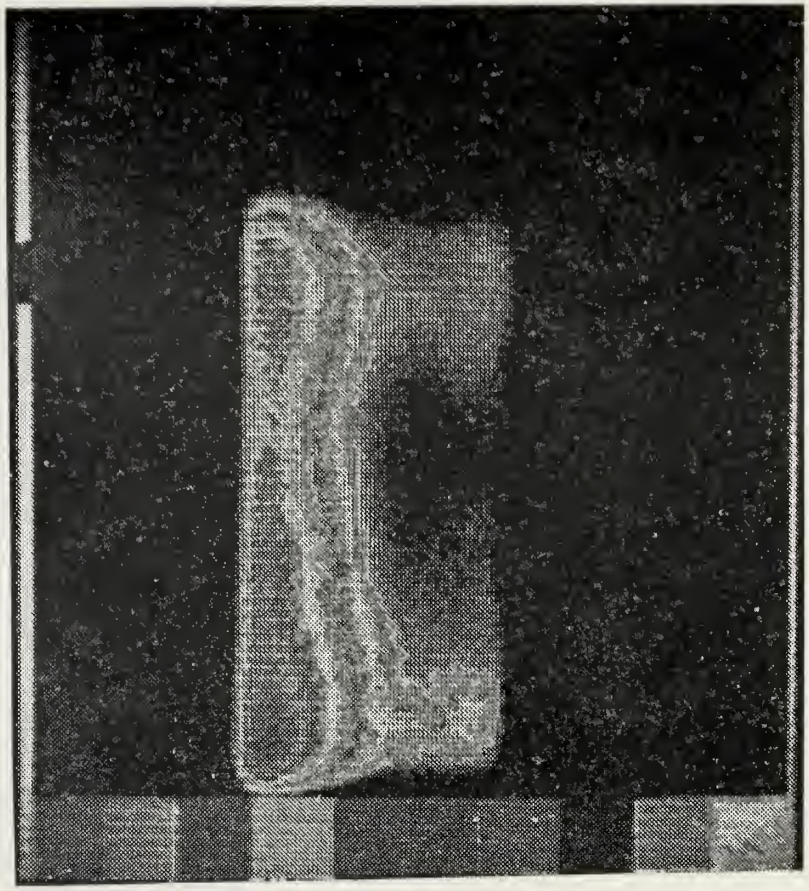

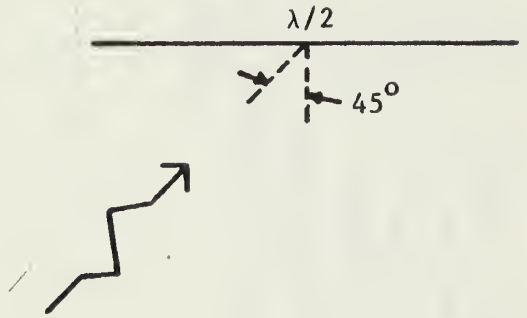

Figure 36 - ONE BY ONE-HALF WAVELENGTH FLAT PLATE CURRENT DISTRIBUTION, 45° INCIDENCE

6. Ninety-Degree Incidence

When the surface normal is 90° from the incident plane wave (Figure 37), the reaction again shows the result of only the leading edge being "driven." The horizontal cross section again exhibits a monotonically decreasing surface current, and insufficient currents exist to create enough localized heating to allow detection of the trailing edge of the surface.

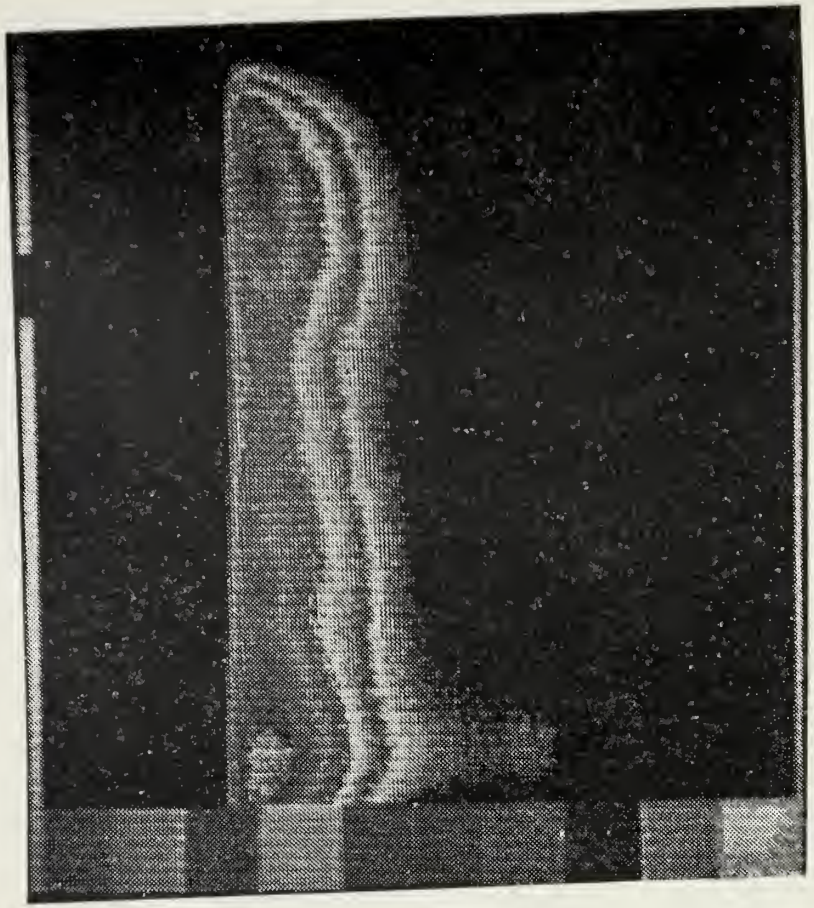

Figure 37 - ONE BY ONE-HALF WAVELENGTH FLAT PLATE CURRENT DISTRIBUTION, 90° INCIDENCE

E. CURVED THREE-QUARTER BY ONE-HALF WAVELENGTH SURFACES ON GROUND PLANE

To show the transition from a flat surface to a cylinder, two sequences of Thermovision pictures were made of surfaces three-quarters of a wavelength high and one-half wavelength wide with varying amounts of curvature. The radii of curvature used were infinity (flat surface), 10.25 centimeters, 7.5 centimeters, and 5.1 centimeters. The 5.1 centimeter radius of curvature corresponds to a cylinder one wavelength (32 centimeters) in circumference that will be studied extensively in the next section.

1. Normal Incidence

This sequence of curved surfaces with the incident signal normal to the center of the surface (Figures 38 through 41), are included to indicate the behavior of the surface currents as the edges become more distant from the source. Because symmetry does not exist on the tubular cylinder with respect to this view, the current distributions shown in this sequence will not exist on the cylinder. However, this sequence does provide insight into the effect of surface curvature.

It is evident from the Thermovision pictures that, as the curvature becomes greater, the surface currents in the center (nearest to the source) become relatively larger. The increase occurs because the effective differential area seen by the source decreases away from the vertical center line and to a lesser degree, because of the spatial attenuation of the incident signal. On the surface with the

smallest radius of curvature (Figure 41), the current magnitudes on a horizontal cross section are nearly constant. The resonant responses of the current magnitudes remain apparent throughout the sequence, with the "monopole-type" response on the edges visible on all but the smallest radius of curvature surface (the half cylinder).

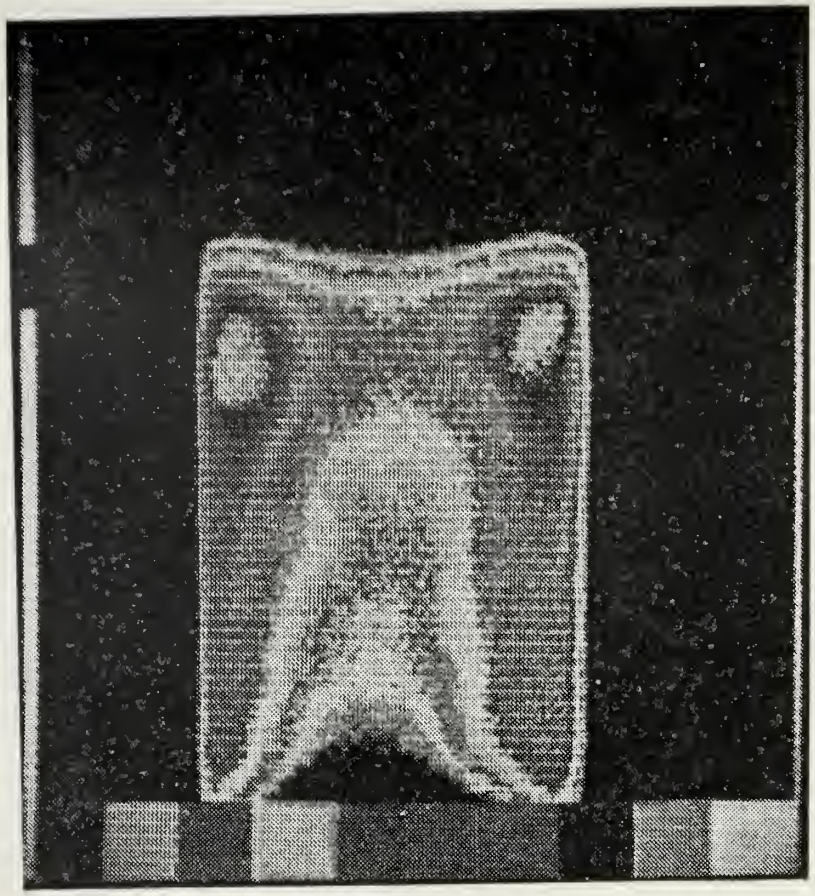

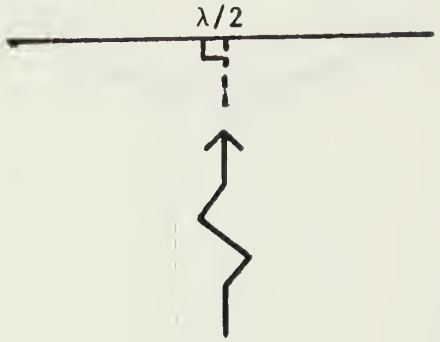

Figure 38 - THREE-QUARTERS BY ONE-HALF WAVELENGTH SURFACE, NORMAL INCIDENCE, r=INFINITY

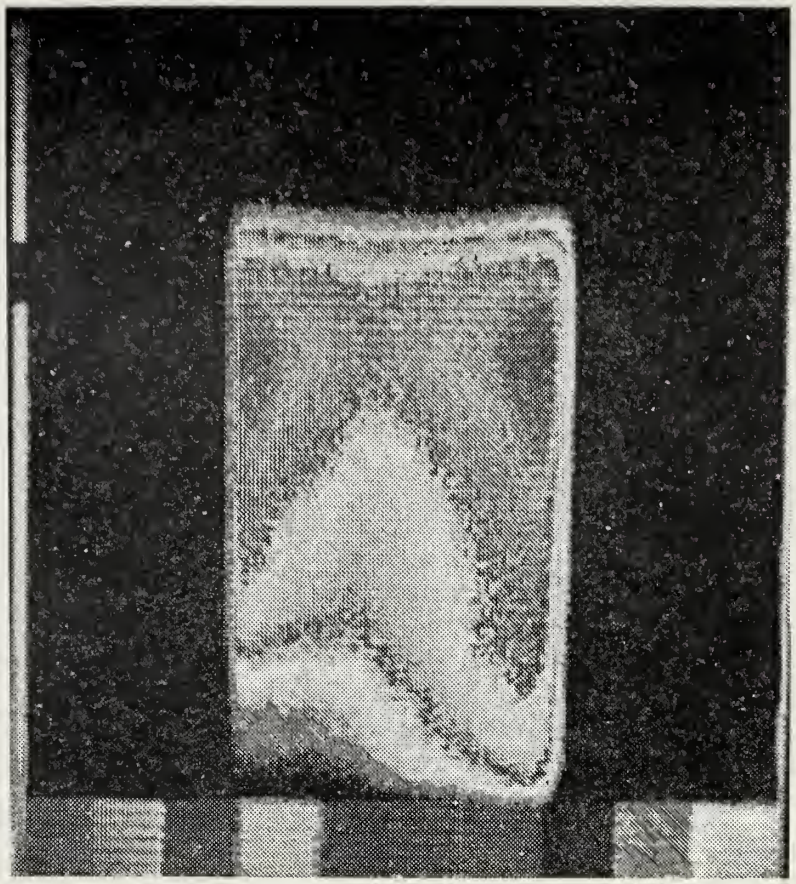

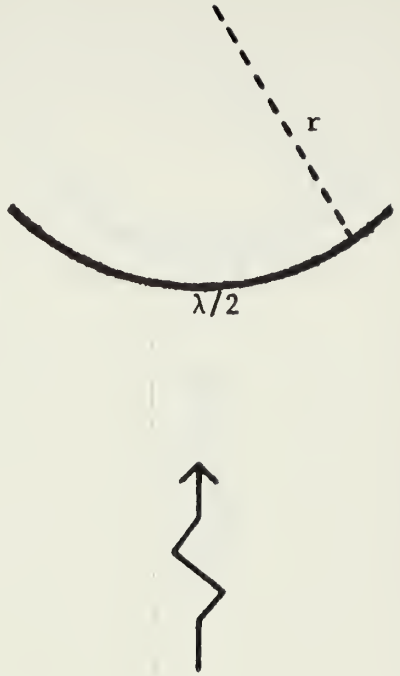

Figure 39 - THREE-QUARTERS BY ONE-HALF WAVELENGTH SURFACE, NORMAL INCIDENCE, r=10.25 cm

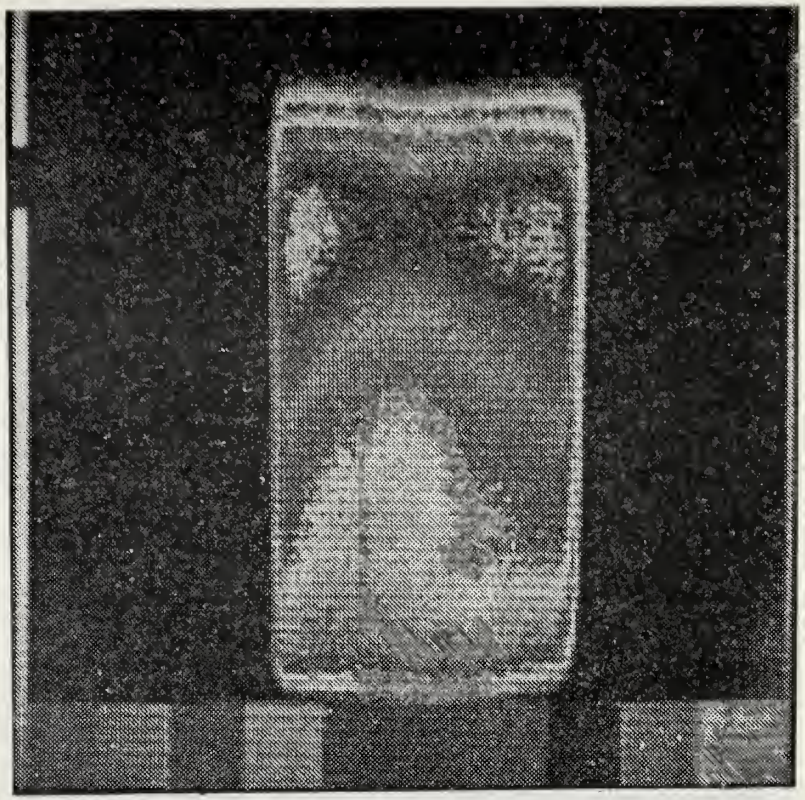

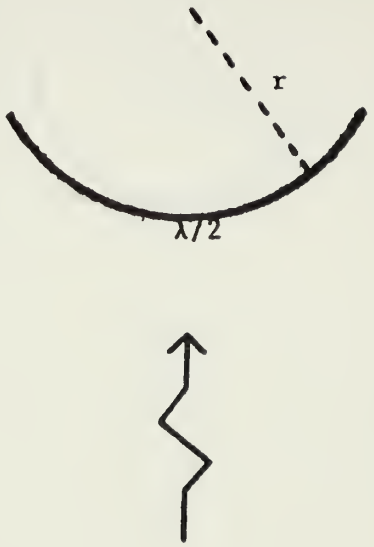

Figure 40 - THREE-QUARTERS BY ONE-HALF WAVELENGTH SURFACE, NORMAL INCIDENCE, r=7.5 cm

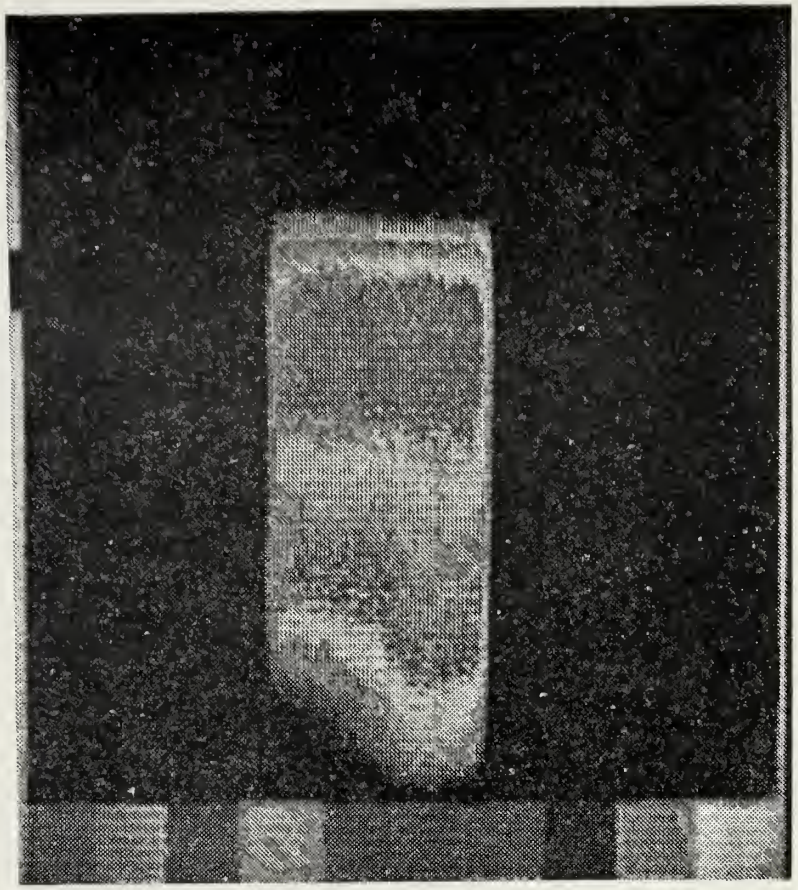

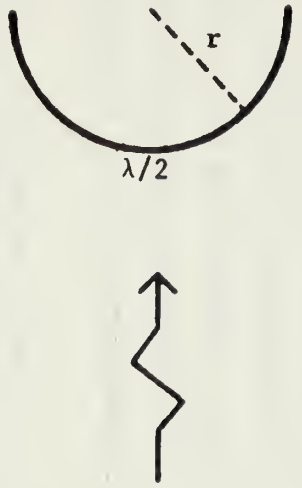

Figure 41 - THREE-QUARTERS BY ONE-HALF WAVELENGTH SURFACE, NORMAL INCIDENCE, r=5.1 cm

2. Ninety-Degree Incidence

Figures 42 through 45 are the Thermovision pictures of the curved surfaces when the incident plane wave is 90° from the normal to the center of the surface. Because of the symmetry of the tubular cylinder with a circumference of one wavelength, the currents in Figure 45 should also be a representation of the currents on that cylinder.

The sequence clearly shows the more distinct formation of the currents on the illuminated portion, as more of the plane wave was incident on the surface with decreasing radius of curvature. Each of the views exhibits the expected resonant response of current magnitudes along the illuminated edge of the surface. The shadowed portion of the surface (the trailing half) in each case was obviously being "driven" by the currents on the illuminated portion.

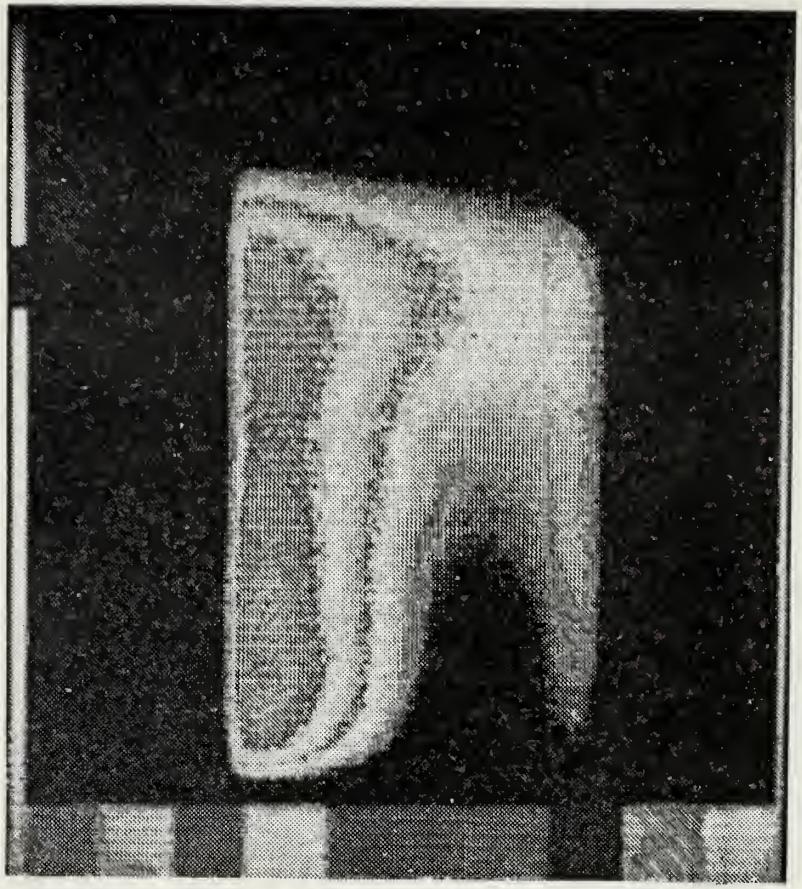

Figure 42 - THREE-QUARTERS BY ONE-HALF WAVELENGTH SURFACE, 90° INCIDENCE, r=INFINITY

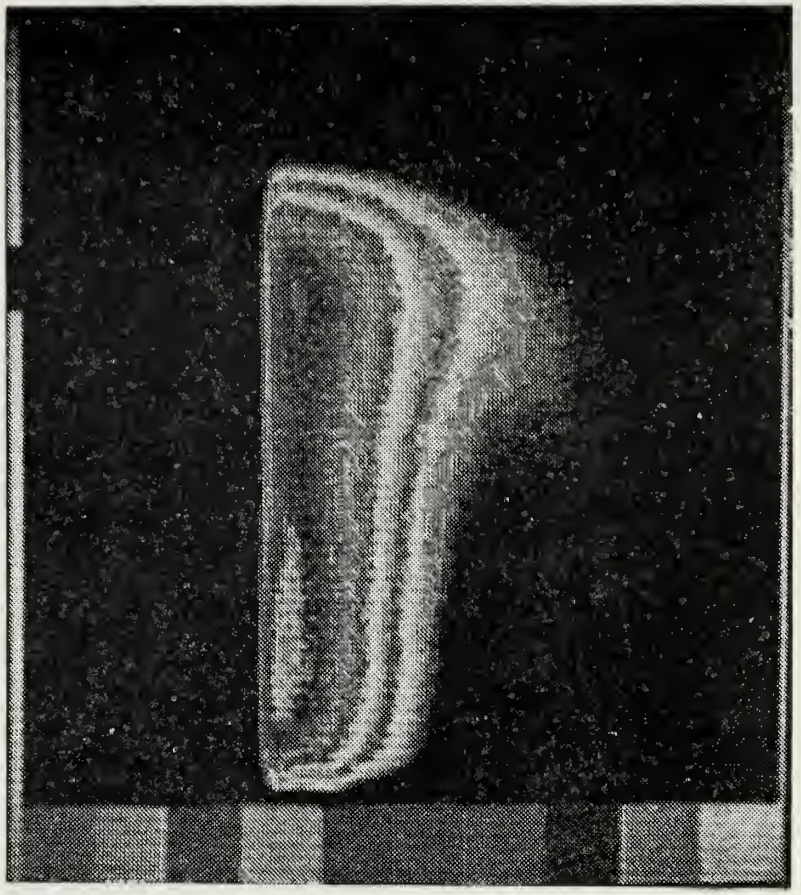

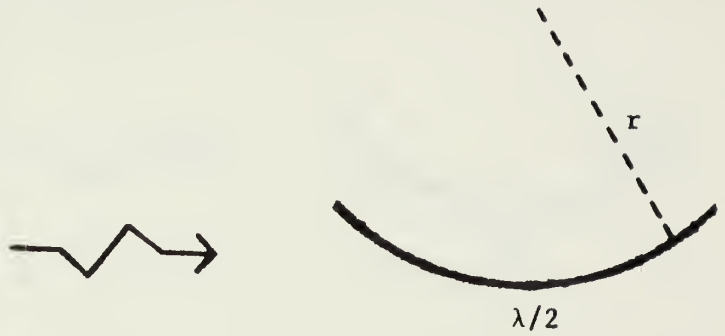

Figure 43 - THREE-QUARTERS BY ONE-HALF WAVELENGTH SURFACE, 90° INCIDENCE, r=10.25 cm

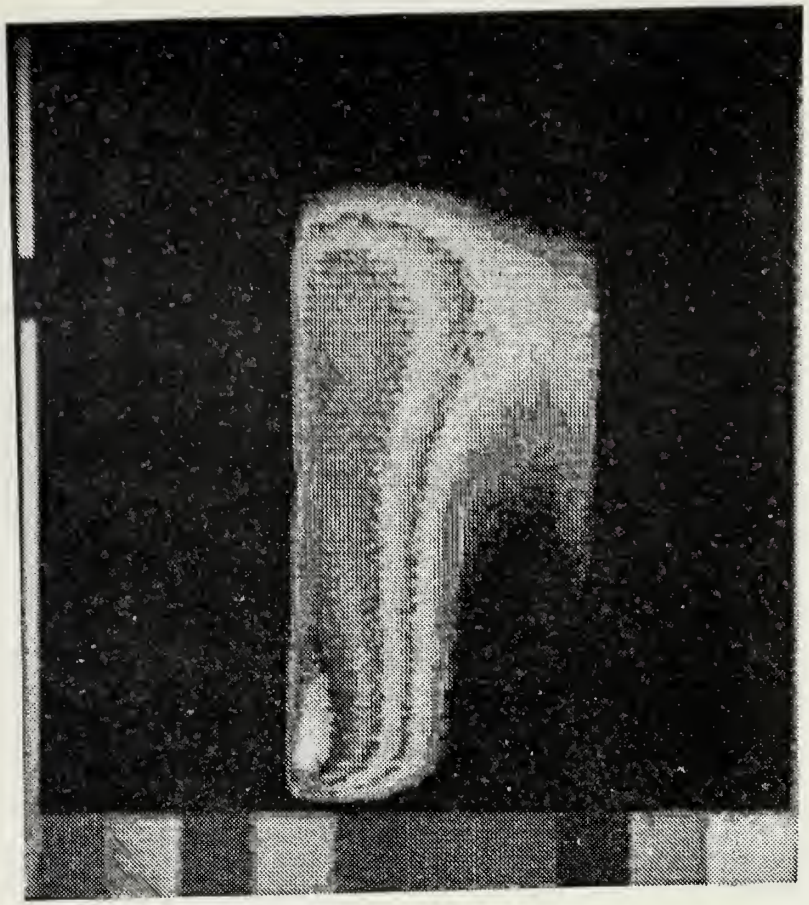

Figure 44 - THREE-QUARTERS BY ONE-HALF WAVELENGTH SURFACE, 90° INCIDENCE, r=7.5 cm

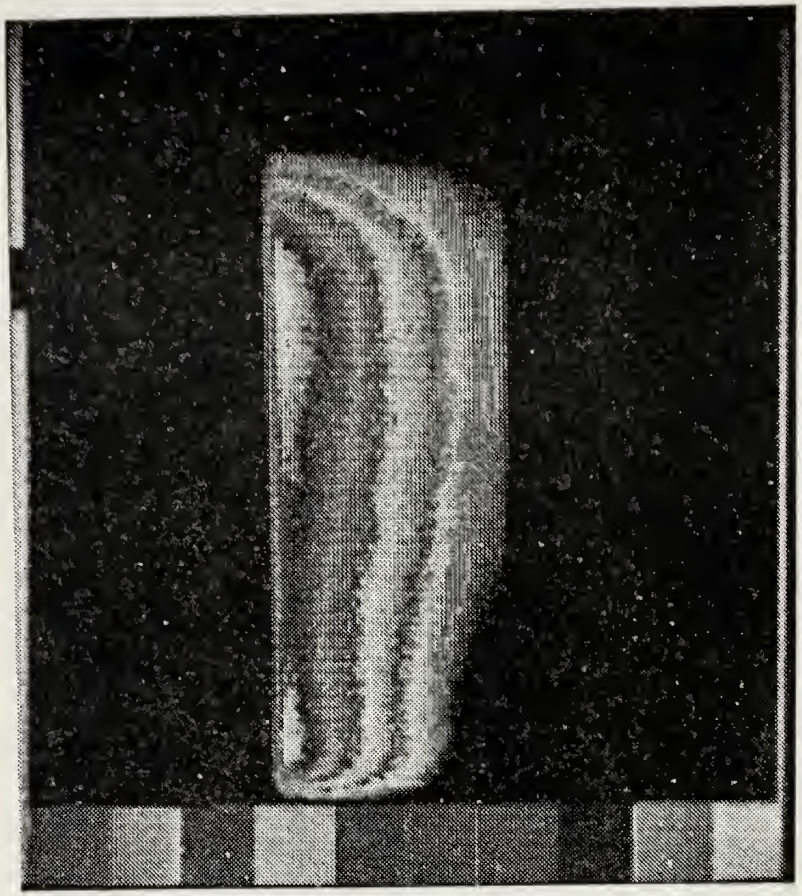

Figure 45 - THREE-QUARTERS BY ONE-HALF WAVELENGTH SURFACE, 90° INCIDENCE, r=5.1 cm

F. THICK CYLINDER ON GROUND PLANE

This section shows the application of the Thermovision surface current determination to a tubular cylinder with ka=1 (circumference of one wavelength) and a height of three-quarters wavelength (24 centimeters), where k is the wavenumber and a is the cylinder radius. Figure 46 shows the resistive paper model of that cylinder.

The model is a five layer resistive paper surface over a polystyrene foam cylinder for rigidity. Again, copper tape was used to insure a uniform connection with the ground plane. Figure 47 exhibits the relative locations of the Thermovision camera and the incident plane wave. Because symmetry exists on the cylinder about a plane perpendicular to the ground plane through the 0°-180° line, the side view was chosen for display. This view then exhibits the relative magnitudes of all currents on the cylinder.

Burton, King, and Blejer (1976) have shown the measured resultant values of surface currents on a cylinder of these dimensions when irradiated by a plane wave, and compared them to the theoretically derived values. These results are shown in Figure 48 with the Thermovision picture of the same situation. The current magnitudes are indicated on an increasing scale from 0 to 9 in ten equal ranges to facilitate comparison with the ten isotherms in the Thermovision picture. Since the Thermovision technique detects steady-state heating of the surface, the relative phases of the currents are not obtained. Thus, the relative phases of the measured results are not indicated in Figure 48. It should be emphasized that the computation of the surface currents on the cylinder is a sophisticated, time

consuming prccedure involving coupled axial and transverse current compcnents.

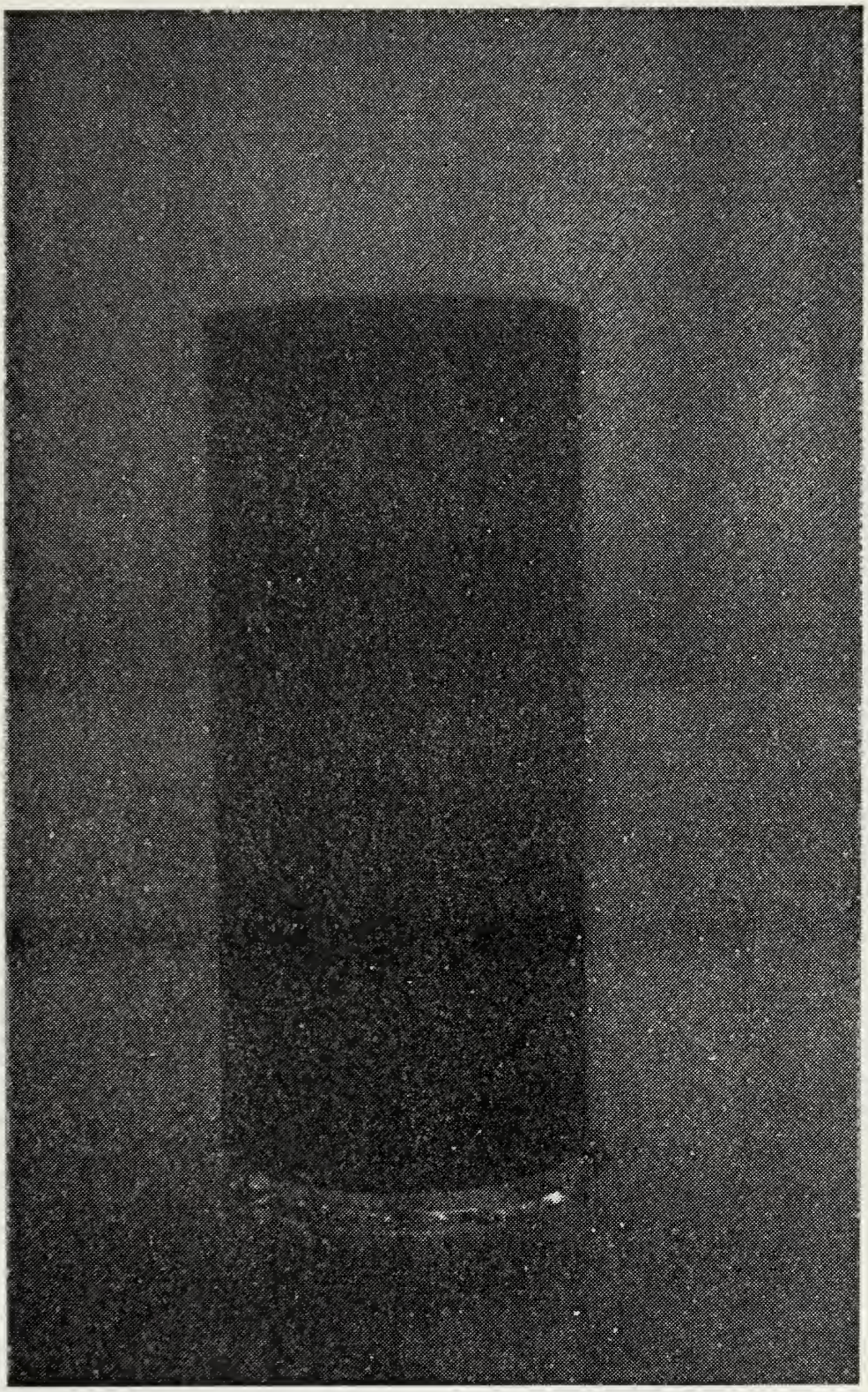

Figure 46 - TUBULAR CYLINDER WITH ka=1 AND HEIGHT OF THREE-QUARTER WAVELENGTH

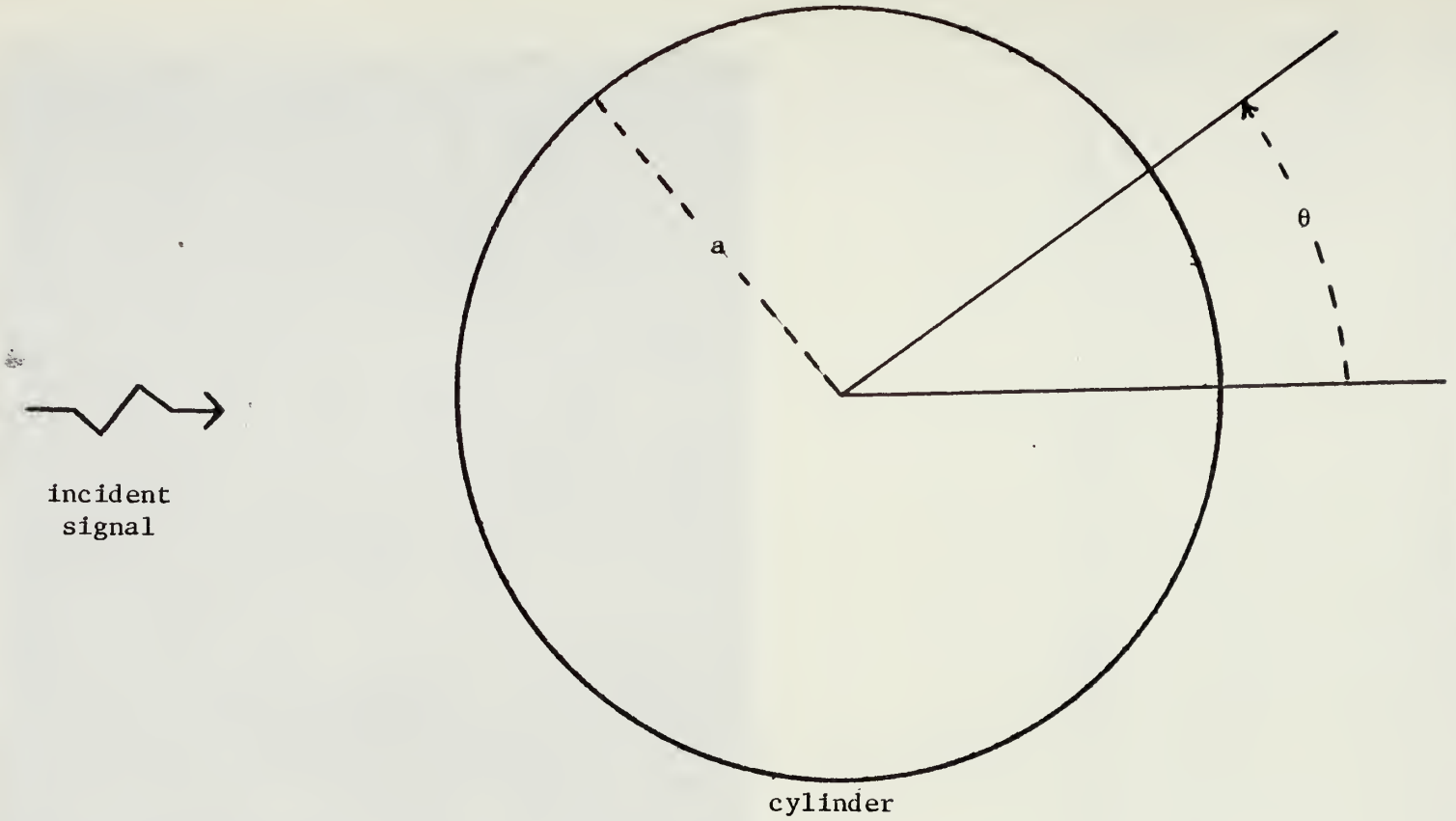

Figure 47 - CYLINDER-CAMERA ORIENTATION

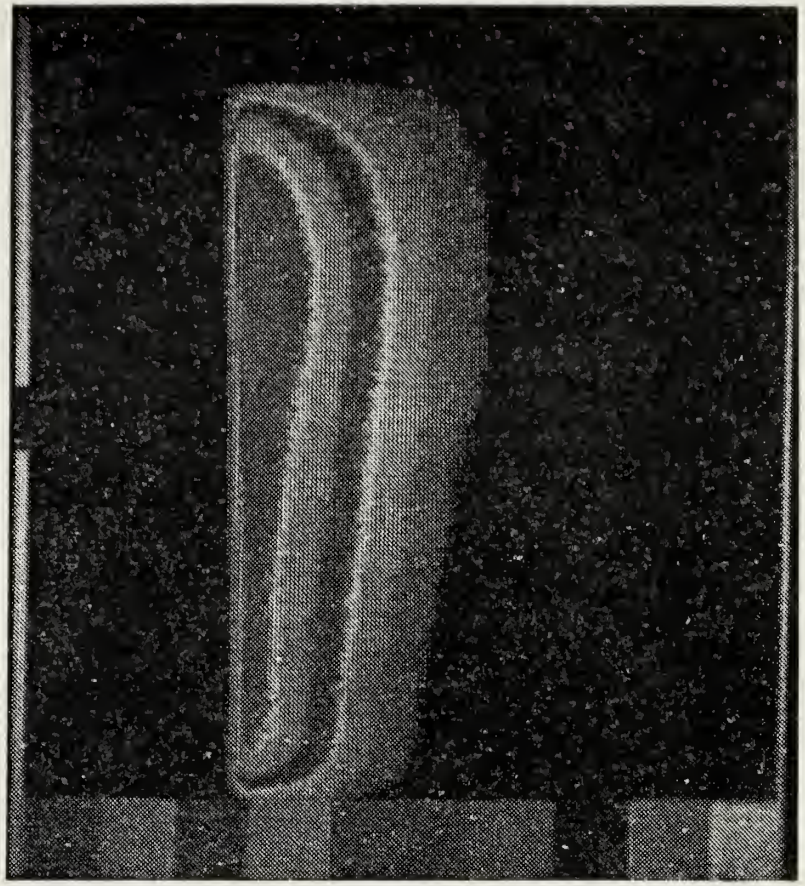

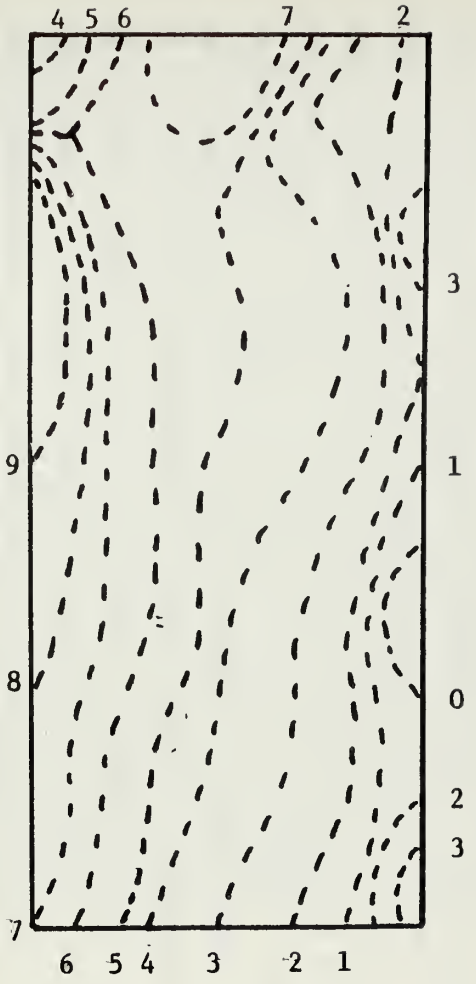

Figure 48 - THICK CYLINDER CURRENT DISTRIBUTION

The temperature window in Figure 48 has been increased to 10°C (each isotherm is 1°C) because of the larger temperature range that exists on the cylinder. Figures 49 through 52 are a sequence of Thermovision pictures of the same cylinder with the temperature window reduced to 2°C for the increased sensitivity (each isotherm is 0.2°C). Each succeeding picture has the bias level changed to lower the temperature window detected. This process causes the increasing size of the white (highest temperature) isotherm, but also allows detection of the smaller currents on the shadowed portion of the cylinder. Comparison of succeeding pictures allows all relative values of current magnitudes to be determined. The temperature window location in Figure 52 is sufficiently low to cause detection of the microwave absorbent material in the background, but the cylinder current values detected are not affected.

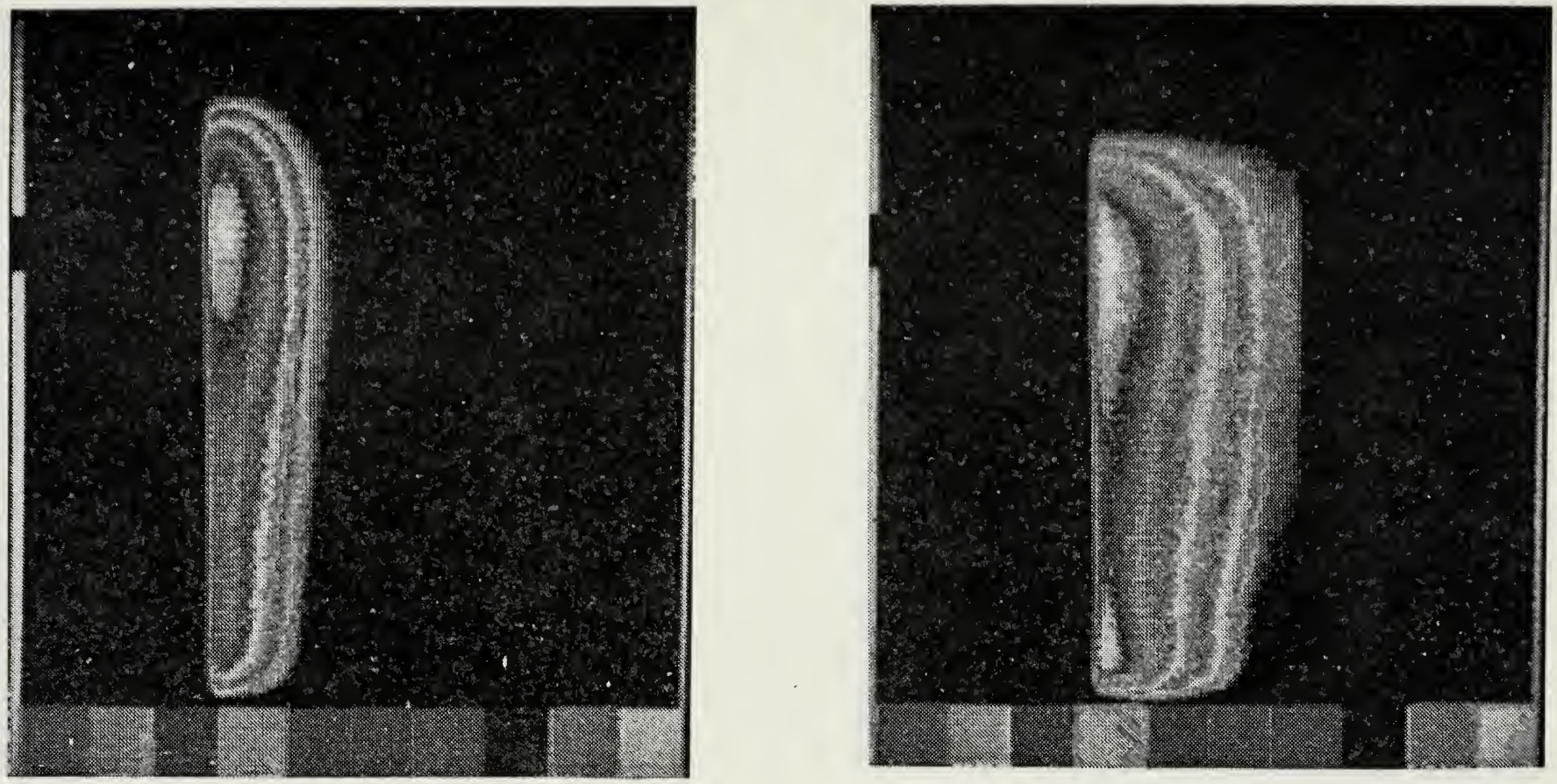

Figure 49 - THICK CYLINDER CURRENT DISTRIBUTION, BIAS SETTINGS 1 AND 2

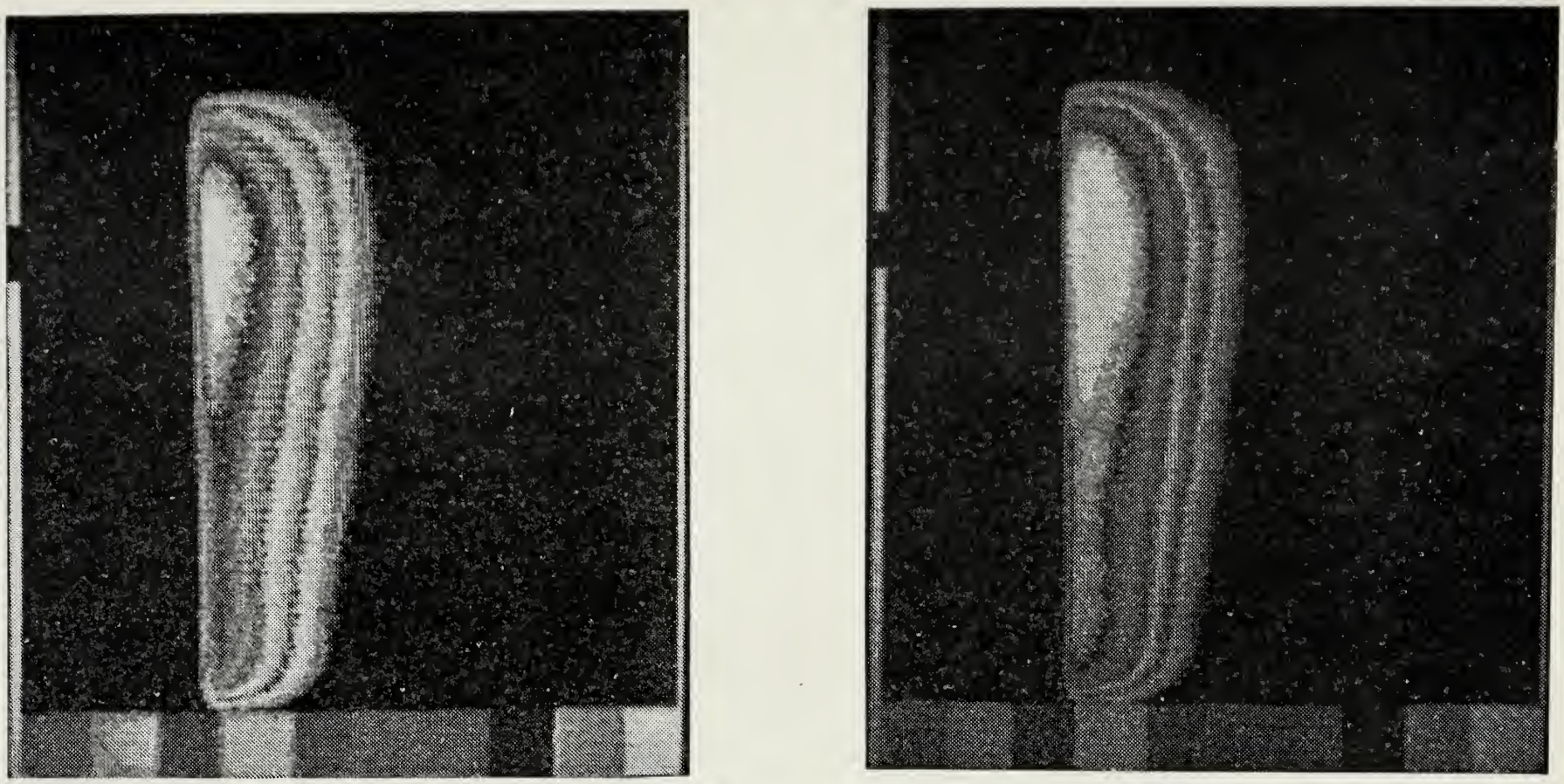

Figure 50 - THICK CYLINDER CURRENT DISTRIBUTION, BIAS SETTINGS 3 AND 4

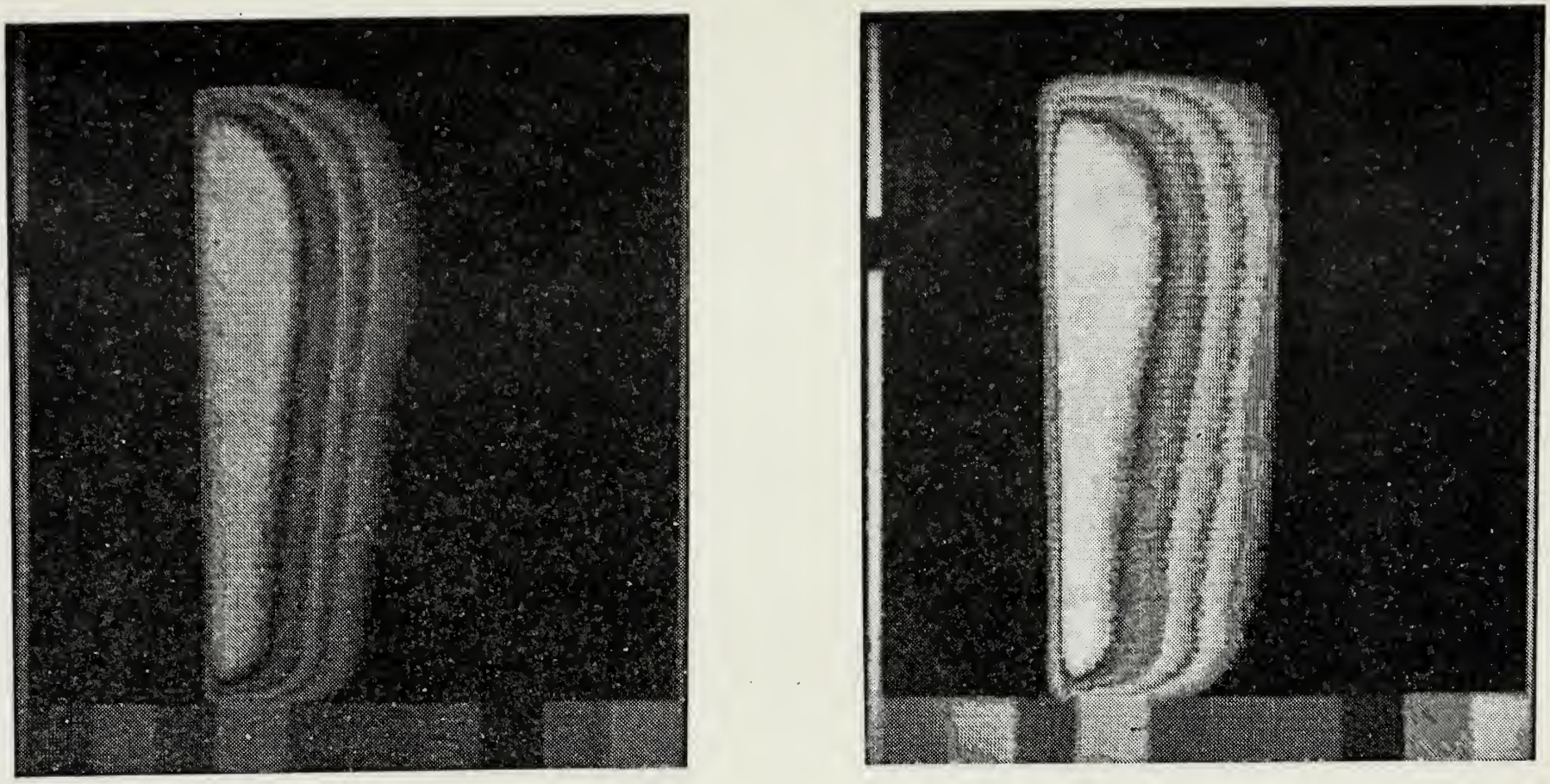

Figure 51 - THICK CYLINDER CURRENT DISTRIBUTION, EIAS SETTINGS 5 AND 6

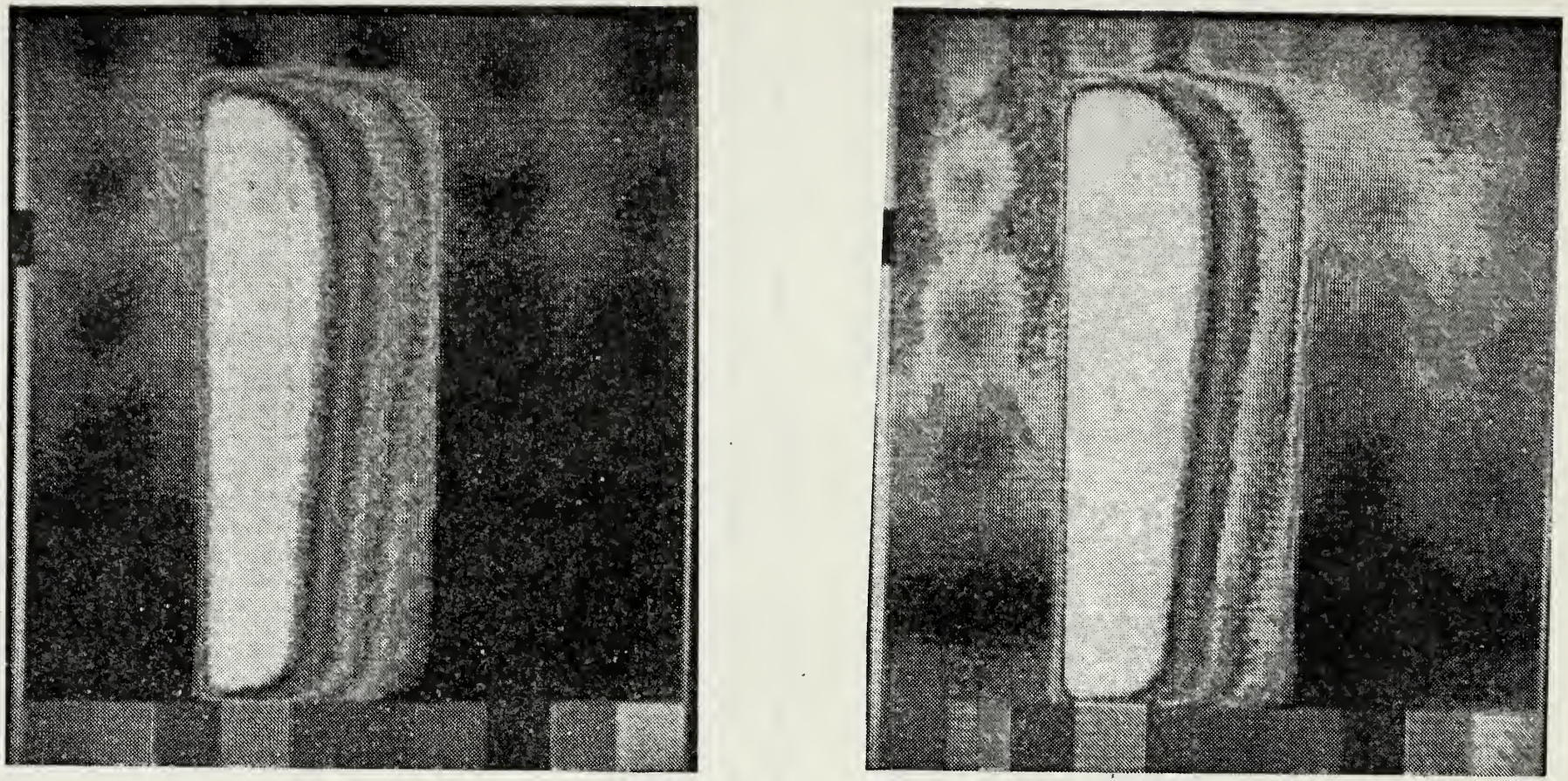

Figure 52 - THICK CYLINDER CURRENT DISTRIBUTION, BIAS SETTINGS 7 AND 8

V. CONCLUSIONS

The infrared imaging technique has been shown to be a valuable tool in the determination of surface charge and current distributions, particularly on complex objects when analytical current determinations are, at best, difficult and time consuming.

The Thermovision technique is particularly important because, with an accurate resistive paper model, subtle differences in current distributions, caused by minor changes in connections and dimensions, can be observed quickly and accurately.

There are some aspects of the Thermovision current detection technique that require care in interpretation. Since this technique uses five layers of resistive paper in the object models, it is possible to have uneven spots or air gaps between the layers. These uneven spots can cause erroneous results because they can alter the thermal conductivity of a portion of the surface. Thus, extreme care must be taken in model construction.

The Thermovision technique must also be used with care at the intersection with the ground plane. Since the surface of the copper tape is a polished metal, with the corresponding low emissivity in the three to five micron wavelength range, the sensitivity of the infrared detection to a given temperature difference is significantly less. Thus, the region covered by the copper tape should not be compared with the remainder of the surface.

It may also be noted that the Thermovision and theoretical results on the tubular cylinder do not match exactly at the top edge of the cylinder. This discrepancy is probably caused by the exposed edges of the resistive paper, which cause a slight surface nonuniformity. This aberration, in turn, slightly changes the thermal conductivity of that edge.

The problems encountered in the application of the Thermovision current detection technique do not significantly affect the general applicability of the procedure. The simplicity of the technique and the near real-time results, make the Thermovision technique an attractive experimental procedure. Infrared detection of surface current distributions will yield reliable results on objects that might otherwise remain unanalyzed.

VI. RECOMMENDATIONS

Since infrared detection of surface charge and current distributions has been shown to be possible and practical, a next logical step is a procedure to allow the application of this technique directly on large metal objects such as ships and aircraft. A surface preparation to increase the emissivity of objects, without significantly altering its electrical properties, would seem to be the correct approach to examine. A proper surface preparation would allow determination of surface currents on materials that do not approach ideal conductors, such as the composite materials currently under study. Such a surface preparation would also solve the problems mentioned in the previous section.

Many objects of interest remain that may be analyzed using carefully constructed resistive paper models. It therefore is important to continue to study these objects using the techniques discussed herein.

APPENDIX A

CURRENT DISTRIBUTIONS ON FLAT SURFACES

The results shown in Figures 53 through 56 indicate the measured surface currents on a flat surface three-quarters of a wavelength high and approximately 0.42 wavelength wide over a conducting ground plane. These results are from current research by Burton and King and indicate the longitudinal and transverse currents on the flat surface with a normally incident plane wave and the same quantities with an incident signal 45° from the normal to the surface.

To allow comparison with the surface currents indicated by the Thermovision pictures in Section IV, the magnitudes were indicated on an increasing scale of arbitrary units from 0 to 9 in ten equal ranges of current magnitudes. Because the relative scales of the transverse and longitudinal currents are being determined, resultant current values are not yet available. However, strong similarities may be seen between the longitudinal current values and the Thermovision pictures.

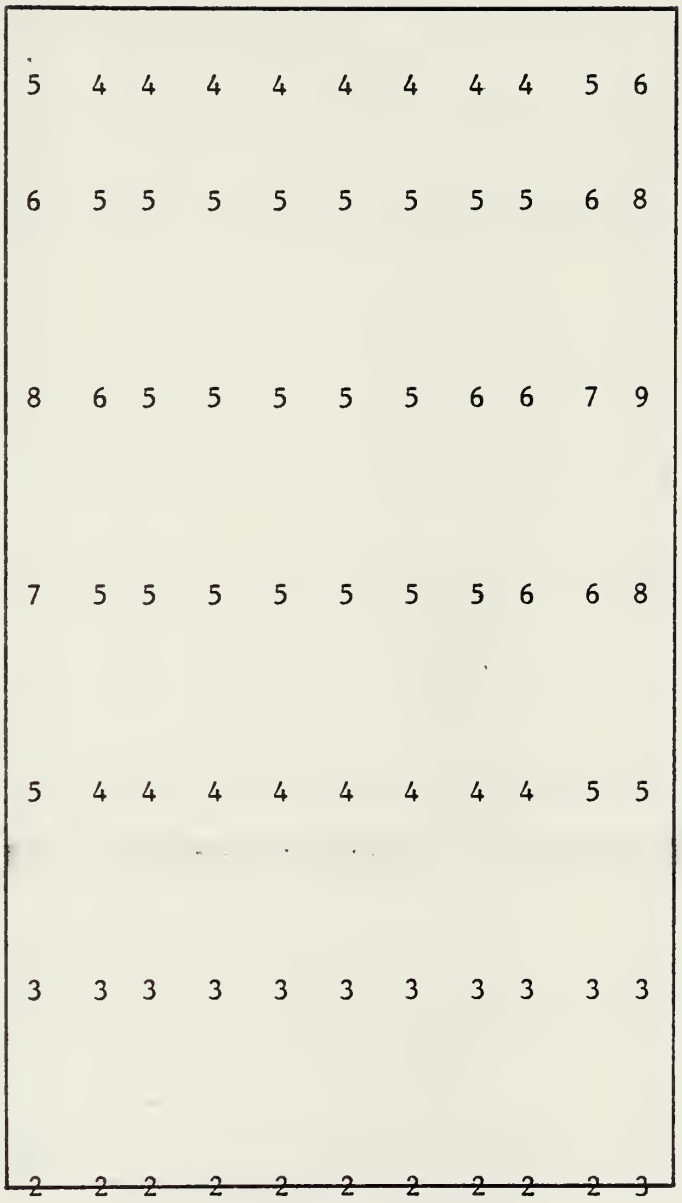

Figure 53 - MEASURED LONGITUDINAL CURRENTS ON A FLAT SURFACE, NORMAL INCIDENCE

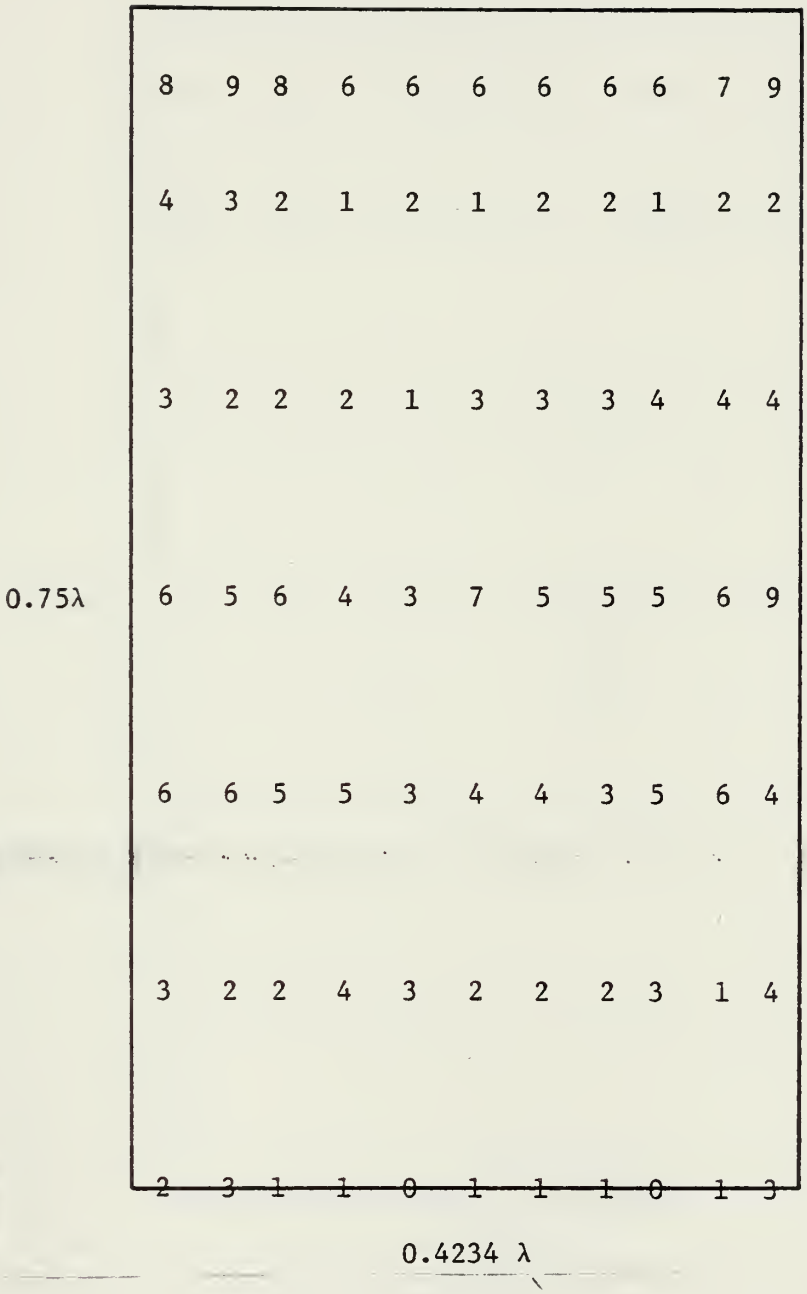

Figure 54 - MEASURED TRANSVERSE CURRENTS ON A FIAT SURFACE, NORMAL INCIDENCE

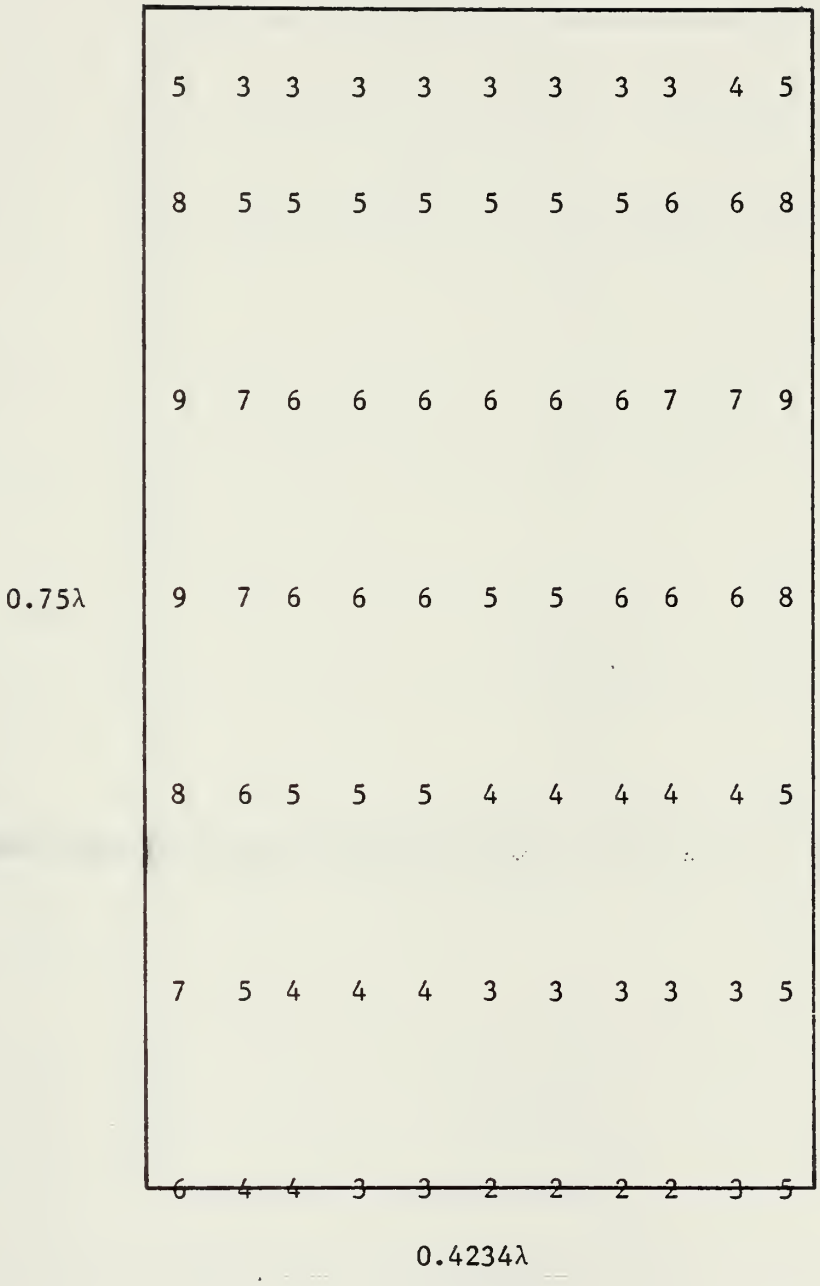

Figure 55 - MEASURED LONGITUDINAL CURRENTS ON A FLAT SURFACE, 45° INCIDENCE

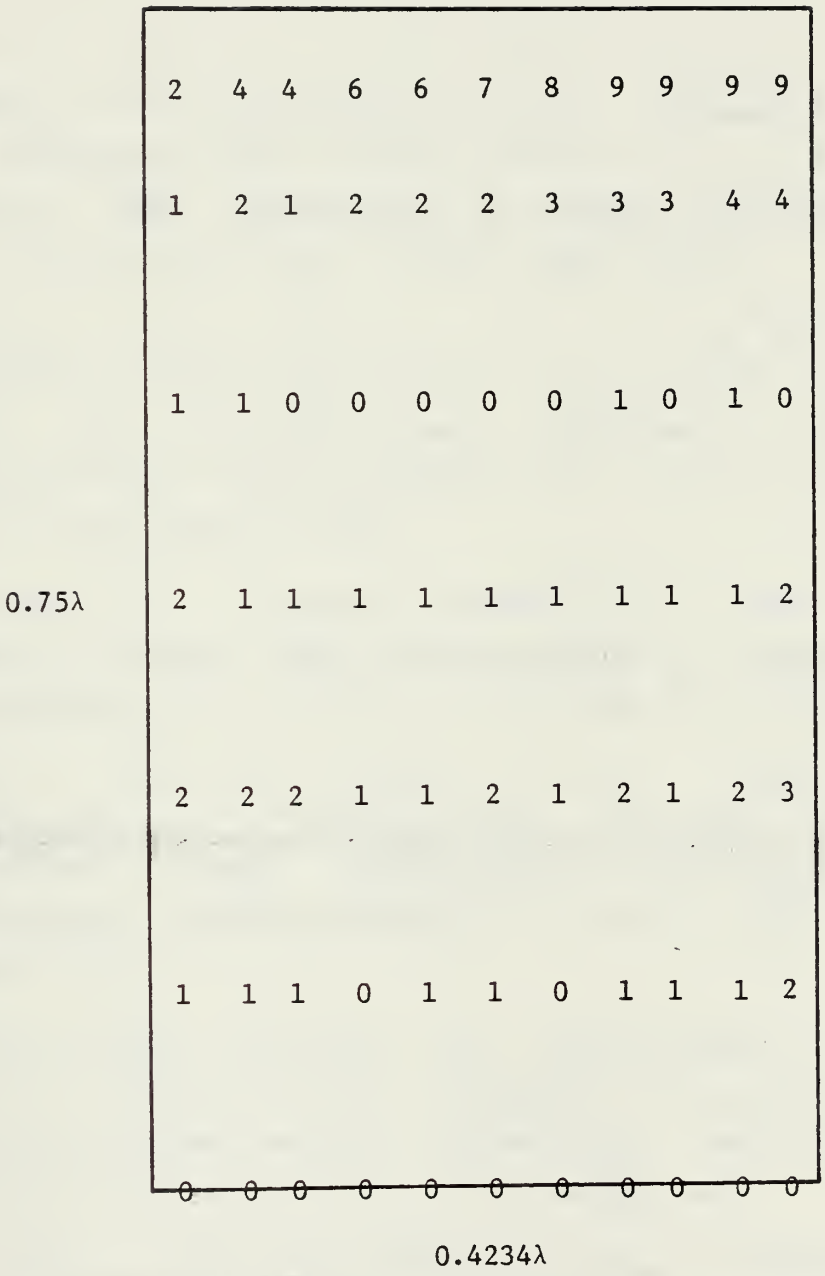

Figure 56 - MEASURED TRANSVERSE CURRENTS ON A FIAT SURFACE, 45° INCIDENCE

BIBLIOGRAPHY

1. Burton, R. W., and King, R. W. P., "Measured Currents and Charges on Thin Crossed Antennas in a Plane-Wave Field," IEEE Transactions on Antnnas and Propagation, Vol. AP-23, No. 5, pp. 657-64, Sept. 1975.

2. Burton, R. W., King, R. W. P., and Blejer, D., "Surface Currents and Charges on a Thick Conducting Tube in an E-Polarized Plane-Wave Field II, Measurements," Radio Science, Vol. 11, No. 8-9, pp. 701-11, Aug.-Sept. 1976.

3. Butler, C. M., "Currents Induced on a Pair of Skew Crossed Wires," IEEE Transactions on Antennas and Propagation, Vol. AP-20, pp. 731-736, Nov. 1972.

4. Chao, H. H., and Strait, B. J., "Radiation and Scattering by a Configuration of Bent Wires with Junctions," IEEE Transactions on Antennas and Propagation (Communications), Vol. AP-19, pp. 701-702, Sept. 1971.

5. Iizuka, Keigo, "A Method for Photographing Microwave with a Polaroid Film," Division of Engineering and Applied Physics, Harvard University, Cambridge, Ma., Technical Report No. 558, p. 3, March 1968.

6. La Varre, C. A., and Burton, R. W., "Thermographic Imaging of Electromagnetic Fields," Thesis Report No. NPS-52 AN 75121, Naval Postgraduate School, Monterey, Ca., Dec. 1975.

7. Nanos, A. G., and Burton R. W., "Infrared Detection of Surface Charge Distributions," Thesis Report, Naval Postgraduate School, Monterey, California, Dec. 1977.

8. Whiteside, H., "Electromagnetic Field Probes," Technical Report No. 377, Cruft Laboratory, Harvard University, Cambridge, Ma., 25 Oct. 1962.

INITIAL DISTRIBUTION LIST

		No. Copies
1.	Defense Documentation Center Cameron Station Alexandria, Virginia 22314	2
2.	Library, Code 0212 Naval Postgraduate School Monterey, California 93940	2
3.	Department Chairman, Code 62 Department of Electrical Engineering Naval Postgraduate School Monterey, California 93940	1
4.	Professor R. W. Burton, Code 62ZN Department of Electrical Engineering Naval Postgraduate School Monterey, California 93940	15
5.	CAPT James D. Selim, USMC 1504 Crescent Drive Bartlesville, Oklahoma 74003	3
6.	Professor J. P. Powers, Code 62PO Department of Electrical Engineering Naval Postgraduate School Monterey, California 93940	1
7.	Mr. Jacob Scherer Post-Doctoral Program RADC-RBC Griffiss AFB, NY 13441	2

8. Professor Glen Smith 1
School of Electrical Engineering
Georgia Institute of Technology
Atlanta, Georgia 30332

9. Professor Lamar Allen 1
University of South Florida
Electrical and Electronic Systems
Tampa, Florida 33620

10. Professor Robert Catellessa 1
Clarkson College of Technology
Potsdam, New York 13676

11. Dr. W. Everett 1
SCEE Cherwood-Oneida Lake
Walnut Grove
Bridgeport, New York 13030

12. Mr. Warren Peele 1
Electrical Engineering Department
Purdue, University
West LaFayette, Indiana 47907

13. Colonel R. E. Thomas 1
DFEE
USAF Academy, Colorado 80840

14. Dr. Richard B. Mack 1
Electronic Technology Division/RADC
LG Hanscom Field
Bedford, Massachusetts 01731

15. Dr. C. E. Baum 1
AFWL/EL
Kirtland AFB
Albuquerque, NM 87118

16. Mr. P. Castillo — 1
AFWL/ELE
Kirtland AFB
Albuquerque, NM 87118

17. LCDR James Charles, USN — 2
NADC (Attn. 02113)
Warminster, Pa 18974

18. Professor K. Iizuka — 1
Department of Electrical Engineering
University of Toronto
Toronto, Canada

19. Dr. Robert Mailloux — 1
Electronics Technology Division/RADC
Hanscomb AFB, MA 01731

20. Professor Walter H. Ku — 1
Department of Electrical Engineering
Cornell University
Ithica, NY 14850

21. Mr. Marlin Kvigne — 2
Naval Ocean Systems Center
San Diego, Ca 92132

22. Mr. Larry Sumney — 2
Code 03E
Naval Electronics Systems Command
Washington, D.C. 20360